

Investigations on some selected conducting polymers and polymer composites for possible optoelectronic applications

Thesis submitted to

COCHIN UNIVERSITY OF SCIENCE AND TECHNOLOGY

in partial fulfillment of the requirements for the award of

DOCTOR OF PHILOSOPHY

by

AMRITHESH.M



**Department of Physics
Cochin University of Science and Technology
Cochin-682022, India**

August, 2009

Investigations on some selected conducting polymers and polymer composites for possible optoelectronic applications

Ph.D thesis in the field of material science

Author:

Amrithesh.M,
Division for Research in Advanced Materials,
Department of Physics,
Cochin University of Science and Technology,
Cochin-682022,
Kerala,
India
Email:amritheshm@gmail.com

T19

T
678-01:621-38
AMR

Supervising guide:

Dr.S.Jayalekshmi,
Reader,
Department of Physics,
Cochin University of Science and Technology,
Cochin-682022,
Kerala,
India
Email:jayalekshmi@cusat.ac.in




August,2009

Declaration

I hereby declare that the work presented in this thesis entitled **“Investigations on some selected conducting polymers and polymer composites for possible optoelectronic applications”** is based on the original work done by me under the guidance of **Dr.S.Jayalekshmi**, Reader, Department of physics, Cochin University of Science and Technology, Cochin-22 and it has not been included in any other thesis submitted previously for the award of any degree.

Cochin-22
12/08/2009


Amrithesh.M



*"Sradhavan labathe jnanam
Tatpara samyamendriya
Jnanam labthwa param santhi
Achiranadhi gachathi"*

*Dedicated to
my beloved Parents & Teachers*

Acknowledgements

Let me humbly express my heart felt thanks to Dr.S.Jayalekshmi (Reader, Department of physics,CUSAT), my guide for her invaluable guidance, wise advices, constant encouragement and above all, the maternal affection and warmth she has extended to me always. She has spared much of her precious time and energy for the successful completion of my research work. I feel blessed to get her as my guide. I would also like to thank the HOD, Physics for rendering me all the necessary facilities. My sincere thanks to Dr.M.K.Jayaraj, Prof K.P.Vijaya Kumar, Prof C.Sudha Kartha, Dr.B.Pradeep, Prof M.R.Anantharaman and Sri P.K.Sarangadharan, faculty members of the Department of Physics,CUSAT for allowing me to use their laboratory facilities. Special thanks to Prof.K.P.R.Kartha, NIPER, Chandigarh for providing me the necessary help. My sincere thanks to Dr.Ashalatha, Reader, K.K.T.M College, Kodungalloor for encouraging me to work in the field of conducting polymers. Prof Rani Joseph, Department of Polymer Science and Rubber Technology, Dr.K.SreeKumar and Dr.Joseph Makkolil, Department of Chemistry have cleared my doubts and given suggestions, which provided a smooth pathway for research. My special thanks to them also.

Ravi sir (Dr.K.Raveendranath) (late), my teacher deserves a special mention. He has been a great inspiration for me always and has helped me in all the ways he could. He is indeed a friend, philosopher and guide. Mr. Rajive and Mr. Aravind have helped me a lot, especially during the early stages of my work. Timely help rendered by Mr. Febin and Ms. Chandni is invaluable. Let me extend my sincere gratitude to them. Mr. Arun, Mrs. Jeeju, Mr. Anil, Mr. Francis, Mr. Sreekanth, Mr. Joseph John

sir and Mrs. Sreevalsa have also provided the necessary assistance and moral support. Thanks to all of them. Timely help rendered by Dr. Joseph Mathai and Dr. Shaji is gratefully acknowledged.

My sincere gratitude to Dr. R. S. Jayasree, Department of Radiology, S.C.T.I.M.S.T, Thiruvananthapuram for spending her precious time in recording the photoluminescence spectra of the samples. Help rendered by Dr. Jyotsna Ravi and Dr. Thomas Lee with the photo acoustics studies of the polyaniline samples is invaluable. I would also like to thank Dr. Ganesh and MS. Swati Pandya, CSR Indore for their help with the thermo power measurements on my samples. Sincere thanks to Dr. Vasanth Sathe of the same institution for recording the Raman spectra of the samples. My heart felt thanks to Dr. D. Sakti Kumar, Bio Nano Electronics Research Center, Toyo University, Japan for the TEM images of the samples. I am also indebted to Ms Honey and Ms Usha of the polymer department who have helped me much with their technical advices. Mr. Baiju John, CIET, Cochin has helped me with the mechanical strength measurements on PANI and PANI-PMMA samples. My special thanks to him also. I remember with gratitude the fruitful discussions with Dr. R. S. Anand, I.I.T., Kanpur about organic optoelectronic devices.

Mr. Sajeev, Mr. Manoj and Mrs. Resmi have helped me a lot during the early stages of my research work. Special thanks to all other research scholars in CUSAT who have helped me in one way or the other during my course of work. My sincere gratitude to all the office, laboratory, library and STIC staff for doing the needful assistance in time. I am very much indebted to K.S.C.S.T.E for providing the research fellowship.

Lots of love to my parents, sister, family members and my fiancée for giving me full support and assistance. The wonderful moments that I have

enjoyed with the family members of my guide, which include Dr.K.P.R.Kartha, Anku, Mr.Jayakrishnan, Smt.RemaDevi, Smt.Jayasri and Mr.Jayaraj still linger in my mind. I would like to thank them all for their love and friendship. I thank God almighty for helping me to complete my research successfully in time.

Amrithesh.M

Preface

Science and technology has revolutionized the modern world. The progress in the areas of electronics, computerscience, health care, communication engineering and information technology over the last two decades is amazing. Progress in theoretical as well as experimental research over the years has sowed the seeds for this abrupt growth. As far as material science is concerned, synthesis and characterization of novel materials with a view on device fabrication has flourished.

Conducting polymers is a fast growing area in materials science research. Materials once considered as insulators have evolved as semiconductors or metals. Conducting polymers are found to have potential applications in the areas of sensors, electromagnetic shielding, microelectronic and optoelectronic devices. They have successfully replaced metals in many areas owing to their lightness, resistance to corrosion, low cost and ease of fabrication. But unfortunately the optical and thermal properties of such systems have not been focused much. Such a study is indispensable for the fabrication of optoelectronic and microelectronic devices capable of operation at high temperatures.

Conducting polymer composites are another area of interest. Despite having good electrical and optical properties, most of the conducting polymers have poor mechanical strength and thermal stability. Making composites with suitable materials is a possible remedy to this problem. Above all, the properties of conducting polymers could be tailored suitably by preparing composites. It is one of the hot areas in conducting polymer research.

The work presented in this thesis is mainly centered on conducting polymers and polymer composites, in bulk and thin film form, for optoelectronic applications. The major areas focused include temperature dependent D.C electrical conductivity, temperature variation of thermopower, photoluminescence, thermogravimetric analysis and mechanical strength measurements in addition to structural and morphological analysis.

A general introduction to conducting polymers, their history, synthesis procedures and applications are dealt with in CHAPTER1.

CHAPTER2 deals with the theoretical aspects. The mechanism of conduction in polymers, effect of doping, various conduction mechanisms and the theory behind the experimental methods employed are detailed in this chapter.

CHAPTER3 is based on polyaniline (PANI) and polyaniline nano rod samples. The effect of doping on the structural, electrical and photo luminescent properties of polyaniline is investigated. Polyaniline nano rod samples are synthesized with various monomer to oxidant feed ratios. The effect of variation in the oxidant feed ratio on the structural, electrical and thermal properties are investigated.

In CHAPTER4, synthesis and characterization of polyaniline-polymethylmethacrylate (PMMA) samples are described. The effect of varying the aniline to PMMA feed ratio on the structural, electrical, photoluminescent and thermal properties are studied.

Detailed investigations on polyaniline-multiwalled carbon nanotube (MWNT) composite samples are described in CHAPTER5. PANI-MWNT composites with various aniline to MWNT

feed ratios are synthesized and their structural, morphological, thermal and electrical (including thermo power) properties are investigated.

CHAPTER6 deals with the optical transition energy gap analysis of some selected conducting polymer films. The films are prepared by solution casting technique. Negative energy gap has been observed for the first time in conducting polymer films, corresponding to indirect allowed transition.

In CHAPTER7, thermal diffusivities of PANI and PANI-MWNT composite samples with various aniline to MWNT feed ratios are investigated, using photo acoustic technique.

The conclusions drawn from the present investigations are summarized in CHAPTER8. The major achievements of the present investigations and the scope for further studies are also highlighted.

The major highlights of the investigations are,

1. A comparative study of the photoluminescence intensities of the PANI(Polyaniline) samples doped with various acids are attempted for the first time. PANI doped with orthophosphoric acid exhibits the highest photo luminescent emission intensity, making it a suitable material for optoelectronic device fabrication.
2. PANI nano rods exhibit good D.C electrical conductivity and thermal stability.
3. The photoluminescence emission intensity as well as D.C electrical conductivity of PANI-PMMA(Polymethylmethacrylate) composites is found to increase with increase in PMMA content in the composite up to a particular feed ratio of aniline to PMMA and thereafter decreases.

4. The D.C electrical conductivity of PANI -MWNT (Multiwalled carbon nano tube) composites increases substantially with increase in MWNT content. The composites show negligible variation of conductivity with temperature in the temperature range 303K-408K, metal like variation of thermo power with temperature and good thermal stability. These observations have been clearly explained and interpreted.
5. The thermal diffusivity of PANI (HCl)-MWNT composites increases with increase in MWNT loading up to a certain limit and thereafter decreases.
6. Negative energy gap has been observed for the first time, corresponding to indirect allowed transition in PANI and PANI-MWNT films in the highly conducting state.

.....203.....

List of publications

In International Journals

1. Enhanced luminescence observed in Polyaniline-polymethylmethacrylate composites, **M. Amrithesh**, S. Aravind, S. Jayalekshmi, R.S. Jayasree, **J.Alloys Compd**, **449(2008)**, 176-179
2. Polyaniline doped with orthophosphoric acid—A material with prospects for optoelectronic applications **M. Amrithesh**, S. Aravind, S. Jayalekshmi, R.S. Jayasree, **J.Alloys Compd**, **458 (2008) 532-535**
3. On the interesting optical transitions observed in polyaniline films in the conducting and insulating states, **M.Amrithesh**, K.P.Chandni, S.Jayalekshmi, Febin Kurian, S.J.Varma, **Optoelectron. Adv.Mater (RC)**,**3(2)(2009)**,149-154
4. Highly conducting PANI-MWNT composites with a flat temperature dependence of conductivity and good thermal stability (**communicated**), **Amrithesh.M**, Febin Kurian, Jayalekshmi.S, Sakthikumar.D

International/National conference presentations

1. *A Novel Synthesis Route for the Preparation of Polyaniline-Polymethylmethacrylate composites* **Amrithesh.M**, Aravind.S, S.Jayalekshmi **International Conference on Science & Technology for sustainable development held in Kottayam during 10-13 Aug 2005, organized by S.B.College, Changanacherry.**
2. *Enhanced Luminescence Observed in Polyaniline-Polymethyl methacrylate Composites* **Amrithesh.M**, Aravind.S, S.Jayalekshmi, R.S.Jayasree **Materials 2005, held in Kuala Lumpur, Malaysia during 6-8 Dec 2005.**

3. TEM studies on PANI nanorods and PANI nanocomposites **Amrithesh.M**, Aravind.S, D.Sakthikumar, Yosuhiko Yoshida, S.Jayalekshmi **4th International Symposium on Bioscience & Nanotechnology, Bio Nano Electronics Research Center, Toyo University, Japan, held during 7-8 November, 2006**
4. Orthophosphoric acid doped Polyaniline-A promising material for optoelectronic device applications. **Amrithesh.M**, Aravind.S, S.Jayalekshmi **International Symposium for Research Scholars, held at IIT Madras during 18-20 Dec 2006**
5. Polyaniline Nano rods with enhanced photoluminescence. **Amrithesh.M**, Aravind.S, S.Jayalekshmi, R.S.Jayasree **National Conference on Smart Electro ceramics, held at C-MET Thrissur during March8-9, 2007**
6. Thermal studies on Polyaniline-carbon nanotube composites **M.Amrithesh**, Febin Kurian, S.Aravind, S.Jayalekshmi **National seminar on Current Trends in Materials Science, held at Christian College Chengannur, during March 25-27, 2007**
7. D.C. conductivity studies on nano pani samples with varying APS ratio **Amrithesh.M**, Chandni K.P., S.Jayalekshmi **National Conference on New Horizons in Theoretical and Experimental Physics, held at Dept of Physics, CUSAT, Cochin-22 during October 8-10, 2007**

Related works

1. Electrical conductivity studies on Polythiophene-carbon nano tube composites **Amrithesh.M**, Febin Kurian, S.Jayalekshmi **National Conference on Nano Materials and Nano Technology (NATCON NAMTECH- 2007) held at University of Luck now, Dec8-10, 2007.**
2. *Interesting Luminescence Behaviour Observed in Polypyrrole-Polymethylmethacrylate composites* **Amrithesh.M**, Aravind.S, S.Jayalekshmi, R.S.Jayasree **Optoelectronic Materials and**

Thinfilms (OMTAT) October 24-27, 2005, Department of Physics, Cochin University of Science And Technology, Cochin.

3. Polypyrrole nanorods with appreciable crystallinity and good optical absorption characteristics Jeeju.P.P, Sreekanth.J.Varma, Amrithesh.M, S.Jayalekshmi, **Cochin Nano, 3-5 January 2009**

.....EOC.....

Contents

Preface
List of Publications

Chapter 1

Introduction	01 - 42
1.1 About polymers	01
1.2 Glass transition temperature	03
1.3 What are conducting polymers?	04
1.4 Progress in conducting polymer research	04
1.5 Synthesis	06
1.6 Gelation of PANI	13
1.7 PANI fibers	14
1.8 Advances in solution processing of PANI	16
1.9 Some important conducting polymers	19
1.10 Conducting polymer composites	20
1.11 Important applications of conducting polymers	20
1.11.1 Opto electronic applications	20
1.11.2 Conducting polymers in micro electronics	29
1.11.3 Gas and liquid separation applications of polyaniline membranes	29
1.11.4 Chemical and biological sensors based on electronically conducting polymers	30
1.11.5 Electrically conducting textiles	30
1.11.6 Electro chemo mechanical devices	31
1.11.7 Conductive polymer/High temperature super conductor assemblies and devices	32
1.11.8 Transparent conductive coatings	33
1.12 Objectives of the present work	35

Chapter 2

Experimental techniques and theory 43 -84

2.1	Introduction	43
2.2	Non-redox doping	45
2.3	Electronic conduction mechanisms	46
2.3.1	Disorder induced metal-insulator transition	47
2.3.2	Hopping in disordered semiconductors	49
2.3.3	Tunneling between metallic islands	50
2.3.4	Space charge limited conduction	52
2.3.5	Schottky effect	53
2.3.6	Poole-Frenkel conduction process	53
2.4	Experimental techniques	54
2.4.1	FTIR spectroscopy	54
2.4.2	X-ray diffraction	56
2.4.3	D.C electrical conductivity measurements	58
2.4.4	Photoluminescence (P.L) measurements	62
2.4.5	TEM studies	65
2.4.6	SEM studies	67
2.4.7	Thermo gravimetric Analysis (T.G.A)	70
2.4.8	UV/Vis/NIR Absorption Spectroscopy	70
2.4.9	Photo acoustics measurements	73
2.4.10	Raman measurements	73
2.4.11	Mechanical strength measurements	74
2.4.12	Thermo power measurements	76
2.4.13	Film thickness measurements	78
	References	79

Chapter 3

Studies on PANI and PANI nano rods 85-104

3.1	Introduction	85
3.2	Synthesis	86
3.3	FTIR studies	86
3.4	Raman studies	88
3.5	X.R.D Analysis	89
3.6	Photoluminescence studies	91
3.7	D.C electrical conductivity studies	93

3.8	Studies on PANI nano rods	95
3.8.1	Synthesis of PANI nano rods	95
3.8.2	FTIR Analysis	96
3.8.3	X.R.D Analysis	97
3.8.4	TEM Analysis	98
3.8.5	D.C electrical conductivity studies	98
3.8.6	T.G.A Analysis	100
3.9	Conclusions	101
	References	102

Chapter 4

Studies on PANI(HCl)-PMMA composites 105-126

4.1	Introduction	105
4.2	Preparation of PMMA sheets	106
4.3	Synthesis of PANI-PMMA composites	107
4.4	FTIR Analysis	107
4.5	Raman studies	109
4.6	Photoluminescence studies	110
4.7	D.C electrical conductivity studies	114
4.8	Thermo Gravimetric Analysis	118
4.9	Mechanical strength measurements	120
4.10	Conclusions	122
	References	123

Chapter 5

Studies on PANI(HCl)-MWNT composites 127-146

5.1	Introduction	127
5.2	Synthesis of PANI and PANI-MWNT composites	128
5.3	TEM Analysis	128
5.4	SEM Analysis	130
5.5	X.R.D Analysis	131
5.6	Raman Analysis	132
5.7	FTIR Analysis	133
5.8	D.C electrical conductivity studies	135

5.9	Thermo electric power studies	139
5.10	T.G.A	142
5.11	Conclusions	143
	References	143

Chapter 6

Optical transition gap analysis in polymer films		147-164
6.1	Introduction	147
6.2	Synthesis of powder samples	149
6.3	Film preparation	149
6.4	Film thickness measurement	149
6.5	FTIR Analysis	149
6.6	Optical absorption studies	150
6.7	Conclusions	161
	References	162

Chapter 7

Photoacoustics: Theory and experiment		165-200
7.1	Introduction	165
7.2	History of photo acoustic effect	169
7.3	Photo induced processes	172
7.4	Detection methods	174
7.5	Photo acoustic effect in condensed media	177
7.6	Rosencwaig-Gersho theory	178
7.7	Open Photo Acoustic Cell configuration	185
7.8	Thermal diffusivity measurements on PANI (HCl) and PANI (HCl)-MWNT composites	189
7.9	Experimental set up	190
7.10	Experimental procedure	192
7.11	Analysis of thermal diffusivity results	193
7.12	Conclusions	197
	References	197

Chapter 8

Summary and future prospects 201-210

8.1	Towards conducting polymers	201
8.2	Missing links	202
8.3	Focus of the present work	202
8.4	Summary of the work done	203
8.5	Scope for further work	210

.....*EOB*.....

Chapter 1

INTRODUCTION

<i>C o n t e n t s</i>	1.1 About polymers
	1.2 Glass transition temperature
	1.3 What are Conducting Polymers?
	1.4 Progress in conducting polymer research
	1.5 Synthesis
	1.6 Gelation of PANI
	1.7 PANI fibers
	1.8 Advances in solution processing of PANI
	1.9 Some important conducting polymers
	1.10 Conducting polymer composites
	1.11 Important applications of conducting polymers
	1.12 Objectives of the present work

1.1 About polymers

Polymers are everywhere! From tooth brushes to computers, from polythene bags to automobiles, polymers have conquered our day to day life.

A polymer is a material whose molecules contain a very large number of atoms linked by covalent bonds, which makes it a macromolecule. The fundamental repeat unit in a polymer is known as a 'monomer'. A large number of such identical units link together to form a polymer chain. The structure of the polymer depends on the

way in which monomer units are linked. There can be linear structures, cross linked structures and ladder like structures. By branched polymer, we refer to the presence of additional polymeric chains issuing from the backbone of a linear molecule. Substituent groups such as methyl or phenyl groups on the repeat units are not considered branches. Branching is generally introduced by intentionally adding some monomers with the capability of serving as a branch. Polymers are of two types-natural polymers and synthetic polymers or plastics. Natural polymers include proteins, cellulose (plants), starch (food) and natural rubber. Nowadays, the use of synthetic polymers is shooting up in a fast pace. The technologically important polymers have the added advantage of easy manufacturability, recyclability, excellent mechanical properties, light weight and low cost compared to alloys and ceramics. Also the macromolecular structure of synthetic polymers allows them to perform many tasks that cannot be performed by other synthetic materials, which include drug delivery, use of grafts for arteries and veins and use in artificial tendons, ligaments and joints.

Polymerisation reactions can be classified into two major groups on the basis of the mechanisms of growth reactions [1-3]. One is step-growth polymerization and the other chain growth polymerization [4]. In step growth polymerization, a polymer is formed by the stepwise repetition of the same reaction over and over again. Here two polyfunctional molecules condense together to produce a larger molecule by eliminating small molecules like water. In step growth

polymerization, each growth step is a chemical reaction between two **molecules**. In chain growth polymerization, a long chain molecule is **formed** by a series of consecutive steps that is completed in a very short **time**. Unlike in the case of step growth polymerization, intermediate **size** molecules cannot be isolated here and the products are final **polymers**. In chain growth polymerization, each individual growth step is a chemical reaction between a chain carrying species and a molecule. In these reactions, the chain is carried by an ion or a free radical. Free radical is a reactive substance with an unpaired electron formed by the decomposition of an unstable molecule called initiator. The chain **growth** is started by initiators, which initially undergo decomposition to form radicals. Free radical polymerization is perhaps the most widely studied reaction among chain growth polymerization mechanisms. Here there are three steps-initiation, propagation and termination. Initiation means the formation of initiator radical by the decomposition of the initiator. The initiator radical then acts on the monomer forming monomer radicals. The first monomer radical reacts with a monomer molecule to form a dimer radical. The dimer radical then reacts with a monomer molecule to produce a trimer radical and the process propagates.

1.2 Glass transition temperature

Glass transition temperature is the temperature below which a polymer is hard and above which it is soft[5]. The hard, brittle state is known as the glassy state and the soft, flexible state as the rubbery or viscoelastic state. On further heating, the polymer becomes a highly

viscous fluid and starts flowing. This state is termed the viscofluid state and the transition takes place at its flow temperature T_f .

1.3 What are Conducting Polymers?

Conducting polymers belong to a special class of polymers in which electrical conductivity can be tuned from insulating to metallic through proper doping [6-7]. They have a conjugated structure with alternate σ and Π bonds. The Π bonds are delocalized throughout the entire polymer network. This results in enhanced electrical conductivity. Examples for conducting polymers include polyaniline, polypyrrole, polythiophene, polyacetylene etc.

1.4 Progress in conducting polymer research

The initial impetus for conducting polymer research is the finding that the inorganic polymer, polysulphur nitride shows metallic behaviour when doped with halogens and below 0.3K, it exhibits superconductivity. In 1976-77, it was observed that the room temperature electrical conductivity of polysulphur nitride could be increased to several orders of magnitude upon exposure to bromine and similar oxidizing agents. But the explosive nature of the material limited its applications [8].

Polyacetylene is an intrinsically insulating organic polymer. It has an intrinsic conductivity much lower than 10^{-5} S/cm. But on exposure to iodine, the electrical conductivity shoots up to 10^3 S/cm [9-11]. Subsequent research in similar conducting polymers has revealed that the conductivity of conjugated polymers could be

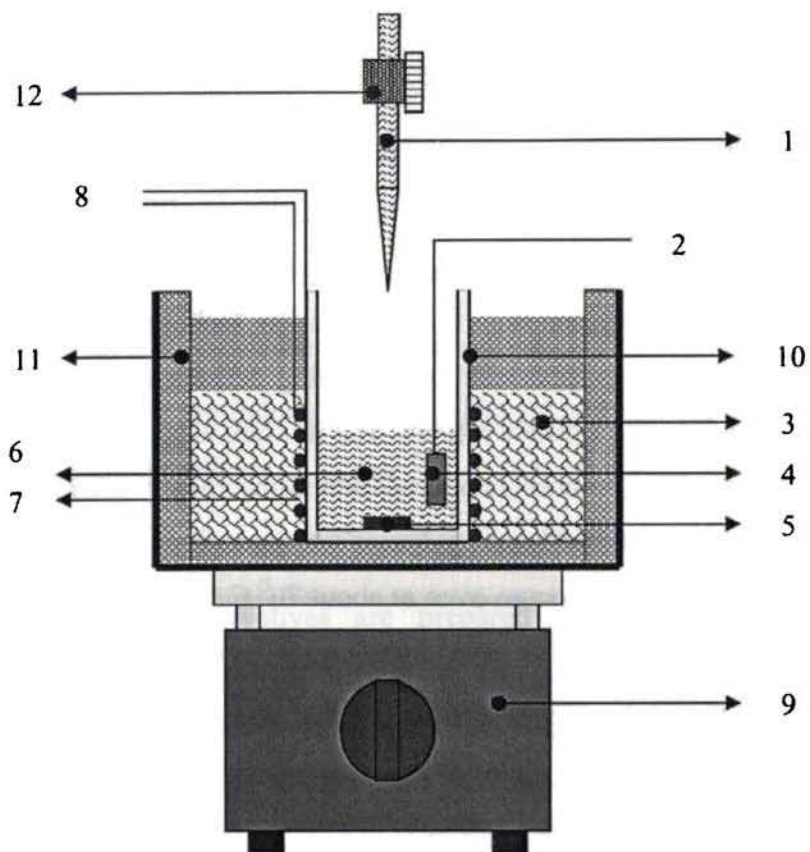
increased by several orders of magnitude upon doping with suitable dopants. Prof. Alan.J. Heeger, Prof. Alan. G. Macdiarmid and Prof. Hideki Shirakawa were awarded the nobel prize in the year 2000 for their pioneering contributions to the field of conducting polymers. Thereafter a host of research groups all over the world initiated research in conducting polymers which significantly contributed for the development of newer fields like organic and molecular electronics, polymer optoelectronics, polymer nanophotonics etc.

Inspite of the impressive progress in improving the electrical conductivity and achieving truly metallic behaviour in polymers, a proper understanding of the origin of metallic transport is still limited by the disordered structure of conducting polymers [9, 12-17]. The band structure of metallic conducting polymers is characterized by a continuous density of states with a well defined Fermi energy. The existence of Pauli spin susceptibility, a quasilinear temperature dependence of thermopower and a linear term in the specific heat provide ample evidence for this structure. However the real finger prints of metallic behaviour such as finite d.c electrical conductivity as $T \rightarrow 0$, a positive temperature co-efficient of resistivity and metal like reflectivity in the infrared are missing [9,18-25]. Recent years have envisaged the development of improved synthesis and processing routes for the preparation of more ordered and homogeneous samples, both in bulk and thin film forms [17,26-27]. The counter ion induced processibility of polyaniline[28] using dopants such as Camphor Sulphonic Acid (CSA), Dodecyl Benzene Sulphonic

Acid(DBSA) and Napthalene Sulphonic Acid(NSA) has resulted in enhanced conductivities and a weaker temperature dependence of conductivity[8-9]. This group of doped conducting polymers exhibit a significant positive Temperature Co-efficient of Resistance (TCR) in the temperature range 160-300K [8-9,29-31]. Recently polyaniline samples prepared using self-stabilised dispersion polymerization [32], are found to have room temperature conductivities in excess of 1000S/cm with a monotonic decrease in conductivity from room temperature to 5K[17]. However a lot of work is still left to be done in improving the microscopic and macroscopic order in these polymers.

1.5 Synthesis

Chemical oxidative polymerization [33] is a common method employed to synthesise conducting polymers in bulk form. Here the monomer is dissolved in the dopant acid solution .The oxidant dissolved in appropriate solvent (water is the commonly used solvent) is added dropwise to the mixture with continuous stirring for 4-5 hours. The precipitate obtained is filtered, washed and dried. This is one of the easiest methods adopted for synthesizing conducting polymers in bulk form and is used to prepare conducting polymers such as polyaniline, polypyrrole etc.



- | | |
|-------------------------------|---|
| 1. Oxidant for polymerization | 2. Connection to temperature controller |
| 3. Freezing mixture | 4. Temperature sensor |
| 5. Magnetic fish | 6. Reaction mixture |
| 7. Heater coil | 8. Connections for heater coil |
| 9. Magnetic Stirrer | 10. Glass beaker |
| 11. Insulating wall | 12. Burette |

Fig. 1.1 Custom made polymerization set up

For the synthesis of conducting polymers such as polyacetylene, more complicated methods such as catalytic polymerization, non catalytic

polymerisation, isomerization, Durham method, dehydrochlorination and dehydration are used [9].

A variety of techniques can be employed to get conducting polymers in thin film form. Solution casting, spin coating, plasma polymerization and electro chemical polymerization are some of the commonly used polymer thin film deposition techniques [9,34-37]. Solution cast films are prepared by dissolving definite amounts of the polymer in a selected suitable solvent. The mixture is stirred for several hours. The resulting solution is poured onto ultrasonically cleaned glass plates and spread uniformly using doctor's blade technique. The film is left to dry in a hot air/vacuum oven at about 70⁰ C for one or two days. Commonly used solvents are meta-cresol (m-cresol), N-Methyl Pyrrolidinone (NMP), Para-cresol (p-cresol), Cyclohexanol and Xylene [9,36-37]. Metacresol is preferred over the rest because of its better solvation properties. Also the polymer-solvent interactions are greater for the m-cresol solution compared to others[9,38]. Still the solubility of conducting polymers in organic solvents remains a lot to be improved, the main reason being the rigid polymer back bone. The Π conjugation imparts stiffness to the polymer back bone which makes the polymer intractable. The Π electron delocalization leads to large electronic polarizability, giving rise to Π - Π interchain attraction. This favours polymer aggregation rather than solvation. Also the rigidity of the polymer back bone thus formed creates an unfavourable entropy for solution. The polymer chains complexed with ionic dopants also contain hydrophobic organic segments. It is very difficult to find

solvents capable of solvating both hydrophilic and hydrophobic segments [9].

Several strategies are employed to overcome this problem [9]. Some of these are [39-41],

- a) Preparation of colloidal dispersions and coated latexes.
- b) Preparation of substituted derivatives
- c) Counter ion induced processibility of polyaniline (PANI) and similar methods

The last two methods are commonly employed nowadays.

Substituted derivatives are prepared by adding solubilizing substituents to the monomer unit of the polymer back bone. The addition of solubilizing substituents creates steric consequences, reducing the ability of the polymer to form delocalized Π electron density over the chain. Some of the examples are listed below.

- a) Phenyl substituted polyphenylene is soluble in chloroform.
- b) Polypyrrole derivatives containing alkyl or alkoxy substituents at either N-,3, or 4 positions are soluble in several common organic solvents such as chloroform, tetrahydrofuran (THF), and ortho dichlorobenzene.

However these substituents induce steric repulsion which distorts the planarity of the polymer. This puts a limit to the extent of Π electron overlap and thereby reduces the electrical conductivity. All the

more, many of the solutions of these substituted polymers are unstable and precipitation occurs after some time. Derivatized polythiophenes form an exemption in this regard [42-46]. Adding substituents on the polythiophene chain has only a minor effect on chain planarity. Alkyl substituted thiophenes have good mechanical and electrical properties in film and fiber forms. The major hurdle in this regard is the tedious synthesis procedure of modified monomers and limited solubility of the doped polythiophene derivatives[9].

Another method involves the inclusion of solubilizing monomeric structures along a modified chain[47]. Though this method increases the solubility to certain extent, it adversely affects the conductivity, because charge transport along the chain gets hindered. The morphology and crystallinity of the polymer may also be adversely affected by this process[9].

The precursor polymer approach is another recently explored method for synthesizing soluble conducting polymers. The steps adopted in this method are outlined below[47].

- a) A precursor polymer is prepared.
- b) It is converted to the form of the desired end product.
- c) Finally it is transformed into dopable Intrinsically Conducting Polymer (ICP), usually by the application of heat.

Most of the precursor polymers used in this approach have a polyelectrolyte structure, which is highly water soluble. Usually films

and fibers can be prepared from the precursor polymer by spin casting or wet spinning respectively. The films and fibers thus formed are thermally converted into the final undoped ICP.

Synthesis of undoped poly (p-phenylenevinylenes) (PPVs) is outlined here as an example[9,48].The PPV precursor polymer is converted to the undoped PPV by heating at temperatures above 200⁰C.Sulphor compounds and acid gases are eliminated by this process. The converted PPV is then doped with solutions of acids and oxidizing agents to attain conductivities of the order of 100S/cm.

This method has its own advantages as well as disadvantages. The main advantage is that good orientation can be achieved before doping using the existing fiber drawing methods. The disadvantages include the difficulty in the synthesis of precursor polymers and the high cost of large scale production.

Another frequently employed technique to synthesise soluble conducting polymers is the copolymerization technique. The additional advantage offered by this method is that it is possible to blend the distinct advantages of various polymers in one system[49-51].For example, this technique is largely employed to impart dyeability to nonreactive fiber forming polymers such as acrylics[9].Here the polymer is copolymerized with monomeric groups that form anionic moieties at the proper pH. The so formed product can be readily dyed with cationic dyes.

Generally there are four different methods for copolymerization [9].

- a) Insitu polymerization of both monomers to form a random copolymer
- b) Grafting of the solubilizing polymer onto the backbone of the insoluble polymer
- c) Grafting of the insoluble polymer onto the backbone of the soluble polymer
- d) Combination of both soluble and insoluble polymers to form a block copolymer by various synthetic methods
- e) Insitu polymerization of an insoluble polymer onto the matrix of a soluble polymer.

Examples include composites of polyaniline and polypyrrole formed by in situ polymerization in matrices such as poly (vinyl chloride) (PVC), polyvinylalcohol (PVA), poly (vinylidenechloride-co-trifluoroethylene) and brominated poly (vinyl carbazole) [37,50].

- f) Counterion-induced processibility of conducting polyaniline (PANI)

Cao et al [28] have reported that the processibility of highly conducting PANI with reasonably high molecular weight could be improved by using functionalized protonic acids. The functionalized protonic acid has the form $H^+(M-R)$. $(M-R)$ is the counterion anionic species. R is the functional group chosen to be soluble in nonpolar or weakly polar organic solvents. Dodecyl benzene sulfonic acid (DBSA) and

camphor sulphonic acid(CSA) are examples for functionalized protonic acids. The long alkyl chains of the functional group make PANI soluble in common organic solvents such as m-cresol, toluene, xylene and chloroform. It is the anionic part (SO_3) of the molecule that dopes PANI[9].The soluble PANI thus formed can also be blended with other nonconductive polymers soluble in the same solvent so as to tailor the properties of the composite polymer. Menon etal[16] have observed positive temperature co-efficient of resistance in CSA doped PANI in the range 150-300K.

1.6 Gelation of PANI

Macdiarmid etal [52] have discovered in 1989, that the solutions of polyaniline Emeraldine Base(PANI(EB)) in NMP gelled after some time. The gelation is due to the interactions or cross-linking between the micro-crystalline areas of PANI[9].

There are mainly two types of gelation. One is the gelation caused by primary valence linkages in a polyfunctional system. Due to the primary bond formation between the polymer chains, the polymer structure gets immobilized. For example, polyethylenes are chemically cross-linked by radiation or chemical agents such as peroxides. This type of gelation is irreversible[9,53].The other type arises from physical cross-links resulting from secondary bonding forces such as hydrogen bond formation, van der waals forces, or other types of interactions that do not involve primary valence bond formation[9,53]. Gelation of this kind is called thixotropic gelation and such gels are called thixotropic

gels. In thixotropic gels, polymer-polymer interactions are greater than polymer-solvent interactions. Thixotropic gels can be broken to a certain extent by simple stirring. But a thixotropic gel, once redissolved will re-form upon sitting. Another method to break a thixotropic gel is to add a suitable second solvent. Hsu et al [54] reported that gels of PANI (EB) in NMP could be redissolved by exposing to gaseous ammonia. The gels can either be doped in the gel form itself and then cast into a film or it can be first cast into a film and then doped [9].

1.7 PANI fibers

PANI could also be processed in the form of fibers. A polymer can be considered as spinnable, if it is capable of assuming large irreversible deformations on applying uniaxial stress [9]. But all spinnable fluids do not form fibers. Examples include honey and highly viscous mineral oils. The spinning solution (spin dope) should have considerable molecular weight also in addition to being spinnable. The spin dope must be capable of forming some type of chain-chain interactions such as hydrogen bonding, dispersion interactions, mechanical entanglement of the polymer chains, or some combination of these or other mechanisms.

Generally fiber spinning is of two types-melt spinning and solution spinning [9]. In melt spinning, the polymer softens and interchain interactions are minimized upon heating. Thus deformation of the polymer is facilitated without deterioration of the chains. Such materials are referred to as thermoplastics. The fiber forming material is spun through a device called spinnerette. Spinnerette is a highly

engineered metal or ceramic plate with several small diameter holes. The cross sectional shape of the holes determines the fiber cross sectional type. The fluid is delivered into the spinnerette by a metering device called the gear pump. Additionally there is a long metallic rotating screw held in an extruder barrel. Its purpose is to transport the polymer through several heating, melting and mixing zones. Finally the metallic screw is interfaced with the gear pump and subsequently with the spinnerette. Solution spinning consists of the following steps. At first the polymer is dissolved in a suitable solvent. The resulting solution is spun into a coagulating solvent bath in which the original polymer is not soluble. The resulting mixture is pumped to the spinnerette and into a coagulation bath.

In both the cases, knowledge of the rheology of the spinning fluid during the spinning process is essential for forming fiber with reproducibly uniform mechanical and electrical properties. For this constitutive equations are developed that describe the mass balance and momentum of the fluid during the spinning process. In solution spinning, the thermodynamics of the coagulation bath and the kinetics of diffusion of the solvent into and out of the forming fiber must be considered

Angelopoulos et al. [55] have reported that N-methylpyrrolidinone (NMP) could dissolve PANI (EB). But solutions of PANI (EB) in NMP above 6% concentration get gelled after some time [56-58]. Unfortunately solutions of at least 6% concentration are necessary for fiber spinning. This limits the usability of NMP as a solvent for PANI.

Hsu et al [54] have discovered that adding certain amines to the polymer solution prevents gelation. They have found out that PANI/1, 4-diaminocyclohexane is a stable spin dope and good quality fibers can be extruded by continuous dry jet spinning. The thus formed fiber could then be drawn at 215^oC.

The spin dope for these films is prepared by adding gaseous ammonia or pyrrolidinone to the NMP solutions of PANI (EB) in required concentrations. The fibers prepared from derivatized PANI and poly (o-toluidine) show much higher electrical conductivity and weaker temperature dependence than similarly prepared HCl doped PANI powders and films.

1.8 Advances in solution processing of PANI

Some research groups have successfully developed a technique to process PANI in its conducting form [28,54,59-60]. This method removes subsequent doping steps, thus reducing cost and speeding production. Work along these lines has resulted in counterion processible PANI and other conductive fiber and film processing methods [54,59]. Efforts to improve the mechanical properties of PANI(EB) by elucidating the structure of the polymer in thermodynamically stable solvents are also in progress. To achieve good solubility, polymer-solvent interactions have to be increased as compared to polymer-polymer interactions. If the polymer is relaxed in solution, the probability of chain entanglement for the purpose of developing fiber and film strength, on extrusion is enhanced. This entanglement should remain after doping to produce conductive fiber or

film with reasonable mechanical properties [61-62]. The chain entanglement enhances the electronic transport between the polymer chains, giving better segment to segment electrical reproducibility. This is achieved by investigating the rheology of polymer-solvent interactions in various solvent systems and spin dopes. The stability of the solution is necessary to produce fibers and films with segment to segment reproducible mechanical and electrical properties on extrusion. Shacklette and Ilan [63] have pointed out that the solubility of PANI(EB) could be understood employing standard solubility parameters that measure the likelihood of a solvent and a polymer engaging in dispersive, polar or hydrogen bonding. Such forces are called secondary bonding forces. They are responsible for holding the polymer chains together to provide strength, as in the case of nylons, or as the interactive forces between solvent and polymer for the purpose of solvation. These researchers have found out that the doped PANI compositions are more polar and hydrogen bonding than PANI (EB). The strong possibility for hydrogen bonding in doped PANI systems is responsible for PANI self associating in solution and phase separating from its host or solvent, forming micro dispersions[9]. Cao et al [64] have reported that fully protonated PANI can be dissolved in organic solvents only when PANI-(acid)_{0.5} complex is solvated by at least an additional 0.5 mole of solvating agent per PANI repeat unit. In the case of solvents with strong hydrogen bond interactions, this solvating agent can be the solvent itself. With the proper choice of solvent and cosolvent, the resultant electrical conductivity of films cast from solution could be much higher or lower than that of the initial

PANI powder. Metallic transport over the whole range of temperatures below room temperature has been reported in dispersion polymerized PANI [17] where PANI is prepared by self-stabilized dispersion polymerization (SSDP). In contrast to conventional homogeneous/dispersion polymerization using an aqueous medium containing aniline, acid and oxidant, this new polymerization is carried out in a heterogeneous biphasic (organic and aqueous) mixture without any stabilizers. Aniline dissolved in acid solution is like a surfactant, with a polar hydrophilic part and an organic hydrophobic part. The monomers and growing polymer chains act as interfacial stabilizers, resulting in excellent dispersion of the organic phase inside the aqueous reaction medium. The aniline monomers and grown PANI chains are separated from the reactive ends of the chain in the aqueous phase by the organic phase and thereby the undesirable side reactions are suppressed. The reaction mixture is filtered, washed and deprotonated to the emeraldine base (EB) form, and then dried. Thus high quality PANI (EB) samples with low density of structural defects can be produced. The resulting PANI (EB) powder, doped with Camphor Sulphonic Acid (CSA) can be cast into free-standing films from solution in meta-cresol. The highest conducting samples synthesized by this method has recorded a room temperature D.C electrical conductivity value of around 1300S/cm with a positive temperature co-efficient of resistance from 300K to 5K. The exciting results obtained may be due to the improved molecular structure of the samples, as revealed from the X-ray Diffraction(XRD) studies.

1.9 Some important conducting polymers

The structures of certain widely studied conducting polymers are given below.

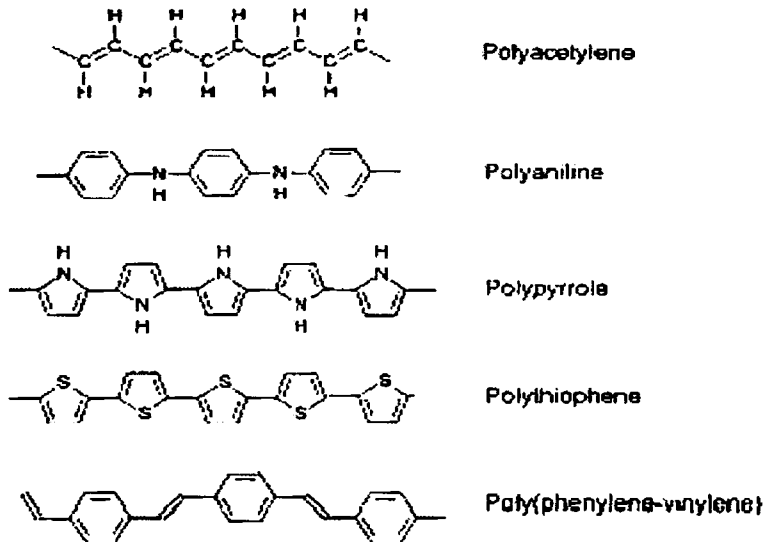


Fig. 1.2 Chemical formulae of some important conducting polymers

As mentioned earlier, the electrical conductivity of polyacetylene can be increased by several orders of magnitude upon doping. But it is highly susceptible to atmospheric oxidation which limits its applications. The electrical conductivity of polyaniline as well as polypyrrole can be tuned from the insulating to the metallic region upon suitable doping. These two conducting polymers, especially polypyrrole exhibits high electro magnetic shielding (EMI shielding) properties. Polythiophene and poly (phenylene-vinylene) are more known for their photoluminescent as well as electroluminescent properties[9].

1.10 Conducting polymer composites

Despite having many attractive properties such as good electrical conductivity and environmental stability, conducting polymers suffer from many limitations. For example some of the conducting polymers have poor mechanical strength and thermal stability. Preparing conducting polymer composites is a clever way to overcome these drawbacks and tailor the properties of these systems to our desired levels. In conducting polymer composites, properties of the host polymer are beautifully blended with those of the guest. Polyaniline (PANI)-polyvinylchloride (PVC), PANI- polymethylmethacrylate (PMMA) and polypyrrole (PPY)-PMMA are some of the examples for polymer composites.

1.11 Important applications of conducting polymers

1.11.1 Optoelectronic applications

Electroluminescence is the generation of light by electrical excitation. This phenomenon has been reported in a wide range of semiconductors. The process of electroluminescence consists of the following steps-injection of electrons and holes from respective electrodes, the capture of one by the other and the radiative decay of the excited state(exciton) produced by this recombination process. An exciton is a bound electron-hole pair. Excitons are classified into three major types-tightly bound excitons (Frenkel excitons), weakly bound excitons (Mott and Wanier excitons) and intermediate excitons (charge transfer excitons)[9]. Tightly bound excitons are localized over one molecular unit. while Mott and Wanier excitons are delocalized over

several molecular units. Tight binding excitons or Frenkel excitons are characterized using tight binding approximation. The basis set of wave functions have their excited states localized on different molecular units. The nearest neighbour interactions lead to the overlap of wavefunctions and the formation of exciton bands. Charge transfer excitons are delocalized over adjacent molecular units. Electron-phonon interactions reduce the coherence in excitons. Now it is more convenient to think of it as a localized state which moves by hopping between different sites. Disorder in site energies is the major cause for losing coherence. Hopping is caused by either tunneling or foster transfer. Foster transfer occurs by near field dipole-dipole interactions without wavefunction overlap. Foster transfer is mainly operative in singlet excitons with a strong dipole matrix element to the ground state as in PPV. In contrast, foster transfer is ineffective in triplet excitons. They hop by tunneling. In molecular crystals such as anthracene with high effective mass and low permittivity, Mott and Wanier theory does not apply. But in polymers, effective mass is low so as to allow mobility along polymer chains. Taking into account the electron-electron interactions, the inference is that singlet excitons are more delocalized than triplet excitons. Triplet excitons are confined over only a few molecular units due to the negative value of exchange interaction. Studies on PPV imply that triplet exciton in PPV lie 0.65eV below the singlet level. The exciton can move along the polymer chain to minimize the energy without interchain crossing. But this is valid only for conjugated polymers with low Π - Π^* band gap. For polymers with higher band gap, interchain crossing of excitons leads to the

formation of extended excited states which would be described as charge transfer excitons within the frame work of molecular semiconductors. Excimers are excitons extending over identical molecular units. Exciplexes are excitons extending over two or more different molecular units.

Organic thin film electroluminescence started to flourish since the early 1970s. Electroluminescence from conjugated polymers was first reported using poly (p-phenylenevinylene) (PPV) as the single semiconductor layer between organic electrodes [65]. The Π - Π^* energy gap of PPV is about 2.5eV. It produces luminescence in a band below this energy. The major drawback of PPV is that it is an intractable material with a rigid rod microcrystalline structure. So it is infusible and insoluble in common solvents. But PPV can be synthesized conveniently by in situ chemical conversion of films of a suitable precursor polymer that itself is processed from solution by spin coating [9]. Most frequently used derivative of PPV is poly(2-methoxy-5-(2 ethyl) hexyloxy-p-phenylenevinylene) (MEH-PPV).

In a polymer LED, positive and negative charge carriers are injected from opposite electrodes. These oppositely charged carriers combine within the polymer layer, resulting in the formation of a singlet exciton. The singlet exciton thus formed decays radiatively to the ground state resulting in light emission [9].

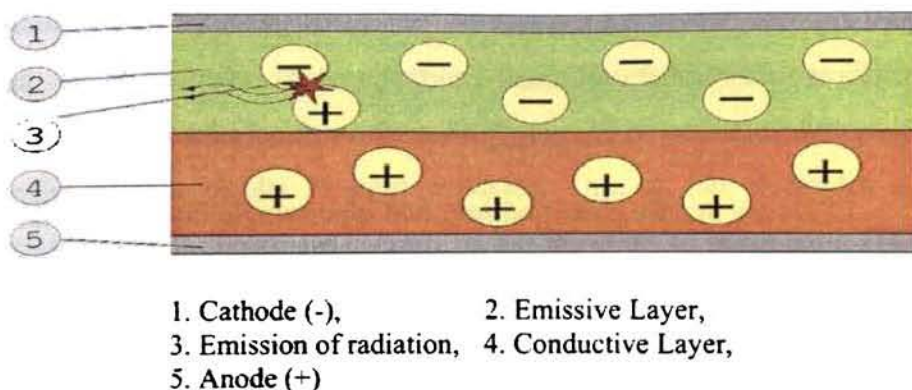


Fig. 1.3 Schematic diagram of an organic polymer LED

During the initial stages, the efficiencies of LEDs based on PPV, fabricated with negative aluminium electrodes were very low. But the internal and external quantum efficiencies have risen sharply over the past few years owing to improved understanding of the operation of these devices and optimization of the device characteristics.

The existence of metallic conductivity in doped conjugated polymers and the non-similarity of electrical and optical properties with traditional metals imply that the exciton formation mechanism in conjugated polymers is completely different. In conjugated polymers, bonding is anisotropic. So an electronic excitation can be accommodated with a local arrangement of polymer bonds without any strain in a direction perpendicular to the chains. This leads to polaron formation in conjugated polymers. Charged excitations between the ground states of two non-degenerate structures is called polarons or bipolarons (doubly charged polarons are called bipolarons (bp^{2-}/bp^{2+})) and their formation is accompanied by a local rearrangement of chain

geometry. The wave like excitations between degenerate ground state structures are called solitons. In conjugated polymers such as polyacetylene, transport of energy occurs through solitons.

LEDs are mainly classified into two types-single layer LEDs and heterolayer LEDs.

Single layer LEDs

The major components of a single layer LED are,

- a) Electron injecting electrode
- b) Hole injecting electrode
- c) Intermediate polymer layer

Consider for example, a ITO/PPV/Al LED. Here ITO is the hole injecting electrode and aluminium is the electron injecting electrode. The schematic diagram for the device is given below.

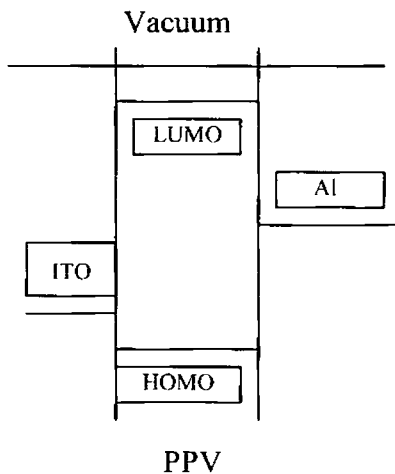


Fig. 1.4 Schematic diagram for an ITO/PPV/Al LED

Here holes are injected into the valence band of PPV from ITO and electrons into its conduction band from aluminium. Their recombination takes place in the PPV layer. The radiative decay of singlet exciton results in light emission. One of the electrodes is semitransparent. There are barriers to the injection of holes from ITO and electrons from aluminium. Considering the ionization potential and electron affinity of PPV, it is inferred that barrier to injection of electrons is greater than barrier to injection of holes. The internal quantum efficiency of the device(η) is defined as the ratio of number of photons produced within the device to the number of electrons flowing in the external circuit. It is given by,

$$\eta = \gamma r q$$

where γ is the ratio of exciton formation events in the device to the number of electrons flowing in the external circuit, r the fraction of singlet excitons and q the efficiency of radiative decay of singlet excitons

To get good internal quantum efficiency, the following conditions must be satisfied.

- a) Electron and hole currents must be balanced
- b) There must be sufficient capture of electrons and holes within the emissive layer
- c) Efficient radiative decay of singlet excitons should take place.

Electroluminescence spectrum of PPV LED is similar to that of its photoluminescence spectrum, implying that singlet excitons are responsible for both the processes.

Several models have been proposed for studying the charge injection and transport in single layer devices. The important among them are the Marks model [66], Parker model [67] and Schottky barrier model [68-69]. The major assumptions of the Marks model are,

- a) At lower voltages, I-V characteristics show a power law dependence due to space charge limited current with significant trapping.
- b) The effective mobilities obtained are very low, indicating the presence of current due to low mobile carriers.
- c) At higher voltages, current is predominantly an interface limited hole current.
- d) The injection mechanism proved difficult to fit with simple models and it is tentatively proposed that the current is limited by thermionic emission through an interfacial barrier.

Parker has studied the characteristics of MEH PPV LED. He chose electrode materials to give currents that are almost entirely due to holes or almost entirely due to electrons. At high fields, he obtained good fits to Fowler-Nordheim theory for tunneling through a triangular barrier with barrier heights in reasonable agreement with the values predicted by electrode work functions. He proposed that there are no space charge limited currents and the width of the schottky barrier is

less than the width of the device. But the observed values of currents are found to be reasonably lower than that predicted by theory. Also Parker model fails to give evidence for the prepondence of triangular barrier over schottky barrier.

Reiss etal have proposed schottky barrier model for ITO/PPV/Al device. In this model, currents are assumed to be predominantly due to holes. Hole currents are limited more by PPV/Al interface than by ITO/PPV interface. They model the current-voltage characteristics using the equation for thermionic emission across a schottky barrier from a semiconductor into a metal. Doping levels estimated for these devices are considerably higher than those estimated by Marks etal. But none of these models is universally accepted. Each has its own merits and demerits.

Heterolayer LEDs

Electron and hole flow can be optimized by forming heterojunctions between the semiconducting layers.

An example is an ITO/PPV/CN-PPV/Al device. PPV is processed from a standard precursor polymer onto ITO on a glass substrate. Cyano PPV (CN-PPV) is spin cast on the top of it. Top electrodes are coated using thermal evaporation. Basic scheme for the device is given below.

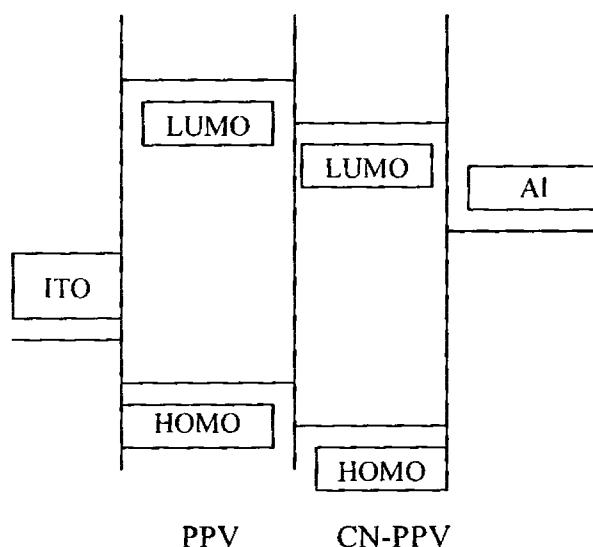


Fig. 1.5 Schematic diagram of a ITO/PPV/CN-PPV/Al LED

Holes injected into the homo of the PPV from ITO are trapped at the heterojunction due to potential step between the homo of PPV and CN-PPV. Electrons injected from the top electrode to the LUMO of CN-PPV have to surmount the potential step to cross to the LUMO of PPV. It is desirable to use high work function metals such as aluminium or gold in place of calcium for efficient electron injection into the LUMO of CN-PPV. Electron-hole combination takes place at the heterojunction and subsequent radiative decay of the singlet excitons gives rise to photo luminescence. Reported internal and external quantum efficiencies of the device are high. It is also observed that current density as well as luminescence intensity increases with voltage.

1.11.2 Conducting polymers in microelectronics

The electrical conductivity of the conducting polymers can be suitably tuned by selecting proper dopants, varying the dopant concentration and synthesis temperature and by preparing polymer blends and composites. In addition, they offer light weight, processibility and flexibility. Possible microelectronic applications include manufacture of devices such as diodes and transistors, metallization, electrostatic discharge protection, electromagnetic shielding, corrosion protection of metals, interconnection technologies and lithography. Recently it has been discovered that water soluble polyanilines may be used as charge dissipators in Scanning Electron Microscopy (SEM) [70]. The use of conducting polymers in the future for IC fabrication and flat panel display manufacture is another exciting area. But higher mobilities and long term stability are required from the semiconducting conjugated polymers before they can compete with silicon based devices.

1.11.3 Gas and liquid separation applications of polyaniline membranes

Membrane based purification systems have wide range of applications such as separating oxygen and nitrogen from air, desalinating sea water, removing organics from waste streams, and separating pure ethanol from its azeotropic mixture with water. Polymer membrane purification systems have proved to be more energy efficient than standard industrial purification techniques. The distinct advantages of polymer membranes include their ease of synthesis and processibility. Polymers can be easily cast as flexible thin

sheets or high surface area hollow fibers that allow large fluxes of gases or liquids through the membranes. The large differences in the permeability of gases through doped and undoped polyaniline films have led to detailed investigations of polyaniline and other conjugated polymers for possible gas sensing applications. Redoping with small amounts of dopants can lead to very high selectivity for important pairs such as O_2/N_2 , H_2/N_2 and CO_2/CH_4 [9]. It is reported that polyaniline has the highest O_2/N_2 selectivity of any polymer membrane. The use of different protonic acids and the preparation of polymer blends provide scope for future developments in this field.

1.11.4 Chemical and biological sensors based on electrically conducting polymers

An electroconductive polymer plays a major role as a membrane component of a chemical and/or biological sensor device. It may be active or passive. When active it may serve as a catalytic layer, a redox mediator, an on/off switch, or a resistor with a resistance value that is modulated by a targeted chemical reaction [9].

1.11.5 Electrically conducting textiles

Textiles, in addition to their initial use as apparel, have been used in several early structural materials. Semiconducting textiles including yarns and woven, nonwoven and knitted fabrics, have been produced by impregnating textile substrates with conductive carbon or metal powders [9]. These products have wide spread applications in electromagnetic interference (EMI) shielding and static dissipation. However, the incorporation of carbon above 40% degrades the

mechanical properties in the polymer/filler blend and results in considerable processing problems in the production of textile fibers. Conducting polymers offer an interesting alternative to coated or filled plastics and textiles. However films and fibers of many conjugated polymers are brittle, expensive to produce, and difficult to manufacture on a large scale. Textiles of various kinds represent a reasonable choice as a substrate for thin coatings of such polymers. Conductive textile composites show surface resistances in the same range as metallised fabrics and carbon based blends. Moreover they show excellent adhesion and noncorrosive character as compared to metal coated fabrics.

1.11.6 Electro chemo mechanical devices

The basic principle behind the fabrication of electro chemo mechanical devices using conducting polymers is that the free volume of a conducting polymer increases during oxidation and decreases during reduction[71]. Contraction and expansion of gel fibers provide a means of converting chemical energy into mechanical energy, which can be used to develop artificial muscles and actuators. Artificial muscles are able to describe angular movements of greater than 360° , trailing several hundred times of their own weight. Flory [72] has proposed an equation of state for the equilibrium swelling of gels that consists of four terms-an elasticity term, a mixing entropy term, a polymer-solvent interaction term and a term for osmotic pressure due to free counterions. The other factors influencing the gel volume are temperature, the kind of solvent, the free ion concentration, the degree

of cross-linking, and the degree of dissociation of groups on polymer chains. Polyelectrolyte gels show a bending motion by shrinking in an electric field, but their response time is very slow. On the other hand, piezoelectric polymers exhibit fast and reversible charge polarization processes induced by high potentials. Response times obtained is very low (of the order of milliseconds). But their attained dimensional variations are lower than 0.3% in volume and 0.1% in length. In the case of electronically conducting polymers, small changes in potential (0.1-0.5V) produce length variations of about 30% with high reversibility. Their response times (3-50 s) are longer than in piezoelectric systems, but shorter than polyelectrolyte gels. However conjugated polymers can generate mechanical stresses of around 100MPa as electrochemomechanical devices, whereas polymer gels yield only 1MPa. But the current efficiency of conducting polymers in the production of mechanical work is only within the range 0.1-1%. Fabrication of artificial muscles using polypyrrole, polyaniline and poly (3-alkylthiophene)s have been reported by several research groups [73-75].

1.11.7 Conductive polymer/High temperature superconductor assemblies and devices

A doped polymer in intimate contact with a superconductor displays interesting electronic interactions, such as proximity effect. The initial work completed in the area of high T_c thin film devices deposited onto Si and GaAs surfaces has shown that these semiconductors are not chemically compatible with the cuprate materials. Although the use of metal oxide buffer layers and low

temperature processing has shown to inhibit somewhat this adverse reactivity between the semiconductor and cuprate materials, the search for new semiconductor materials that do not degrade the cuprate compounds is warranted. In this context, conductive polymer systems combined with high- T_c superconductor structures may be used for the construction of new types of superconductor circuits, sensors and devices. The major highlights of such types of structures are[9],

- a) They provide an excellent platform for the study of novel molecule-superconductor electron and energy transfer phenomenon.
- b) Chemical compatibility between polymer and superconductor components can be evaluated.
- c) The fabrication of conductive polymer/superconductor structures may lead to the development of new prototype devices and sensors in which the properties of the superconductor are controlled by the influence of the conductive polymer element.
- d) High T_c superconductors may be used to drive conductive polymer systems into the superconducting state at temperatures well above 100K.

1.11.8 Transparent conductive coatings

One of the limitations of intrinsically conducting polymers (ICPs) is their poor processibility. But significant advances in the area of solution processing over the last decade have led to the development of

transparent, highly conducting coatings and films[9]. The so prepared conductive coatings are suitable for a wide range of industrial applications-from electrostatic dissipation to electrochromic displays. The details regarding synthesis of processible polyaniline and its film preparation have already been given at the beginning of this chapter. Recently water soluble conducting polyanilines have been synthesized by oxidative polymerization of aniline complexed to a polymeric acid.

Some of the possible applications of conductive polymer films and coatings are given below.

- a) Antistatic coatings
- b) Absorption of radar frequencies
- c) Corrosion prevention
- d) EMI/RFI shielding
- e) Electrochromic displays
- f) Electrochemical actuators
- g) Lithographic resists
- h) Lightning protection
- i) Microelectronics
- j) Polymer electrolytes
- k) Photovoltaics
- l) Rechargeable batteries
- m) Smart windows
- n) Solar cells
- o) Sensors-pressure, temperature, chemical and biological

Applications such as electrochromic windows, displays, sensors and electromechanical tools are unique to conducting polymers. For example, electrochromic devices and smart windows use the colour change from doped to dedoped polymer. Electromechanical tools, on the other hand use the dimensional changes.

1.12 Objectives of the present work

The samples chosen for the present study include PANI doped with three different acids-hydrochloric acid (HCl), orthophosphoric acid (H₃PO₄), camphorsulphonic acid (CSA)), PANI-polymethylmethacrylate (PMMA) composites, PANI-Multiwalled carbon nanotube (MWNT) composites, doped PANI nano rods, all in bulk forms and solution cast films of PANI(EB), PANI(HCl) and PANI (HCl)-MWNT composite.

PANI is well known for its ease of synthesis, environmental stability and excellent electrical and optical properties [53]. Though there are extensive reported work on the electrical properties and sensor applications of this polymer, much attention has not been given to its photoluminescent properties. One of the objectives of the present work is to carry out a systematic investigation on the photoluminescent properties of PANI doped with different acids and the composites of PANI with PMMA. Attempts have also been made to correlate the electrical properties of PANI doped with acids such as HCl, CSA and H₃PO₄ with the structural aspects of the polymer.

Recently nanostructured polymers are extensively investigated owing to their tunable electrical and optical properties [25-26]. The

present work also includes investigations on the structural, electrical and thermal properties of HCl doped polyaniline nano rods synthesized by chemical oxidative polymerization technique.

PMMA is a highly transparent material with excellent mechanical strength [49]. In the present work, the motivation for synthesizing PANI-PMMA composites is to blend these remarkable properties of PMMA with the excellent electrical transport properties of PANI. The Photoluminescence (P.L) investigations are also carried out on PANI-PMMA composites with various aniline to PMMA feed ratios. PANI-PMMA composites are found to exhibit high P.L emission. Moreover, most of the photoluminescent polymers are highly electroluminescent also [76].

PANI-MWNT composites are widely explored nowadays [77-79], thanks to their excellent electrical and thermal properties. However detailed investigations on the temperature variation of D.C electrical conductivity of these composites, especially in the high temperature region is quite scarce. Also the nature of interaction between PANI and MWNT is still controversial. In the present work, attempts have been made to carry out a systematic study on the temperature variation of D.C electrical conductivity of these composites with special emphasis on this interaction.

In addition to these investigations, part of the present work is devoted to studies on polyaniline films. Extensive work has already been carried out in highly conducting doped PANI films, unraveling the

mechanisms of electrical transport properties and highlighting the application oriented optoelectronic properties. However the nature and origin of various optical transitions in films of PANI and its composites is not extensively investigated. An indepth investigation on the “how and why” of different optical transitions in PANI films has hence been initiated in the present study.

References

- [1] F W Billmayer Jr, Text Book of Polymer Science, John Wiley & Sons, New York,1970
- [2] D B V Parker, Polymer Chemistry, Applied Science Publishers Ltd,London,1974
- [3] David J William, Polymer Science and Engineering, Prentice-Hall, New Jersey,1971
- [4] H Yasuda, Plasma Polymerisation, Academic press,Orlando,1985
- [5] David I Bower, An introduction to polymer physics, Cambridge University Press,Cambridge,2002
- [6] Bernhard Wessling, Chemical innovation31(2001)34
- [7] Sajan D George, S Saravanan, M R Anantharaman, S Venkatachalam, P Radhakrishnan, V P N Nampoore,C P G Vallabhan, Phys. RevB69 (2004) 235201
- [8] A B Kaiser,Rep.prog.Phys.64(2001)1
- [9] Terje A Skotheim, L Ronald, Elsenbaumer, John R Reynolds, Handbook of Conducting Polymers, Marcel Dekker, INC, New York,1998
- [10] C K Chiang, C R Fincher, Y W Park, A J Heeger, H Shirakawa, E J Louis, S C Gua, A G Mac Diarmid, Phys.Rev.Lett.39 (1977)1098

- [11] C K Chiang, M A Druy, S C Gua, A J Heeger, H Shirakawa, E J Louis, A G Mac Diarmid, Y W Park, *J. Am. Chem. Soc.*, 100 (1978) 1013
- [12] H Naarmann, N Theophilou, *Synth. Met.*, 22(1987)1
- [13] N Basescu, Z N X Liu, D Moses, A J Heeger, H Naarmann, Theophilou, *Nature* 327(1987)403
- [14] Th. Schimmel, D Glaser, M Schwoerer, H Naarmann, *Conjugated Polymers*, Kluwer Academic, Dordrecht, 1991
- [15] J Tsukamoto, *Adv. Phys.*, 41(1992)509
- [16] Reghu Menon, C O Yoon, D Moses, A J Heeger, *Phys. Rev B*, 48 (1993)17685
- [17] K Lee, S Cho, S H Park, A J Heeger, C W Lee, S H Lee, *Nature* 441(2006) 65
- [18] A J Heeger, S Kivelson, J R Schrieffer, W P Su, *Rev. Mod. Phys.*, 60 (1988)781
- [19] A B Kaiser, *Synth. Met.*, 45(1991) 183
- [20] A J Heeger, *Rev. Mod. Phys.*, 73(2001) 681
- [21] A B Kaiser, *Adv. Mater.*, 13(2001) 927
- [22] A J Heeger, *phys. Scr. T102* (2002) 30
- [23] R Kiebooms, R Menon, K Lee, *Handbook of Advanced Electronic and Photonic Materials and Devices*, Vol8, Academic, Santiago, 2001, p1-102
- [24] R S Kohlman, J Joo, A J Epstein, *Physical Properties of Polymers Handbook*, AIP, New York, 1996, p453-478
- [25] K Lee, *Encyclopedia of nanoscience and Nanotechnology*, vol5, American Scientific publishers, San Diego, 2004, p537-549
- [26] J Jang, J Bae, K Lee, *Polymer* 46 (2005) 3677
- [27] H Liu, X B Hu, J Y Wang, R I Boughton, *Macromolecules* 35 (2002)9414

- [28] Y Cao, P Smith, A J Heeger, *Synth. Met.*, 48 (1992) 91
- [29] E R Holland, S J Pomfret, P N Adams, A P Monkman, *J.Phys: Condens. Matter*, 8(1996)2991
- [30] A B Kaiser, C J Liu, P W Gilbert, B Chapman, N T Kemp, B Wessling, A C Patridge, W T Smith, J S Shapiro, *Synth. Met.*, 84 (1997) 699
- [31] C O Yoon, M Reghu, D Moses, A J Heeger, Y Cao, *Synth. Met.*, 63 (1994)47
- [32] S H Lee, D H Lee, K Lee ,C W Lee, *Adv. Funct.Mater.*,15 (2005),1495
- [33] M Amrithesh, S Aravind, S Jayalekshmi, R S Jayasree, *J.Alloys Compd* 458 (2008) 532
- [34] J Mort, F Jansen, *Plasma Deposited Thin Films*, CRC press, Florida, 1988
- [35] W N G Hitchon, *Plasma Processes for Semiconductor Fabrication*, Cambridge University Press,Cambridge,1999
- [36] Y Long, Z Chen, N Wang, J Li, M Wan, *Physica B* 344 (2004) 82
- [37] P Juvin, M Hasik, J Fraysse, J Planes, A Pron, I K-Bajer, *J. Appl. Polym. Sci* 74 (1999) 471
- [38] D L Wise, G E Wnek, D J Trantalo, T M Cooper, J D Gresser, *Electrical and optical polymer systems Fundamentals, Methods and Applications*, Marcel Dekker INC, New York,1998(chapter10)
- [39] S P Armes, M D Aldissi, S F Agnew,*Synth.Met.*,28(1989)C837
- [40] S P Armes: *Conducting polymer colloids: a review in Colloidal Polymer Particles*, Axcademic, New York, 1995, p-207-231
- [41] S Maeda, R Corradi, S P Armes, *Macromolecules*, 28 (1995) 2905
- [42] K Y Jen, T R Jow, R E Elsenbaumer, *J.Chem. Soc. Chem. Commun.* (1987)1113

- [43] M R Bryce, A Chissel, P Kathirgamanathan, D Parker, N R M Smith, *J. Chem. Soc. Chem. Commun.* (1987)466
- [44] K Y Jen, M Maxfield, L W Shacklette, R L Elsenbaumer, *J. Chem. Soc. Chem. Commun.* (1987)309
- [45] R L Elsenbaumer, K Y Jen, G G Miller, H Eckhardt, L W Schacklette, R Jow, *Electronic properties of conjugated polymers*, Springer-Verlag, Berlin, 1987, p-400
- [46] K Y Jen, R L Elsenbaumer, L W Schacklette, *PCT Int. Patent WO 8800, 954* (1988); *Chem. Abstr.*,109 (1988)191098q
- [47] J R Reynolds, M Pomereantz, *Electroresponsive Molecular and polymeric Systems*, Marcel Dekker, New York,1989,p-187-256
- [48] T Murase, T Ohnishi, Noguchi, *Chem. Abstr.*, 104 (1990)169124v
- [49] M Amrithesh, S Aravind, S Jayalekshmi ,R S Jayasree , *J.Alloys Compd* 449(2008)176
- [50] A Mirmohseni, G G Wallace, *Polymer* 44 (2003) 3523
- [51] S Yun, J Kim, *J.Phys. D: Appl. Phys.*, 39 (2006) 2580
- [52] A G Mac Diarmid, A J Epstein, *Faraday Discuss. Chem. Soc.*, 88 (1989)17
- [53] G Odian, *Principles of Polymerisation*, Wiley-Interscience, New York, 1991, p17-19
- [54] C H Hsu, J D Cihen, R F Tietz, *Synth. Met.*, 983 (1993) 37
- [55] M Angelopoulos, C E Asturier, S P Ermer, E Ray, M E Scherr, A G Mac Diarmid, A M Akhtar, Z Kiss,A J Epstein, *Mol. Cryst. Liq. Cryst.*, 160(1988)151
- [56] Oka, S Morita, K Yoshino, *Jpn. J. Appl. Phys.* 29 (1990) L679
- [57] K T Tzou, R V Gregory, *Synth. Met.*, 983 (1993) 55
- [58] E J Oh, Y Min, S K Manohar, A G MacDiarmid, A J Epstein, *Abstr. Am. Phys. Soc. Mtg.* 1992 M30

- [59] T Ikkala, J Laakso, K Vakiaparta, E Virtanen, H Ruohonen, H Jarvinen, T Taka, P Passiniemi, J E Osterholm, Y Cao, A Andreatta, P Smith, A J Heeger, *Synth. Met* 69 (1995) 97
- [60] J D Cohen, R F Tietz, *Eur. Patent Appl.*, 0446943 A2(1991)
- [61] A Ziabicki, *Fundamentals of Fibre Formation, Wet and Dry-Spinning from Solutions*, 1976,p249-350
- [62] F Grulke, *Polymer Process Engineering*, Prentice Hall, Englewood Cliffs, NJ,1994, p363-434
- [63] L W Shacklette, C C Han, *Mat. Res. Soc. Symp.*, 328 (1994)
- [64] Y Cao, J Qui, P Smith, *Synth. Met.*, 69 (1995)187
- [65] J H Burroughes, D D C Bradley, A R Brown, R N Marks, K Mackay, R H Friend, P L Burn, B Holmes, *Nature* 347 (1990) 539
- [66] R N Marks, D D C Bradley, R W Jackson, P L Burn, A B Holmes, *Synth. Met.*, 57 (1993) 4128
- [67] I D Parker, *J. Appl. Phys.*, 75 (1994)1656
- [68] S Karg, W Riess, V Dyakanov, M Schwoerer, *Synth. Met.*, 54 (1993) 427
- [69] J Gmeiner, S Karg, M Meier, W Riess, P Stroehriegl, M schwoerer, *polymer* 44 (1993) 201
- [70] M Angelopoulos, J M Shaw, M A Lecorre, M Tissier, *Microelectron. Eng.*, 13 (1991) 515
- [71] R H Baughman, L W Schacklette, R L Elsenbaumer, E J Plichta, C Becht, *Molecular Electronics*, Kluwer, Dordrecht, 1991
- [72] P J Flory, *Principles of Polymer Chemistry*, Cornell Univ. Press., Ithaca, Ny, 1953, chapter 13
- [73] T F otero, R J Rodriguez, *Intrinsically Conducting Polymers-An Emerging Technology*, Kluwer, Dordrecht,1993, p-179
- [74] W Takashima, M Kaneko, K Kaneto, A G MacDiarmid, *Synth.*

- [75] X chen, O Ingnas, Synth. Met., 74 (1995)159
- [76] M Wohlgenannt, Z V Vardeny, J. Phys: Condens. Matter, 15 (2003), R83
- [77] R Sainz, A M Benito, M T Martinez, J F Galindo, J Sotres, A M Baro, B Corraze, O Chauvet, A B Dalton, R H Baughman, W K Maser, Nanotechnol., 16 (2005) S150
- [78] H Zengin, W Zhou, J Jin, R Czerw, D W Smith, Jr., L Echevoyen, D L Carroll, S H Foulger, J Ballato, Adv. Mater. 14 (2002) 1480
- [79] X Zhang, J Zhang, Z liu, Appl. Phys. A,80 (2005) 1813

.....SCB.....

Chapter 2

EXPERIMENTAL TECHNIQUES AND THEORY

<i>Contents</i>	2.1 Introduction
	2.2 Non-redox doping
	2.3 Electronic conduction mechanisms
	2.4 Experimental Techniques

2.1 Introduction

The common feature of conducting polymers is their Π conjugated structure. Three of the four electrons from one s and two p states in the outermost shell of carbon occupy sp^2 hybridized states. These electrons form three strong σ bonds that play a key role in forming the polymer structure. The remaining valence electron occupies a p orbital and is called a Π electron. The Π electron wave functions from different carbon atoms overlap to form a Π band. Sigma bonds are strong and localized, while the Π bonds are weak and thus delocalized. The delocalized Π electrons are responsible for the high electrical conductivity of conducting polymers [1, 2]

But in systems such as polyacetylene, adjacent CH bonds move towards each other to form alternate short and long bonds, thereby

lowering the electronic energy of the system. This is called Peierls distortion. The resulting ground state can be described in terms of the inequality of the transfer integrals for the single and double bonds t_1 and t_2 , which opens up an energy gap, $2\Delta=2(t_1-t_2)$, separating the Highest Occupied Molecular Orbital (HOMO) from the Lowest Unoccupied Molecular Orbital (LUMO)[3-5].

The value of the symmetry breaking parameter or distortion U_0 can be related to the one dimensional energy gap through the relation $2\Delta=8\beta U_0$, where β is the electron phonon coupling constant which describes the modulation of the Π electron transfer integral due to the atomic motion. Here, in quasi one-dimensional conjugated systems, the domain walls separating the degenerate ground state structures are called solitons. In such systems (e.g. Polyacetylene), solitons take the place of electrons and holes in semi conductors. They are responsible for the transport of electrons and holes along the polymer chains. In short, solitons are excitations of a system leading from one minimum of the potential to another minimum of the same energy. Solitons can propagate without energy loss. There are three types of solitons- positive, negative and neutral [2].

For conducting polymers other than polyacetylene, different solitonic states have different energies. So solitonic conduction mechanisms are not expected. However, states appear in the band gap due to the formation of polarons (electrons localized in an electric potential minimum formed by lattice distortions). Polarons have both charge and spin and their motion can contribute to charge transport.

Polarons of opposite spin often pair up to form bi polarons with zero spin.

2.2 Non-redox doping

Polyaniline is a mixed oxidation state polymer composed of reduced benzenoid units and oxidized quinonoid units (scheme 2.1a). The average oxidation state is given by $1-y$. It can exist in several oxidation states ranging from the completely reduced leucoemeraldine base state (scheme 2.1b), where $1-y=0$, to the completely oxidized pernigraniline base state (scheme 2.1c), where $1-y=1$. The “half” oxidized ($1-y=0.5$) emeraldine base state (scheme 2.1d) is an insulator and is composed of an alternating sequence of two benzenoid units and one quinonoid unit.

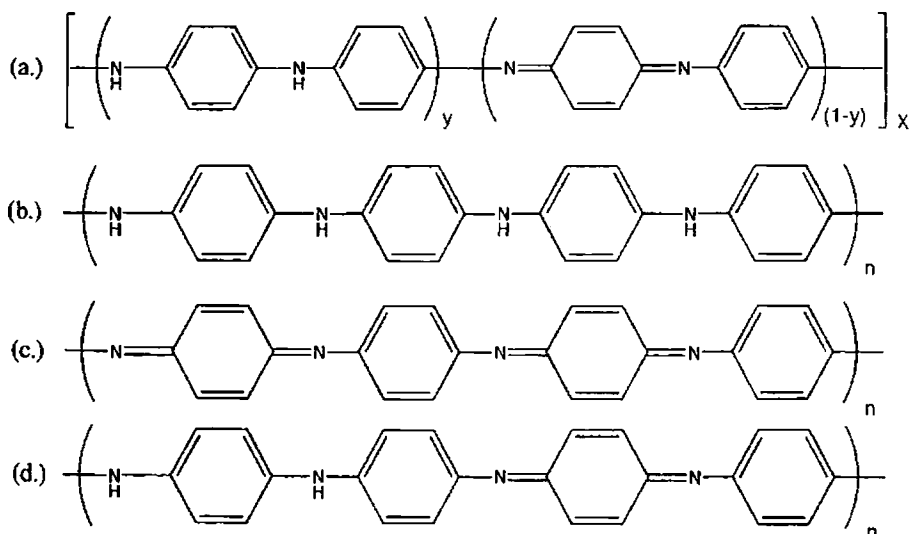


Fig. 2.1 Different oxidation states of polyaniline

However, emeraldine base can be non-redox doped with acid[6] to yield the conductive emeraldine salt state of polyaniline as shown in fig 2.2.

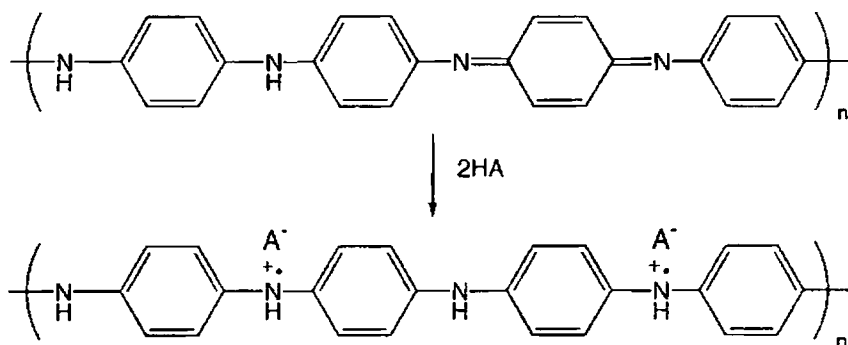


Fig. 2.2 Protonic acid doping of polyaniline (emeraldine base) to polyaniline (emeraldine salt)

This non-redox doping differs from redox doping in that it does not involve the addition or removal of electrons from the polymer backbone.

2.3 Electronic conduction mechanisms

Employment of the above described doping techniques and sophisticated synthesis methods provide a conceptual framework for understanding the electronic structure of these novel polymer semiconductors at low doping levels [7-11]. The origin of metallic nature in conducting polymers is still controversial[12,13].

Though such systems exhibit a Pauli spin susceptibility[12], a quasilinear temperature dependence of thermo power[14] and a linear term in the specific heat[15], the real fingerprints of metallic

behaviour (e.g.-finite D.C conductivity as $T \rightarrow 0$, a positive temperature co-efficient of resistivity and metallic reflectivity in the infrared) are absent. Nowadays new methods of synthesis and processing of conducting polymers have resulted in systems with improved homogeneity and long range order, providing opportunities for investigating the metallic state through transport and optical measurements [16-26].

2.3.1 Disorder induced metal-insulator transition

Anderson [27] reported that the localization of electronic wave functions can occur if the random component of disorder potential is large enough compared to the band width. The mean free path (λ) in such systems is given by,

$$1/\lambda = 0.7(1/a) (V_0/B)^2 \dots\dots\dots (2.1)$$

where a is the interatomic distance, V_0 is the random potential, and B is the bandwidth. According to Anderson, the states will become localized throughout the band for a critical value of V_0/B that is estimated to be of the order of unity in three dimensions.

Later on, Mott [28, 29], pointed out that the states in the band tails are more susceptible to localization. The critical energy called the mobility edge (E_c) separates the localized states from the non localized states and it plays an important role in cases of significant disorder, even when V_0/B is below the critical value.

In 1970, Anderson [30] proposed that a degenerate electron gas in a random disorder potential tends to localize if the magnitude of the disorder potential is large compared with the bandwidth. Such a system is called a “Fermi glass”. It is an insulator with a continuous density of localized states (no energy gap) occupied according to Fermi statistics. If the extent of disorder is sufficiently large so that the Fermi energy (E_F) lies in the region of localized states, there is a transition from the metallic state (finite value of conductivity as $T \rightarrow 0$) to a nonmetallic state (conductivity $\rightarrow 0$ as $T \rightarrow 0$). This disorder induced metal-insulator (M-I) transition is called Anderson transition [28, 29]. The critical region is characterized by a universal power law temperature dependence of conductivity, $\sigma_{crit} \propto T^{-\beta}$. The localization length increases as E_F approaches E_c . Mott proposed the concept of minimum metallic conductivity σ_{min} , treating M-I transition as discontinuous and employing the Ioffe-Regel criterion that the lower limit of mean free path is the interatomic spacing [31].

$$\sigma_{min} = 0.03(2 \pi e^2) / (3 \hbar a) \dots\dots\dots (2.2)$$

for $\sigma \sim \sigma_{min}$, the system is near the M-I transition, whereas systems with $\sigma < \sigma_{min}$ is on the insulating side of the M-I transition. An important parameter for characterizing the disorder is the product of Fermi wave vector (K_F) and the mean free path (λ).

In short, if $K_F \lambda \ll 1$, $\sigma \ll \sigma_{min}$, the sample is on the insulating side of the M-I transition and if $K_F \lambda \geq 1$, $\sigma \geq \sigma_{min}$, the sample is on the metallic side of the M-I transition. Though conducting polymers are in general quasi 1D systems, strong interchain coupling suppresses the localization, facilitating the formation of 3D metals [32,33]. When such

a material is oriented (e.g., by tensile drawing), it behaves like an anisotropic 3D metal.

2.3.2 Hopping in disordered semiconductors

For many of the amorphous materials, electronic conduction is governed by Mott's variable range hopping [28]. In disordered semiconductors with localized states in the band gap, conduction occurs by phonon assisted tunneling between electronic localized states centered at different positions.

Mott and Davis have formulated an expression for variable range hopping as,

$$\sigma(T) = \sigma_0 \exp [-(T_0/T)^\gamma] \dots\dots\dots (2.3)$$

for hopping in three dimensions, the exponent has the value $\frac{1}{4}$. It is assumed that the electronic wave functions decay with distance r as $\exp(-r/L_{loc})$, where L_{loc} is the localization length and T_0 is a constant. According to this model, in three dimensions,

$$\sigma_0 = e^2 v R^2 N(E) \dots\dots\dots (2.4)$$

and

$$T_0 = \lambda \alpha^3 / KN(E) \dots\dots\dots (2.5)$$

where

- e: the electronic charge
- λ : a dimensionless constant with its value approximately equal to 18.1
- $N(E)$: the density of states at the Fermi level.
- α : the inverse rate of fall of the wave function and
- K: the Boltzmann constant

The hopping distance,

$$R = [9/8\pi \alpha kN (E)]^{1/4} \dots\dots\dots (2.6)$$

The average hopping energy W can be estimated by knowing R and $N (E)$ from the relation,

$$W = \frac{3}{4} \pi R^3 N(E) \dots\dots\dots (2.7)$$

T_0 and σ_0 can be obtained from the slope and intersection with the conductivity axis respectively.

α is approximated as 10 \AA^0 and the characteristic phonon frequency $\nu, 10^{13} \text{ s}^{-1}$.

At sufficiently high temperatures, hopping is to nearest neighbours with $\gamma = 1$. This is a case similar to that in a crystalline semiconductor. For 2D hopping, $\gamma = 1/3$ and for 1D hopping, $\gamma = 1/2$. Quasi 1D hopping plays a key role in conducting polymers where polymer chains traverse disordered regions to connect crystalline islands. Charge carriers would diffuse along such electrically isolated disordered chains as part of the conduction path, but would readily localize owing to the 1D nature of the chains. Quasi 1D variable range hopping along disordered chains dominates the overall resistance of the polymers in such cases.

2.3.3 Tunneling between metallic islands

Calculations by Sheng and Klafter(1983) and Sheng (1992) [34,35] reveal that, if conduction is by electronic tunneling through non-conducting

material separating mesoscopic metallic islands, rather than between localized states, the expression for the tunneling conductivity approximately takes the form (2.3), with $\gamma=1/2$. This model is appropriate for a granular metal in which small metallic grains are surrounded by non-conducting shells. Here the conductivity is limited by the electrostatic charging energy when an electron is transferred from one island to the next. The inhibition of tunneling when the thermal energy kT is less than the charging energy is referred to as Coulomb blockade.

If the metallic regions are large enough that the electrostatic charging energy is much smaller than the thermal energy kT , tunneling can occur between metallic states of the same energy on different sides of the barrier without thermal excitation, provided that the wave functions overlap. Fluctuations in the voltage across the tunneling junction can greatly increase the tunneling current as temperature increases according to Sheng (1980) [36].

Conductivity due to this fluctuation assisted tunneling for a simple parabolic barrier shape can be approximated as,

$$\sigma(T) = \sigma_0 \exp [-(T_0 / (T+T_0))] \dots\dots\dots (2.8)$$

where,

T_0 : The temperature at which the thermal voltage fluctuations become large enough to raise the energy of electronic states to the top of the barrier

T_0/T_0 : determines the tunneling in the absence of fluctuations

$\sigma(0)$: low temperature limit

The prefactor σ_1 is approximated as independent of temperature.

2.3.4 Space charge limited conduction

In the metal-polymer-metal configuration, where the contacts are ohmic, carriers can be injected from the metal electrode into the conduction band of the polymer under an applied electric field. If the amount of injected carriers is more than that which can be transported across the pellet, a space charge will be build up at the metal polymer interface. So electrons flowing through the system under an electric field will be impeded and controlled by the space charge collected at the metal-polymer interface and this gives rise to the phenomenon known as space charge limited (SCLC) conduction [37]. For a trap free material, the current density under SCL conduction is given by

$$J_{sclc} = (9/8) \epsilon \epsilon_0 \mu (V^2/d^3) \dots\dots\dots (2.9)$$

ϵ : the dielectric constant of the material

V : the applied voltage and

D : the thickness of the sample

SCL currents are important because the injected current is independent of the mechanism of carrier generation and depends only on the transport and trapping of the carriers within the sample. SCLC shows three to four distinct regions in the current- voltage plots. The first region corresponds to the low field conduction region where the variation of current density with voltage is ohmic. As voltage is increased, the injected carriers outnumber the thermally generated ones and SCLC starts. The equation (2.9) shows that J is directly

proportional to V^2 and inversely proportional to d^3 . The transition from ohmic to square law shows the onset of SCLC conduction.

2.3.5 Schottky Effect

The potential barrier at the metal-insulator interface region can be overcome by the electrons and they can flow from the metal electrode to the conduction band of an insulator under an applied field. This effect called Schottky effect is a field assisted conduction process. When an electron jumps from the metal surface, the latter becomes polarized and exerts an attractive force on the electron. Due to the resulting image force, the potential step at the metal polymer interface changes smoothly. The potential energy of the electron due to the image force is

$$\Phi = -e^2 / (16 \pi \epsilon \epsilon_0 x) \dots\dots\dots (2.10)$$

Here x is the distance of the electron from the electrode surface

2.3.6 Poole-Frenkel Conduction Process

Upon the application of an electric field to a sample, the potential barrier height caused by Coulombic forces on an atom will be reduced. This phenomenon is known as Poole-Frenkel effect. The potential energy of an electron in the field of a trapping center is given by the usual Coulomb expression,

$$\Phi = -e^2 / (4 \pi \epsilon \epsilon_0 x) \dots\dots\dots (2.11)$$

Here x is the distance from the center.

The potential energy here is four times that due to the image force in Schottky mechanism.

2.4 Experimental Techniques

In this section, a detailed description of the techniques employed for structural, morphological, electrical, optical, thermal and mechanical characterization of the samples investigated in the present work is included.

2.4.1 FTIR spectroscopy

Fourier Transform InfraRed (FTIR) spectroscopy is employed for the identification of functional groups.

Fig 2.3 depicts a schematic diagram of FTIR setup.

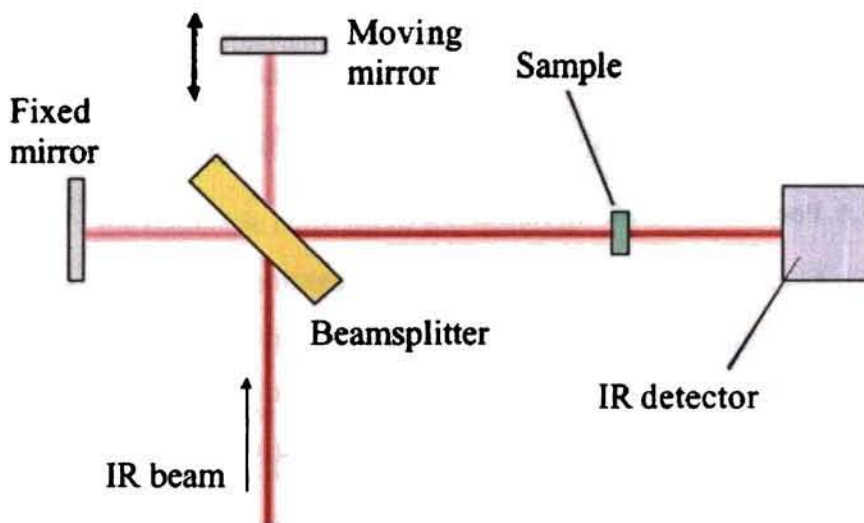


Fig. 2.3 Schematic diagram of FTIR spectrometer

The basic optical component of Fourier transform spectrometers is the Michelson interferometer. Light from an infrared source—a heated element or a glow bar—is collimated and directed on a beam splitter. An

ideal beam splitter creates two separate optical paths by reflecting 50% of the incident light and transmitting the remaining 50%. In the near and middle infrared region, germanium deposited on a KBr substrate is used as a beam splitter. In one path the beam is reflected back to the beam splitter by a fixed position mirror, where it is partially transmitted to the source and partially reflected to the detector. In the other leg of the interferometer, the beam is reflected by the movable mirror that is translated back and forth, while maintained parallel to itself. The beam from the movable mirror is also returned to the beam splitter where it, too, is partially reflected back to the source and partially transmitted to the detector. Although the light from the source is incoherent, when it is split into two components by the beam splitter, the components are coherent and can produce interference phenomenon when the beams are combined. The detector is usually a deuterated triglycene sulfate pyroelectric detector and the movable mirror rides on air bearing for good stability. Other detectors such as cooled HgCdTe are also used.

Different functional groups in the sample absorb characteristic frequencies of I.R radiation. IR spectrometers could analyze gases, liquids and solids using various sampling accessories. Thus FTIR spectroscopy is an important and popular tool for structural elucidation and compound identification. The spectrum obtained, representing the molecular absorption and transmission is a molecular fingerprint of the sample. Different functional groups absorb at their unique characteristic frequencies. This makes infrared spectroscopy useful for several types of analysis [38-41].

In the present work, FTIR spectrum is taken using an Avatar 370 spectrometer employing a DTGS KBr detector. The resolution of the instrument is 4cm^{-1} .

2.4.2 X-ray diffraction

X-ray topography or X-ray diffraction is a non-destructive technique for structural study[42-45]. Though it is not a high resolution technique, it gives microscopic information. The schematic diagram corresponding to crystal diffraction is given below.

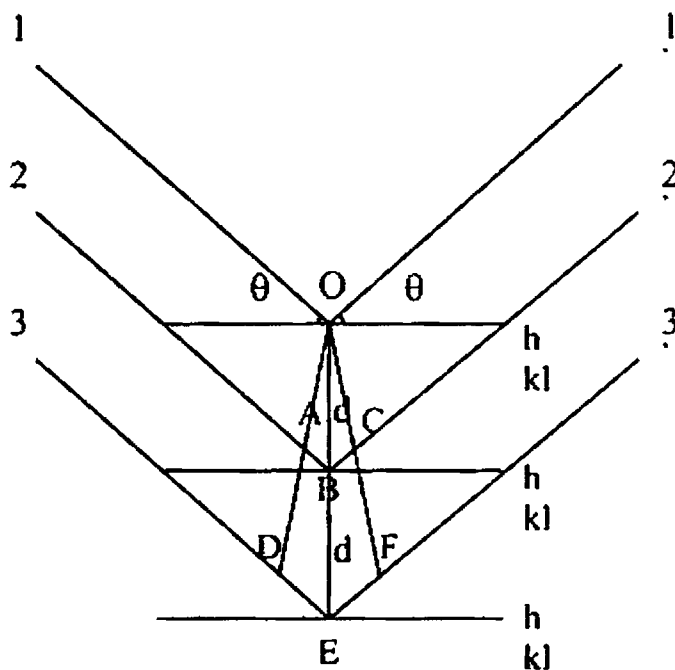


Fig. 2.4 Crystal diffraction

Monochromatic X-rays impinge on a crystal with lattice spacing 'd'. They emerge out at twice the Bragg diffraction angle θ .

The Bragg equation is,

$$2d\sin\theta = \lambda \dots\dots (2.12)$$

$$\text{Or } \theta = \sin^{-1}(\lambda/2d) \dots\dots (2.13)$$

The diffracted X-rays are made to fall on a photographic plate or film, placed as close to the sample as possible. The film must be perpendicular to secondary X-rays to get a good image. Dislocations or defects produce a highly intense diffracted beam than that from a perfect plane.

$$\text{Strain}(S) = (d_{\text{unstrained}} - d_{\text{strained}}) / (d_{\text{unstrained}}) \dots\dots\dots (2.14)$$

Topography is generated when the sample and film are scanned in synchronism with the screen.

X-ray topography is of two types-reflection X-ray topography and transmission X-ray topography. In reflection X-ray topography, developed by Berg and Barret, X-rays are incident on the crystal plane at small angle α . The reflected X-rays fall on the photographic plate placed close to the sample. Reflection X-ray topography is helpful in the study of crystal dislocations. Transmission X-ray topography is developed by Lang. Monochromatic X-rays are made to fall on the crystal through a slit. The X-rays transmitted through the crystal passes through a slit on the screen and then to the photographic plate. Transmission X-ray topography [46, 47] is used in the study of crystal defects. In section topography, the sample and the film is kept stationary [48, 49]. A small section of the sample-the cross-section is imaged. Section topography provides “defect depth” information.

The XRD analysis of the samples is carried out using a fully automated Rigaku 1710 X-ray Diffractometer. In our set-up, filtered Cu-K α radiation having wavelength $\lambda = 1.542 \text{ \AA}$ is used for diffraction. The accelerating potential applied to the X ray tube is 30KV and the tube current is 20 mA

2.4.3 D.C electrical conductivity measurements

The four-point probe technique is the most common method for measuring the semiconductor resistivity/conductivity. It is an absolute measurement without recourse to calibrated standards. It is often used to provide standards for other resistivity measurements. Though two-point probe method is easier to implement, the interpretation of measured data is difficult. In two-point probe, each probe serves as a current and as a voltage probe. The total resistance R_T between the two probes is given by,

$$R_T = V/I = 2R_P + 2R_C + 2R_{sp} + R_s \dots \dots \dots (2.15)$$

Where R_P is the probe resistance, R_C the contact resistance at each metal probe/semiconductor contact R_{sp} , the spreading resistance under each probe, and R_s the semiconductor resistance. We assume R_C and R_{sp} to be identical for both the contacts. The contact resistance arises from the mechanical metal probe contacting the semiconductor. The spreading resistance accounts for the resistance encountered by the current when it flows from the small metal probe into the semiconductor and from the semiconductor to the probe. R_{sp} is a measure of resistivity, because for typical four-point probes $R_{sp} \gg R_s$.

Neither R_C nor R_{sp} can be accurately calculated for a mechanical probe contact. So they cannot be accurately extracted from the total resistance. R_P can be separately determined by shorting the two probes and measuring the resistance.

The solution to this dilemma is the four point probe technique originally proposed by Wenner [50]. Here two probes carry the current and the other two probes sense the voltage. The two current carrying probes have contact and spreading resistance associated with them. But this is not true for the two voltage probes. The voltage is measured either with a potentiometer which draws no current at all, or with a high impedance voltmeter, which draws very little current. The parasitic resistances R_C , R_P and R_{sp} are negligible in either case because the voltage drop across them is negligibly small due to a very small current that flows through them. Such four-contact measurement techniques are frequently referred to as Kelvin techniques.

Let I be the current entering through probe 1 and leaving through probe 4. The potential V at a distance r from an electrode in a material of resistivity ρ is given by,

$$V = \frac{\rho I}{2\pi r} \dots\dots\dots (2.16)$$

For probes resting in a semi-infinite medium, with current entering probe 1 and leaving probe 4, the voltage V_0 , measured with respect to zero reference potential becomes,

$$V = \frac{\rho I}{2\Pi} \left(\frac{1}{r_1} - \frac{1}{r_4} \right) \dots\dots\dots (2.17)$$

where r_1 and r_4 are the distances from the probes 1 and 4 respectively. The minus sign accounts for current leaving through probe 4. For probe spacing s_1, s_2 and s_3 , the voltage at probe 2 is,

$$V_2 = \frac{\rho I}{2\Pi} \left(\frac{1}{s_1} - \frac{1}{s_2 + s_3} \right) \dots\dots\dots (2.18)$$

and at probe 3 is

$$V_3 = \frac{\rho I}{2\Pi} \left(\frac{1}{s_1 + s_2} - \frac{1}{s_3} \right) \dots\dots\dots (2.19)$$

The total measured voltage $V = V_2 - V_3$ becomes

$$V = \frac{\rho I}{2\Pi} \left(\frac{1}{s_1} - \frac{1}{(s_2 + s_3)} - \frac{1}{(s_1 + s_2)} + \frac{1}{s_3} \right) \dots\dots\dots (2.20)$$

The resistivity ρ is given by,

$$\rho = \frac{2\Pi V}{I \left(\frac{1}{s_1} - \frac{1}{(s_2 + s_3)} - \frac{1}{(s_1 + s_2)} + \frac{1}{s_3} \right)} \dots\dots\dots (2.21)$$

ρ is usually expressed in ohm.cm, with V measured in volts, I in amperes, and s in cm. The current is usually such that the resulting voltage is approximately 10mV. For most four-point probes, the probe spacings are equal. With $s = s_1 = s_2 = s_3$, the equation becomes,

$$\rho = \frac{2\Pi SV}{I} \dots\dots\dots (2.22)$$

Smaller probe spacings allow measurements closer to wafer edges.

Semiconductor wafers are not semi-infinite in extent in either the lateral or vertical dimension. So, the equation for resistivity must be corrected for finite geometries.

For an arbitrarily shaped sample, the resistivity is given by,

$$\rho = \frac{2\Pi SFV}{I} \dots\dots\dots (2.23)$$

$$\text{Conductivity } \sigma = \frac{I}{2\Pi SFV} \dots\dots\dots (2.24)$$

where F is a correction factor that depends on the sample geometry. F corrects for probe location near sample edges, for sample thickness, sample diameter, probe placement and sample temperature.

For collinear or in-line probes with equal probe spacing s, the correction factor F is a product of three separate correction factors F₁, F₂ and F₃.

$$\text{Ie, } F = F_1 \times F_2 \times F_3 \dots\dots\dots (2.25)$$

F₁ corrects for sample thickness F₂ corrects for lateral sample dimensions, and F₃ corrects for placement of probes relative to sample edges.

Sample thickness must be corrected for most measurements since semi conducting wafers are not infinitely thick. Their thickness is usually on the order of the probe spacing, or less, introducing the correction factor [51],

$$F_{11} = t/s/2 \ln \{ [\sinh (t/s)] / [\sinh (t/2s)] \} \dots\dots\dots (2.26)$$

This is for a non-conducting bottom surface, where t is the wafer or layer thickness.

For a conducting bottom surface, the correction factor becomes

$$F_{12} = t/s/2 \ln \{ [\cosh (t/s)] / [\cosh (t/2s)] \} \dots\dots\dots (2.27)$$

Conducting bottom surfaces are difficult to achieve. In most of the cases, four-point probe measurements are taken with insulating bottom boundaries. For thin samples,

$$F_{11} = t/s/2 \ln (2) \dots\dots\dots (2.28)$$

Conventional four probe measurements are suitable for moderate or low resistivity materials, while minority carrier injection and sample loading by the voltmeter limit the accuracy of measurement in the case of high resistivity samples.

2.4.4 Photoluminescence (P.L) measurements

P.L measurements are performed using a Jobin Yvon Flurolog 3 Spectrofluorometer. (Model FL3-22). The instrument has a 450W Xenon lamp as source and a PMT detector (Model: R928P). The

sample compartment module is T-box type. Double gratings are used for excitation and emission spectrometers.

Photoluminescence is the process by which light energy is absorbed by the material and a fraction of it is emitted in the visible or near visible region. The excitation source is IR, visible, UV or X-rays. Photoluminescence is mainly divided into two-fluorescence and phosphorescence. In fluorescence, emission occurs during excitation or within 10^{-8} s after excitation. 10^{-8} s is of the order of lifetime of the atomic state corresponding to the allowed electric dipole transitions in the visible region. If emission occurs microseconds or even hours after excitation is removed, it is called phosphorescence. Some samples show characteristic luminescent behaviour. In others activators are mainly responsible for luminescence [52-53].

In polymers, generally excitons are responsible for luminescence. Exciton is a stable, bound electron-hole pair in the sample. An electron from the LUMO of the polymer combines with a hole from the HOMO to form excitons. Generally singlet excitons are delocalized over the polymer chain while the triplet excitons are bound. Obviously singlet excitons are mainly responsible for photoluminescence in conjugated polymers. The singlet exciton formed decays radioactively to the ground state with the emission of light[2]. If emission does not occur, then a non-radiative pathway is dominant and the electronic excitation is converted into rotational or vibrational motion within the polymer and its surroundings. The difference between the absorption and emission maxima of the spectra is called the Stoke's shift. Stoke's shift

occurs when the emission from the lowest vibrational excited state relaxes to various vibrational levels of electronic ground state.

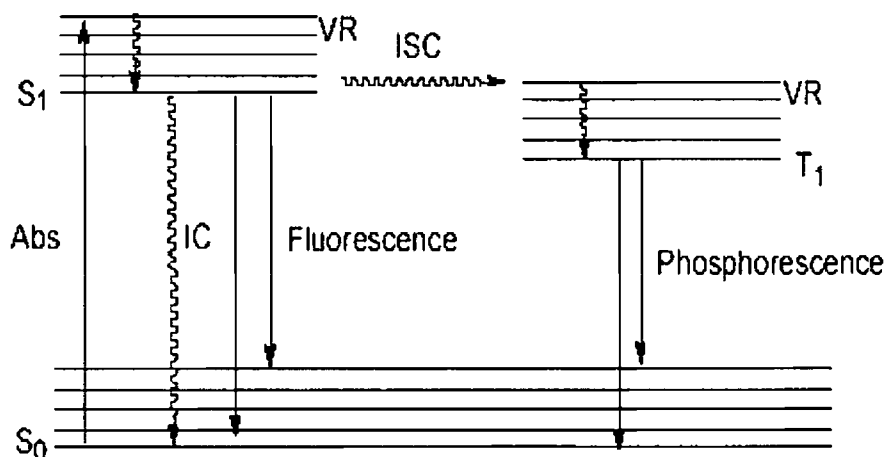


Fig. 2.5 Schematic diagram of various optical processes

Abs = absorption,	VR = vibrational relaxation,
ISC = Intersystem crossing,	IC = internal conversion,
S_0 = ground state singlet,	S_1 = first excited state,
T_1 = first triplet excited state.	

Based on the processes responsible for photoluminescence, the phenomenon of photoluminescence is mainly divided into two—intrinsic luminescence and extrinsic luminescence. Some samples exhibit intrinsic luminescent behaviour. In others, activators are mainly responsible for luminescence. Activators are impurity atoms present in small concentrations in the host material or stoichiometric excess of certain component in the host material (self-activators).

In extrinsic luminescence, there will be some localized energy levels in the forbidden energy gap of the sample. There are two possibilities.

- a) Intermediate level corresponding to the activator atom, A.
- b) Intermediate level corresponding to the host material, G which is under the perturbing influence of activators or belonging to lattice defects, whose existence is associated with the incorporation of activator atoms.

There are mainly three possibilities of excitation.

- a) A photon of appropriate energy may excite an electron from G to A.
- b) Excitons may be formed in some other parts of the sample. They may diffuse to the luminescence center. Under the excitation of the excitons, electrons may be excited from G to A.
- c) Due to the bombardment with electron or photon, an electron may be created in the conduction band and a hole in the valence band. Hole from the valence band may occupy the level G and electron from the conduction band the level A. Their recombination and subsequent deexcitation results in photoluminescence.

2.4.5 TEM studies

The TEM images are obtained using a JOEL JEM 2200 FS electron microscope working under an accelerating voltage of 200 KV. Schematic diagram of a Transmission Electron Microscope (TEM) is given in fig 2.6.

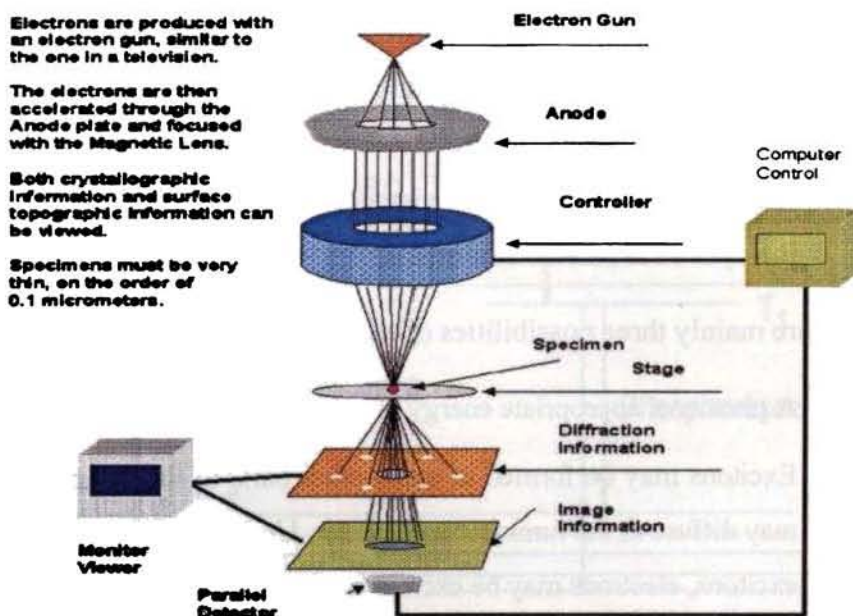


Fig. 2.6 Schematic diagram of transmission electron microscope

In a TEM, electrons from the electron gun are accelerated from 100KV to 400KV and are focused onto the specimen by a combined lens system[54-57].The sample is kept very thin for effective transmission and is placed on a copper grid. The transmitted and forward scattered electrons produce a diffraction pattern in the back focal plane of the lens and a magnified image on the image plane of the lens. Either of it is projected onto a fluorescent screen for photographing or electronic recording. Formation of diffraction pattern helps to study the structural details.

There are mainly three imaging techniques-bright field, dark field and high resolution imaging [38].Contrast depends on diffraction and scattering of electrons. Transmitted electrons give rise to bright field

image and specific diffracted beam the dark field image. Contrast depends on the intensity of electrons transmitted through the sample that pass through the imaging lens. Heavier elements lead to greater scattering of electron beam. So, intensity of transmitted electrons is reduced. Contrast comes about by phase contrast, mass contrast, thickness contrast and diffraction contrast. High resolution TEM (HREM) is used to obtain information on the atomic scale and is particularly used in the interface analysis. Here a number of different diffracted beams are combined together to give an interference image.

2.4.6 SEM studies

The SEM images are obtained using a Joel 6390LV scanning electron microscope. The schematic diagram of a scanning Electron Microscope (SEM) is given in figure 2.7.

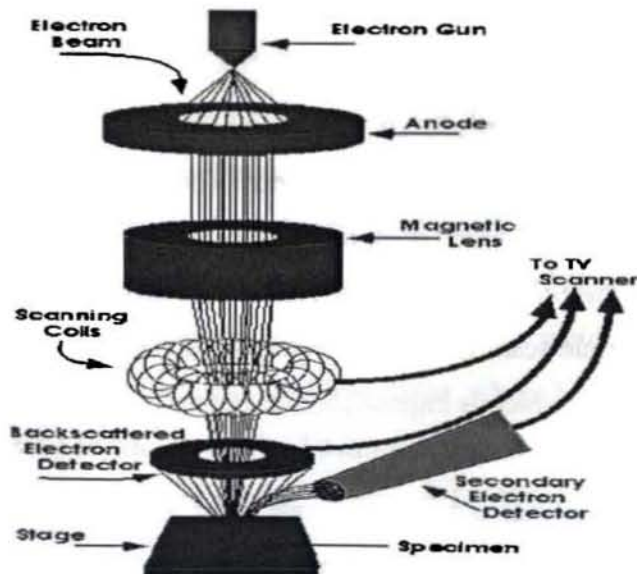


Fig. 2.7 Schematic diagram of a scanning electron microscope

Scanning Electron Microscopy is similar to optical microscopy. But here electrons are used instead of photons. Electrons of energy 10-30KeV impinge on the sample. Secondary electrons, back scattered electrons, auger electrons and X-ray photons are produced. Secondary electrons form the SEM image. Back scattered electrons also form an image [58]. Absorbed electrons are measured as electron beam induced current.

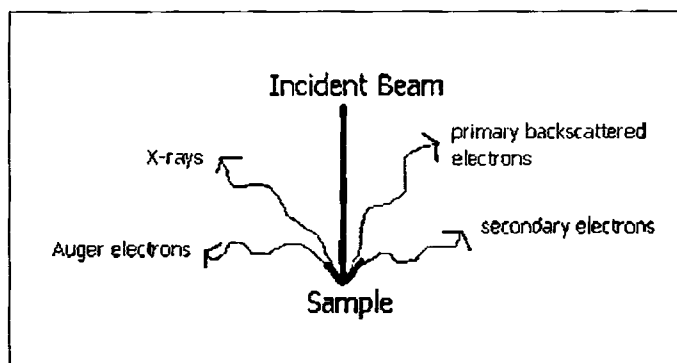


Fig.2.8 Production of secondary electrons

The secondary electrons are detected and amplified. The image of the specimen is mapped onto a C.R.T screen. There should be one to one correspondence between each point on the specimen and each point on the screen. Magnification is defined as the ratio of the length of C.R.T display to length of sample scan. Using SEM, magnification of the order of 10^6 could be achieved, which is impossible through optical microscope. Large magnification is possible because electrons have smaller wavelengths and depth of field produced is large. Contrast is an important parameter for SEM imaging. For flat, uniform samples, there is no contrast. But for samples composed of materials with different atomic numbers, contrast is

observed. Contrast is observed mainly due to back scattered electrons because back scattering co-efficient is a strong function of atomic number than secondary electron emission co-efficient. Other factors affecting contrast are sample surface, surface topography and local electric fields. Secondary electrons are emitted from the top 10nm of the sample surface. When the sample is tilted through an angle θ from the normal beam direction, electron beam path inside the sample increases by $1/\cos \theta$.

$$\text{Contrast-C}=\tan \theta d\theta \dots\dots\dots (2.29)$$

Sample stage is an important parameter. It should allow sufficient tilt and rotation for the sample to be viewed in all directions. In SEM, the detector collects even those electrons moving away from it, unlike an optical microscope.

The electron gun emits electrons. It should have low electron dispersion. Usually tungsten filament is used which produces electron dispersion in the range 2eV. Lithium hexaborate and field emission sources have lower energy dispersion, longer life and higher brightness. The electron beam passes through scanning coils and lens system to the sample. Auger electrons, characteristic and continuous X-rays, photons, back scattered electrons and secondary electrons are produced. Secondary electrons are detected by a detector which is usually a scintillation material which produces light when highly accelerated electrons (10-12KV) fall on it. To accelerate electrons, scintillator is placed in a faraday cage of high electric field. The electrons from the detector are connected to a photomultiplier tube which multiplies the number of electrons several folds. It is finally connected to Cathode

Ray Tube (C.R.T).C.R.T image is a mapping of the scanned signal image. The beam diameter used in SEM is 10nm.Still resolution is not good [38]. The major reasons are,

- a) Large number of electrons is elastically and inelastically scattered. Elastic scattering occurs due to scattering of electrons by positive nuclei and inelastic scattering is due to valence and core electrons.
- b) The shape of electron distribution cloud depends on the ion beam energies and the atomic number of the target. For $Z \leq 15$, the distribution is tear drop shaped. For $15 < Z < 40$, it becomes more spherical. In the case of elements with $Z \geq 40$, the distribution is hemi spherical.
- c) For low atomic numbers, electrons are absorbed and for high atomic numbers, back scattered electrons are large.

2.4.7 Thermo gravimetric Analysis (TGA)

Sample and reference are heated by a single source and the temperatures are measured by thermo couples embedded in the sample and reference, and attached to their pans. Weight loss corresponding to various temperatures is noted [1].

2.4.8 UV/Vis/NIR Absorption Spectroscopy

In this technique, the absorption of light in the ultraviolet (10–420 nm), visible (420–700 nm) and near-infrared (700–2500 nm) regions by a sample is measured. The absorption of light in the

UV/Vis/NIR region depends on the nature of chemical groups present in the structure.

A polymer molecule, in its ground state contains two electrons of equal and opposite spin in each filled molecular orbital. One of the electrons in the highest filled Π molecular orbital absorbs light and is raised to the lowest unfilled Π molecular orbital. If the spins are antiparallel, we get an excited singlet state and if they are parallel, an excited triplet state results. The different possible transitions are,

1. σ - σ^* transition

Here the transition of electron is from a bonding sigma orbital to a higher energy antibonding sigma orbital. Since sigma bonds are very strong, this transition is a high energy process.

2. n - σ^* transition

This transition is observed in saturated compounds having one heteroatom with unshared pair of electrons. These transitions require less energy than σ - σ^* transitions.

n - σ^* transitions are sensitive to hydrogen bonding.

3. Π - Π^* transition

Such transitions occur in compounds with unsaturated centers and requires less energy than n - σ^* transitions.

4. n- Π^* transition

Here an electron of unshared electron pair on a heteroatom is excited to a Π^* antibonding orbital. n- Π^* transition requires the least amount of energy than all the above transitions and consequently this transition gives rise to an absorption band at longer wavelengths.

The absorption co-efficient α is measured, by dividing the absorption values by the film thickness.

The photon absorption in many amorphous materials is found to obey the Tauc relation given by, $(\alpha h\nu) = B (h\nu - E)^n \dots\dots(2.30)$

Here α is the absorption coefficient in eVcm^{-1} , $h\nu$ the photon energy, B a constant and the index n is connected with the distribution of the density of states. For direct allowed transition energy gap, $n=1/2$ and for indirect allowed transition energy gap, $n=2$. $(\alpha h\nu)^2$ as a function of photon energy $h\nu$ gives direct allowed transition energy gap. $(\alpha h\nu)^{1/2}$ as a function of photon energy $h\nu$ gives indirect allowed transition energy gap [59-60].

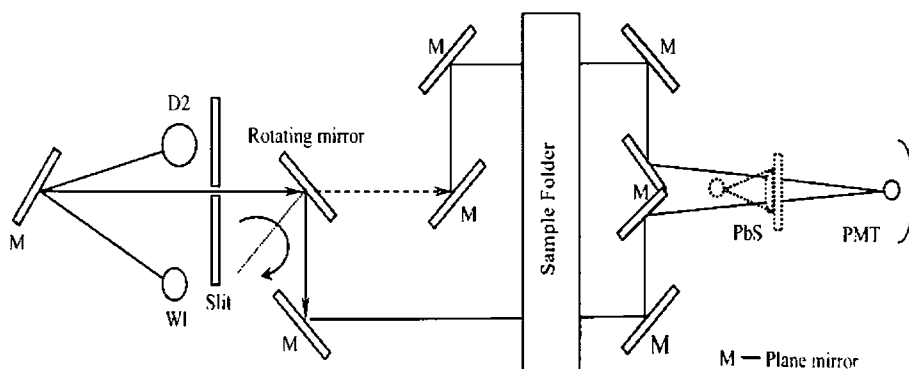


Fig. 2.9 Block diagram of UV/VIS/NIR Spectrometer

In the present work we have used Jasco V 570 UV/VIS/NIR spectrometer employing a Deuterium lamp (190-350nm) and a halogen lamp (330-2500nm). The optical system used is a single monochromator. The spectrometer has two detectors-1. Photo Multiplier Tube (PMT) 2. Lead sulphide (PbS) Photoconduction cell. The instrument has a resolution of 0.1nm in the UV/VIS region and 0.5nm in the NIR region.

2.4.9 Photo acoustics measurements

The Thermal Diffusivities are calculated using thermo elastic bending formula applied to open photo acoustic technique in transmission configuration. The detailed theory regarding this technique is given in chapter 7.

2.4.10 Raman measurements

Raman Spectroscopic measurements of the samples are carried out in the range 200cm^{-1} - 1800cm^{-1} , using a Jobin Yvon Horiba micro Raman system employing a 488nm Argon laser as source.

Raman spectroscopy is based on the Raman effect, first reported by C.V.Raman in 1928[61]. If the incident photon imparts part of its energy to the lattice in the form of a phonon, it emerges as a lower energy photon. This is called Stokes shift. When the photon absorbs a phonon and emerges with higher energy, it is termed Anti-Stokes shift. The Anti-Stokes mode is much weaker than the Stokes mode. So Stokes mode scattering is usually monitored. In Raman scattering, incident light interacts with optical phonons, while in Brillouin

scattering, the incident light interacts with acoustic phonons. Since optical phonons have higher energies than acoustic phonons, giving larger photon energy shifts, Raman scattering is easier to detect than Brillouin scattering.

In Raman spectroscopy, a low power laser beam is pumped onto the sample [62]. The weakly scattered light is passed through a double monochromator, which rejects the Rayleigh scattered light. The Raman shifted wavelengths are detected by a photodetector. The fluorescent background problem is eliminated by combining Raman spectroscopy with FTIR [63]. By using lasers of different wavelengths and hence different absorption depths, it is possible to profile the sample to some depth. The wavelengths of the scattered light are analyzed and matched to known wavelengths for identification.

Raman spectroscopy can be used to detect both organic and inorganic species. It is free from charging effects, which is a disadvantage for electron and ion beam techniques. It is sensitive to strain, allowing it to be used for detecting stress in a semiconductor material or device. The major semiconductor applications of Raman spectroscopy include structural defects, ion damage, laser annealing, alloy fluctuations, interfaces and heterojunctions [64].

2.4.11 Mechanical strength measurements

Mechanical strength measurements are carried out using a *AG I Shimadzu Universal Testing Machine (UTM)* (figure 2.10). The machine can measure a load up to 10kN. The pellets samples are standardized by

applying a uniform pressure. The diameter of the probe employed is 5mm.



Fig. 2.10 Universal testing Machine

For quantitative description of mechanical behaviour, it is necessary to derive stress-strain relationships. An ideal elastic solid obeys Hooke's law.

There are 5 important ways in which the mechanical behaviour of a polymer may deviate from this ideal case. The polymer may exhibit

- a. Time dependence of response
- b. Non-recovery of strain on removal of stress
- c. Non-linearity of response (It does not imply non-recovery).
- d. Anisotropy of response

These are essentially independent effects. A polymer may exhibit all or any of them [1].

2.4.12 Thermo power measurements

Thermo power measurements are conducted using a home made Thermo Electric Power (TEP) set up in dc differential technique using copper electrodes. Copper contribution is properly deducted.

The thermo power, or thermoelectric power (also called the **Seebeck coefficient**) of a material is a measure of the magnitude of an induced thermoelectric voltage in response to a temperature difference across that material. The thermo power has units of (V / K) . The term *thermo power* is a misnomer, since it measures the voltage or electric field (not the electric power) induced in response to a temperature difference.

Classically, an applied temperature difference causes charged carriers in the material, whether they be electrons or holes, to diffuse from the hot side to the cold side, similar to a gas that expands when heated. Mobile charged carriers migrating to the cold side leave behind their oppositely charged and immobile nuclei at the hot side thus giving rise to a thermoelectric voltage (thermoelectric refers to the fact that the voltage is created by a temperature difference). Since a separation of charges also creates an electric field, the buildup of charged carriers onto the cold side eventually ceases at some maximum value since there exists an equal amount of charged carriers drifting back to the hot side as a result of the electric field at equilibrium. Only an increase in the temperature difference can resume a buildup of more charge carriers on the cold side and thus lead to an increase in the thermoelectric voltage. Incidentally the thermo power also measures the entropy per charge

carrier in the material. The thermo power of a material, represented as S , depends on the material's temperature, and crystal structure.

If the temperature difference ΔT between the two ends of a material is small, then the thermo power of a material is conventionally (though only approximately, see below) defined as:

$$S = -\frac{\Delta V}{\Delta T} \dots\dots\dots (2.31)$$

Where ΔV is the thermoelectric voltage seen at the terminals.

This can also be written in relation to the electric field E and the temperature gradient ∇T , by the equation:

$$S = -\frac{E}{\Delta T} \dots\dots\dots (2.32)$$

Strictly speaking, these two expressions are only approximate: The numerator of the first equation should be the difference in (electrochemical potential divided by e), not electric potential. Likewise, the second equation should have the gradient of electrochemical potential divided by e rather than the electric field. However, the chemical potential is often relatively constant as a function of temperature, so using electric potential alone is, in these cases, a very good approximation.[65]. Taking the sign into consideration, the equations 2.31 and 2.32 may be rewritten as,

$$S = -\frac{V_{\text{left}} - V_{\text{right}}}{T_{\text{left}} - T_{\text{right}}} \dots\dots\dots (2.33)$$

$$E = S \nabla T \dots\dots\dots (2.34)$$

where "left" and "right" denote two ends of the material. Thus, if S is positive, the end with the higher temperature has the lower voltage, and vice-versa. The electric field will point in the same direction as the temperature gradient.

Note that there is a minus sign in the first equation, but not in the second. This is because the electric field points from the higher voltage towards the lower voltages, whereas the temperature gradient points from the lower temperature towards the higher temperature [66].

2.4.13 Film thickness measurements

Film thickness is recorded using a DEKTAK 6M STYLUS PROFILER working in the range 0.005 μm to 262 μm .

The thickness of the film can be calculated using a modern technique called stylus profiler. It is an advanced thin and thick film step height measurement tool capable of measuring step even below 100 \AA . One can use this to profile surface topography and waviness as well as measuring surface roughness in a sub nanometer range. The stylus is mechanically coupled to the core of an LVDT (Linear Variable Differential Transformer).As the stage moves the sample, the stylus rides over the sample surface. Surface variations cause the stylus to be translated vertically. Electrical signal corresponding to the stylus movement is produced, as the core position of the LVDT changes. The LVDT scales an ac reference signal proportional to the position change, which in turn is conditioned and converted to digital format, through a

high precision integrating analog to digital converter. This signal is stored in computer memory for display [67-69].

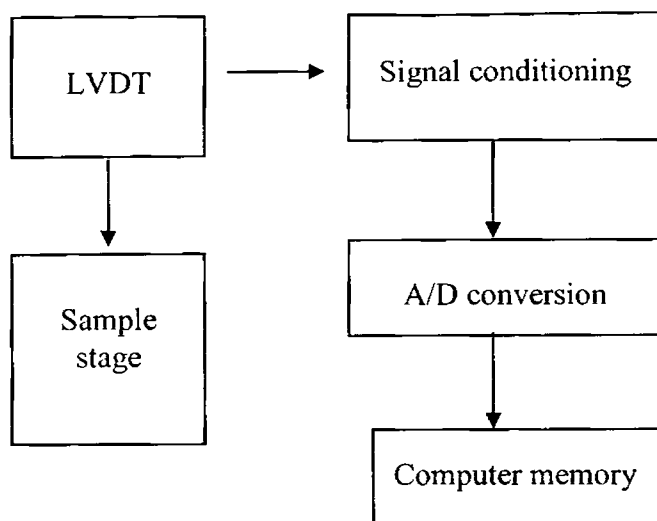


Fig. 2.11 Block diagram of stylus profiler thickness monitor

References

- [1] An introduction to polymer physics, David.I.Bower, Cambridge University Press, Cambridge, UK, 2002
- [2] T A Skotheim,R L Elsenbaumer,J R Reynolds(Eds), Handbook of Conducting Polymers, Marcel Dekker,INC,New York,1998
- [3] W P Su, J R Schrieffer, A J Heeger, Appl.Phys.Lett.42 (1979)1698
- [4] W P Su, J R Schrieffer, A J Heeger, phys.Rev.B.22 (1980)2099
- [5] M J Rice, Phys.Lett.A71 (1979)152
- [6] J Y. Shimano, A G Macdiarmid, Synth.met.123 (2001)251
- [7] S A Brazovskii, N N Kirova, Sov.Sci.Rev.A Phys.5 (1984)99

- [8] S Roth Bleier, *Adv.Phys.*36 (1987)385
- [9] A J Heeger, S Kivelson, J R Schrieffer, W P Su, *Rev.Mod.Phys.*60 (1988)781
- [10] Kiess(Ed), *Conjugated Conducting Polymers*, Springer, New York, 1992
- [11] W R Salaneck, I Lundstrom, B Ranby (Eds), *Conjugated Polymers and Related Compounds*, Oxford Univ.Press, London, 1993
- [12] Reghu Menon, C O Yoon, D Moses, A J Heeger, *Phys.RevB*, 48(1993)17685
- [13] K Lee, S Cho, S H Park, A J Heeger, C W Lee, S H Lee, *Nature*441 (2006)65
- [14] A B Kaiser, *phys.Rev.B*40 (1989)2806 .
- [15] D Moses, A Denenstein, A Pron, A J Heeger, A G MacDiarmid, *Solid State Commun.*36 (1980)219
- [16] J Tsukamoto, A Takahashi, K Kawasaki, *Jpn.J.Appl.Phys.*29 (1990)125
- [17] I Murase, T Ohnishi, T Noguchi, M Hirooka, *Synth.Met.*17 (1984)639
- [18] F E Karaz, J D Capistran, D R Gagnon W Lenz, *Mol.Cryst.Liq. Cryst.*118 (1985)327
- [19] T Hagiwara, M Hirasaka, K Sato, M Yamaura, *Synth.Met.*36 (1990)241
- [20] K Sato, M Yamaura, T Hagiwara, K Murata, M Tokumoto, *Synth.met.*40 (1991)35
- [21] Y Cao, P Smith, A J Heeger, *Synth.Met.*48 (1992)91
- [22] Y Cao, A J Heeger, *Synth.Met.*52 (1992)193
- [23] Y Cao, J J Qiu, P Smith, *Synth.Met.*69 (1995)187

- [24] Y Cao, P Smith, A J Heeger, *Conjugated Polymeric Materials: opportunities in Electronics, Optoelectronics and Molecular Electronics*, (J L Bredas and R R Chance (Eds)), Kluwer Academic, Dodrecht, 1990
- [25] R D McCullough D Lowe, *J.Org.Chem.* 70 (1993)904
- [26] T A Chen, R D Rieke, *J.Am.Chem.Soc.* 114 (1992)10087
- [27] P W Anderson, *Phys.Rev.* 109 (1958)1492
- [28] N F Mott, E A David, *Electronic process in noncrystalline Materials*, Oxford Univ.Press, Oxford, 1979
- [29] N F Mott, *Metal-Insulator Transition*, 2nd ed., Taylor & Francis, London, 1990
- [30] P W Anderson, *Comments Solid State Phys.* 2 (1970)193
- [31] A F Ioffe, A R Regel, *prog.Semicond.* 4 (1960)237
- [32] S Kivelson, A J Heeger, *synth.Met.* 22 (1989)371
- [33] A J Heeger, P Smith, *Conjugated Polymers*(J L Bredas and R Silby(Eds)),Kluwer Academic,Dordrecht,1991,p141
- [34] P Sheng, J Klafter, *Phys.Rev.* B27 (1983)2583
- [35] P Sheng, *Phil.Mag.* 65 (1992)357
- [36] P Sheng, *Phys.Rev.* B21 (1980)2180
- [37] D R Lamb, *Electrical conduction mechanism in thin insulating films*, Methuens and Co ltd, 1967, p56
- [38] Dieter K. Schroder. *Semiconductor material and device characterization*. John Wiley 3rd Ed., 2005.
- [39] J B Pendry, *Low Energy Electron Diffraction*, Academic press, New York, 1974
- [40] K Heinz, *Progr.Surf.Sci.* 27 (1988)239

- [41] B F Lewis J Grunthner, A Madhukar, T C Lee, R Fernandez, J.Vac. Sci.Technol.B3 (Sep/Oct1985)1317
- [42] A R Lang, Modern Diffraction and Imaging Techniques in Materials Science(S.Amelinckx,G.Gevers and J.Van Landuyt (Eds)),North Holland,Amsterdam,1978,p407-479
- [43] B K Tanner-Ray Topography, Pergamon Press, Oxford, 1976
- [44] R N Pangborn, Metals Handbook, 9th ed. (R E Whan, coord) Am.Soc.Metals, Metals Park, OH, 1986, 365-379
- [45] B K Tanner, Diagnostic Techniques for Semiconductor Materials and Devices(T J Shaffer and D K Schroder(Eds)), Electrochem.Soc., Pennington,NJ,1988,p133-149
- [46] A R Lang, J.Appl.Phys.29 (1958)597
- [47] A R Lang, J.Appl.Phys.30 (1959)1748
- [48] B K Tanner-Ray Diffraction Topography, Pergamon Press, Oxford, 1976
- [49] Y Epelboin, Mat.Sci.Eng.73 (1985)1
- [50] F Wenner, Bulletin of the Bureau of Standards12 (1915)469
- [51] J Albers, H L Berkowitz, J.Electrochem.Soc.132 (1985)2453
- [52] H B Bebb,E W Williams, Semiconductors and Semimetals(R K Willardson and A C Beer(Eds)),Academic Press, New York, 1972,181-320
- [53] P J Dean, Prog.Crystal Growth Charact.59 (1982)89
- [54] M V Heimendahl, Electron Microscopy of Materials, Academic Press, New York, 1980
- [55] D B Williams B Carter, Transmission Electron Microscopy, Plenum, NY, 1996
- [56] D C Joy, A D Romig, Jr., J I Goldstein (Eds), Principles of Analytical Electron Microscopy, Plenum Press, New York, 1986

- [57] W R Runyan, T J Shaffner, Semiconductor Measurements and Instrumentation, McGraw Hill, New York, 1998
- [58] V E Cosslet, Advances in Optical and Electron Microscopy (R Barer and V E Cosslet (Eds)), Academic Press, London, 1988, p215-267
- [59] J Bardeen, F J Blatt, L M Hall, Proc photoconductivity Cong., Wiley, New York, 1956, p146
- [60] E A Davis, N F Mott, Phil.Mag.22 (1970)903
- [61] P F Schmidt W Pearce, J.electrochem.Soc.128 (1981)630
- [62] M Grasserbauer, Pure Appl.Chem.60 (1988)437
- [63] R G Downing, J T Maki, R F Fleming, Microelectronic processing: Inorganic material Characterisation (L A Casper (Ed)) American Chemical Soc., Symp.Series, Washington DC, 295(1986)163-180
- [64] R Young Ward Scire, Rev.Sci.Instrum.43 (1972)999
- [65] S Maekawa, T Tohyama, S E Barnes, Physics of Transition Metal Oxides, Springer, 2004
- [66] H J Goldsmid, J Sharp, Thermo electrics: Basic Principles and New Materials Developments, Springer, 2001
- [67] G Stoney, Proc.R.Soc.London Ser.A, 82(1909)172
- [68] R A Jaccodine, W A Schlegel, J Appl.Phys. 37(1966)2429
- [69] W A Brantley, J.Appl.Phys. 44(1973)5344

Chapter **3**

STUDIES ON PANI AND PANI NANO RODS

<i>Contents</i>	3.1 Introduction
	3.2 Synthesis
	3.3 FTIR studies
	3.4 Raman Studies
	3.5 X.R.D Analysis
	3.6 Photoluminescence studies
	3.7 D.C electrical conductivity studies
	3.8 Studies on PANI nano rods
	3.9 Conclusions

3.1 Introduction

The electrical and optical properties of polyaniline (PANI) can be tuned to the appropriate region by doping with protonic acids [1-4]. The doped PANI samples have decent electrical conductivity and excellent stability under ambient conditions. Recently various nanoscale applications have motivated the research on one dimensional (1D) nano scale materials such as nano rods, nano fibers and nano tubes [5-7]. PANI nano materials, in particular have caught much attention due to their enhanced electrical conductivity, environmental stability and colour change corresponding to diverse redox states [8-10]. In this chapter, a comparative study of the structural, morphological, electrical

and thermal properties of PANI and PANI nano rod samples are outlined. The variation of photoluminescence emission intensity and D.C electrical conductivity of micro sized PANI, with the nature of the dopants used, are also studied.

3.2 Synthesis

Freshly distilled aniline (A.R grade) is dissolved in 1.5M dopant acid solution. Ammonium persulphate(APS) dissolved in water is added drop wise to the mixture with continuous stirring for 4-5 hours(Aniline to APS weight ratio is fixed at 3.37). The precipitate obtained is filtered, washed and dried.

3.3 FTIR studies

The FTIR spectra of PANI doped with hydrochloric acid(HCl),camphor sulphonic acid(CSA) and orthophosphoric acid (H_3PO_4) are given in figures3.1-3.3 below.

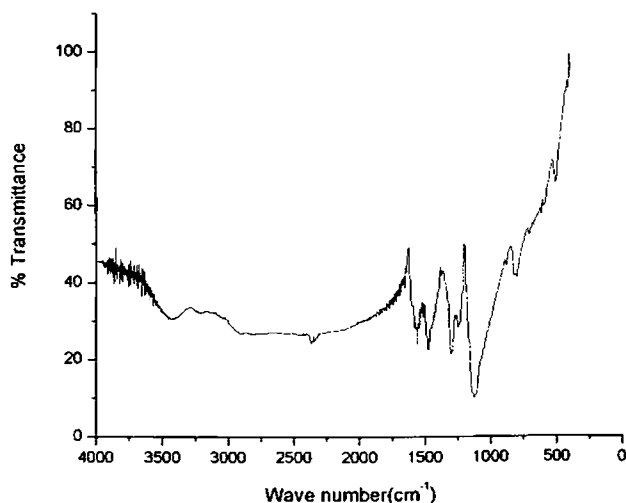


Fig. 3.1 FTIR spectrum of HCl doped PANI

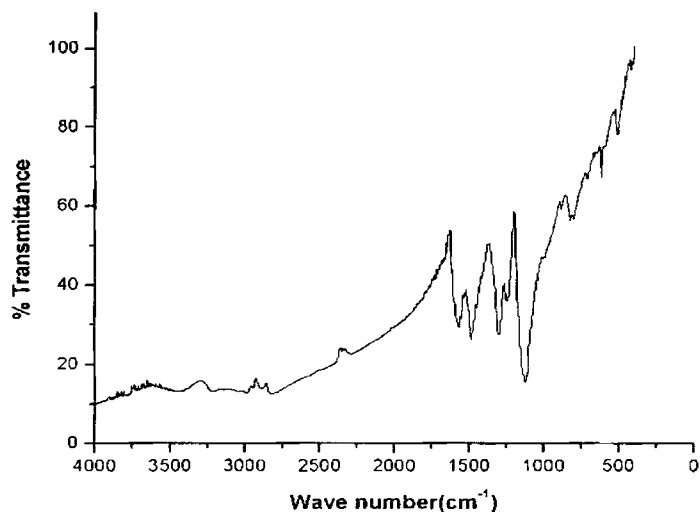


Fig. 3.2 FTIR spectrum of CSA doped PANI

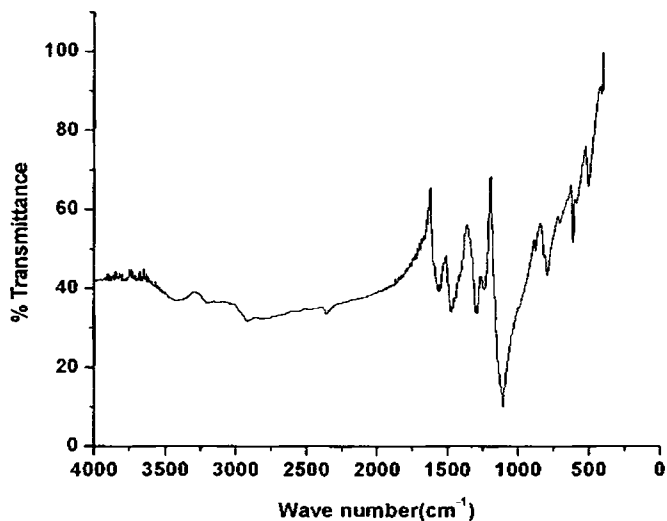


Fig. 3.3. FTIR spectrum of H₃PO₄ doped PANI

The major peaks are at around 3500 cm⁻¹(NH stretching vibration), 2900 cm⁻¹ (CH stretch), 1570 cm⁻¹(C=N stretch of the quinonoid unit of PANI), 1470 cm⁻¹ (C=C stretch of the benzenoid unit of PANI) and 1100 cm⁻¹(quinonoid unit vibration of doped PANI) as reported earlier. [1, 5, 11]

3.4 Raman Studies

The Raman spectra of PANI doped with HCl, CSA and H₃PO₄ are given in figure 3.4.

The major peaks of PANI (HCl) are at 1192 cm⁻¹(C-H bending of the quinonoid ring), 1481 cm⁻¹(C-C in plane deformation of quinonoid ring), 1616 cm⁻¹ (C-C stretching of benzene ring) and 1338 cm⁻¹ (C-N band of polarons) [12-16]. CSA and H₃PO₄ doped PANI samples exhibit a slight shift in vibrational wave numbers and their corresponding intensities. For example, the position corresponding to C-N band of polarons is shifted to 1390 cm⁻¹ and 1409 cm⁻¹ respectively in CSA and H₃PO₄ doped PANI. Both the FTIR and Raman spectra exhibit all the major peaks corresponding to acid doped PANI.

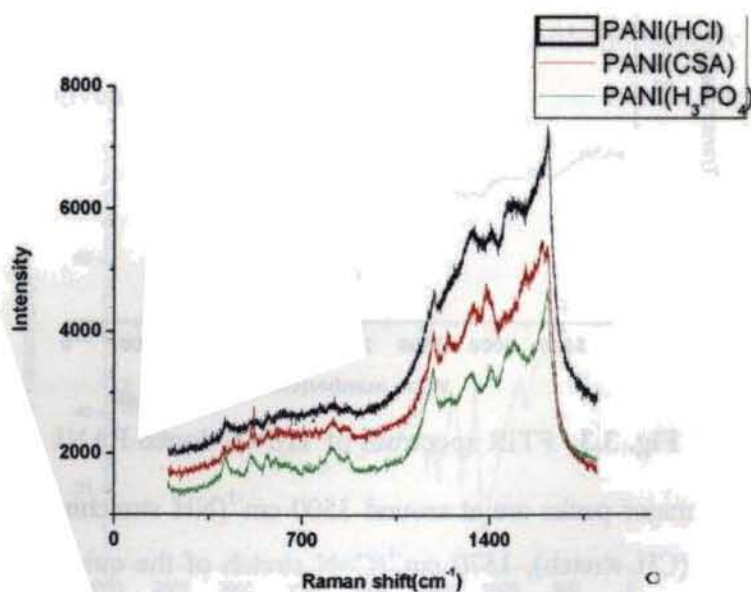


Fig. 3.4 Raman spectra of PANI doped with various acids

3.5 X.R.D Analysis

The X.R.D spectra of PANI doped with HCl, CSA and H₃PO₄ are given in figures 3.5-3.7. All the samples are taken in powder form.

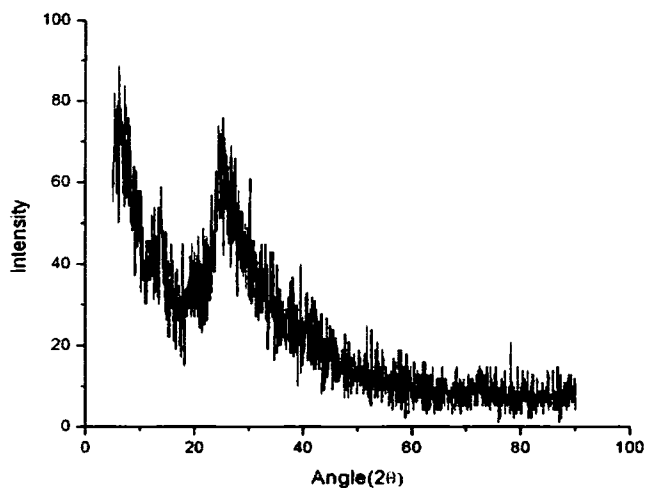


Fig.3.5 X.R.D spectrum of HCl doped PANI

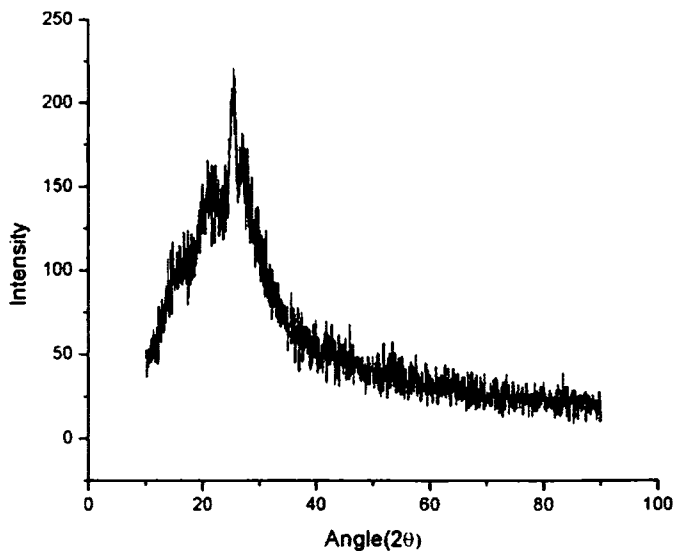


Fig. 3.6 X.R.D spectrum of CSA doped PANI

3.5 X.R.D Analysis

The X.R.D spectra of PANI doped with HCl, CSA and H₃PO₄ are given in figures 3.5-3.7. All the samples are taken in powder form.

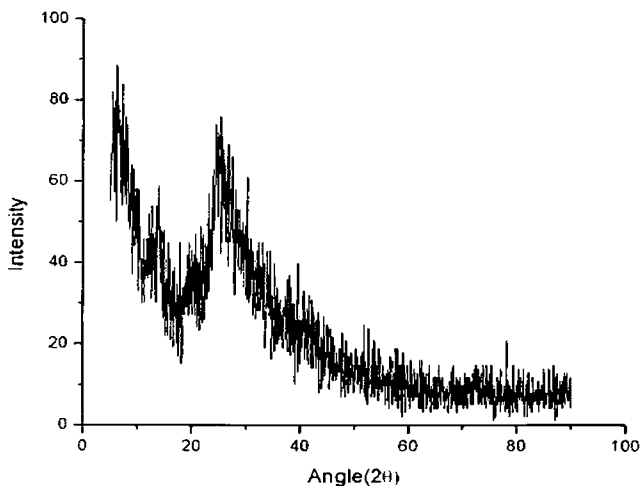


Fig.3.5 X.R.D spectrum of HCl doped PANI

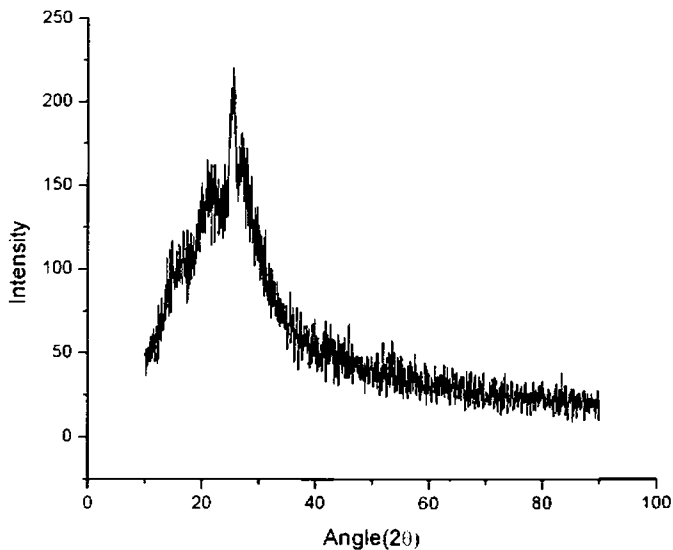


Fig. 3.6 X.R.D spectrum of CSA doped PANI

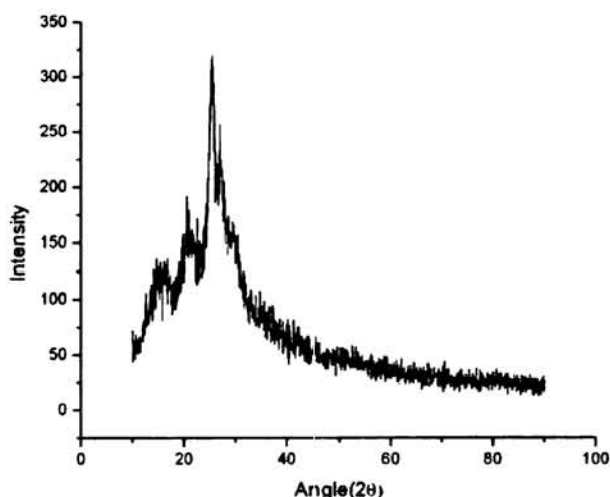


Fig. 3.7 X.R.D spectrum of H₃PO₄ doped PANI

Orthophosphoric acid doped polyaniline shows a crystalline, sharp peak at 25⁰. The peak shown by CSA doped PANI at the same position is less sharp and reduced in intensity, while HCl doped PANI shows only an amorphous peak at the same position. Additionally, orthophosphoric acid doped PANI shows crystalline peaks at 27⁰ and 21⁰ and amorphous peaks at 15⁰ and 30⁰. Peak exhibited by CSA doped PANI at 27⁰ is less crystalline. All other peaks of this sample are amorphous. The peak shown by HCl doped PANI at 15⁰ is also amorphous [16, 17]. Evidently orthophosphoric acid doped PANI shows more crystallinity compared to PANI doped with the other two protonic acids. Accommodating large sized dopant ions such as PO₄⁻ demands greater rearrangement of bonds along the polymer backbone, leading to better crystallinity [1, 18]. This is strongly supported by the fact that the increase in crystallinity of the three PANI samples is in the ascending order of the size of the dopant ion attached. The graphite-

like diffraction peak at around 25° [1, 16, 19] is common to all the samples and is characteristic of the extent of Π conjugation in PANI. Since orthophosphoric acid doped PANI shows the sharpest and the most crystalline peak at 25° , it has the longest order of Π conjugation. In short, the benzenoid and quinonoid units are more orderly arranged in orthophosphoric acid doped PANI compared to PANI doped with the other two acids.

3.6 Photoluminescence studies

The samples in powder form, are excited at 365nm. This is because the π - π^* transition of the benzenoid unit, the unit responsible for photoluminescence in PANI, falls around 330 nm. [20-21]. The samples are excited using a high intense, 450W xenon lamp. The corresponding spectra are shown in figure 3.8.

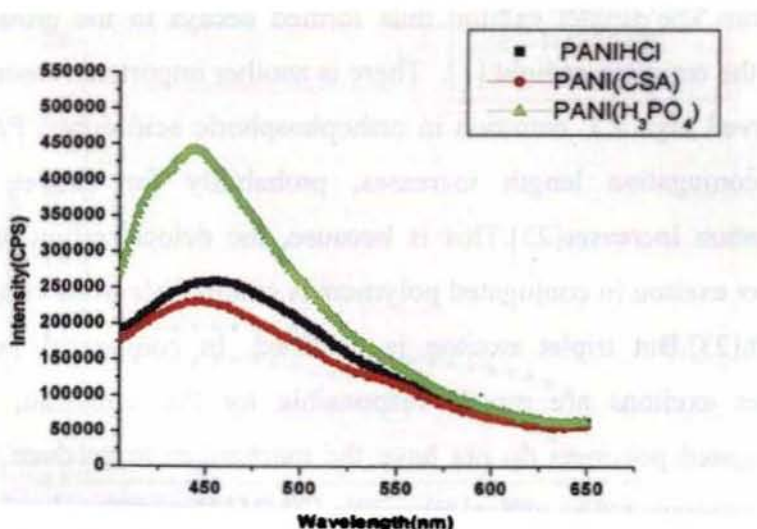


Fig. 3.8 Photoluminescence emission spectra of PANI doped with three different dopants excited using a high intense, 450W xenon lamp (excitation wavelength is 365 nm).

For the three samples, the photoluminescence emission is observed at around 450nm. This corresponds to the HOMO/LUMO transition in the Π - Π^* energy gap [20].

Orthophosphoric acid doped PANI shows the highest luminescence intensity followed by PANI doped with HCl and CSA respectively. The better crystallinity in orthophosphoric acid doped PANI, as evident from its X.R.D spectrum implies that the benzenoid and quinonoid units in it are more orderly arranged, without any unfavourable clustering of quinonoid units. Generally the quinonoid unit quenches the photoluminescence emission due to intrachain energy dissipation [20-22]. The higher extent of Π conjugation coupled with the more orderly arrangement of the benzenoid and quinonoid units observed in orthophosphoric acid doped PANI favours the formation of excitons. The singlet exciton thus formed decays to the ground state with the emission of light [1]. There is another important reason for the observed high P.L emission in orthophosphoric acid doped PANI. As the conjugation length increases, probability for singlet exciton formation increases [23]. This is because, the delocalization length of singlet exciton in conjugated polymers is comparable to its conjugation length [23]. But triplet exciton is confined. In conjugated polymers, singlet excitons are mostly responsible for P.L emission, because conjugated polymers do not have the mechanism to produce the spin flip necessary for an optical transition [24-25]. Hence one should expect higher photoluminescence emission from orthophosphoric acid doped PANI which has a higher extent of Π conjugation. HCl doped PANI

shows slightly better photoluminescence emission compared to the more crystalline CSA doped PANI. The possible reason may be the presence of lighter dopant ions in HCl doped PANI(Cl^-), with greater mobility compared to the heavier dopant ions(SO_3^-) in CSA doped PANI. This favours increased exciton formation and its decay to the ground state results in light emission with enhanced intensity[1].

3.7 D.C electrical conductivity studies

The variation of D.C electrical conductivity with temperature of PANI doped with three different dopants is given in fig 3.9. The temperature range chosen is from 303K to 413K. All the samples are taken in the form of pressed pellets, applying uniform pressure. 4-probe technique has been used to measure the D.C electrical conductivity.

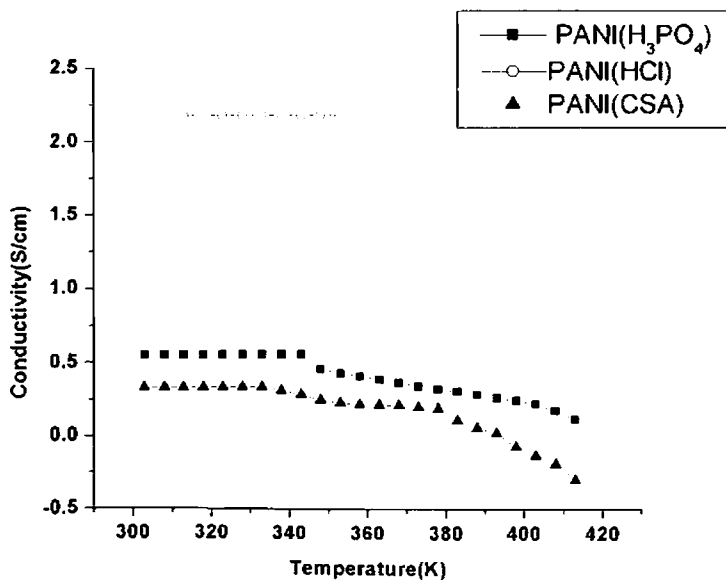


Fig. 3.9 Temperature dependent D.C electrical conductivity plots of PANI doped with various acids

HCl doped PANI shows a flat temperature dependence of D.C electrical conductivity up to about 373K (room temperature conductivity is 2.17S/cm). The reasonably high electrical conductivity of HCl doped PANI is attributed to the high molarity of dopant acid solution used and low mass of Cl⁻ ions. Actually only less than 1% of the available charge carriers contribute to the conductivity of doped PANI. If all the charge carriers contribute, the room temperature conductivity of doped PANI would be comparable to that of copper [20]. In fact PANI is only partially crystalline, with conducting metallic islands separated by large amorphous regions as evident from the X.R.D spectrum (Fig 3.5-3.7). The characteristic metallic conductivity in doped PANI is limited by strong disorder [20, 26]

HCl doped PANI shows the highest room temperature D.C electrical conductivity (2.17S/cm) as compared to CSA (0.30953S/cm) and orthophosphoric acid doped PANI (0.55S/cm). The comparatively higher D.C electrical conductivity of HCl doped PANI as compared to PANI doped with the other two acids may be due to the presence of lighter dopant ions (Cl⁻ ions) in HCl doped PANI as compared to the heavier counterparts in CSA (SO₃⁻) and orthophosphoric acid (PO₄⁻) doped PANI samples. The light weight Cl⁻ ions have greater mobility than the heavier SO₃⁻ and PO₄⁻ ions, resulting in enhanced conductivity. Although PO₄⁻ ions are heavier than SO₃⁻ ions, orthophosphoric acid doped PANI exhibits slightly greater D.C electrical conductivity than CSA doped PANI. The possible reason may be the better crystallinity of orthophosphoric acid doped PANI, due to the large sized PO₄⁻ ions,

demanding greater rearrangement of bonds as explained in the previous section. The more orderly arrangement of the benzenoid and quinonoid units facilitates easier charge transport, compensating for the greater weight of PO_4^- ions. This enhances the D.C electrical conductivity.

The samples show negligible variation of D.C electrical conductivity with temperature, characteristic of polymer samples near the metallic region of metal-insulator transition [27-32].

3.8 Studies on PANI nano rods

Nanoscale materials and devices have grabbed the attention of the scientific community, thanks to their diverse applications [5-7]. PANI nano materials have the added advantage of higher conductivity and better environmental stability. A variety of techniques such as template method, self assembly method, electrochemical polymerization and electro spinning have been employed for the preparation of pani nano rods [8-10]. PANI nano rods could be produced in large scale without undesired byproducts using dispersion polymerization method [33].

3.8.1 Synthesis of PANI nano rods

PANI nano rods with different monomer to oxidant (APS) feed ratios are prepared using dispersion polymerization technique [5]. The synthesis procedure is briefly outlined below.

20 ml of 35 weight% HCl and 2 ml aniline (freshly distilled, A.R grade) are dispersed in 200 ml of distilled water. APS is added to the solution, at a definite monomer to oxidant feed ratio. The resulting mixture

is stirred for 3h. The synthesis temperature is maintained at around -10°C using freezing mixture. The precipitate obtained is filtered, washed and dried. Samples are prepared with different aniline to APS feed ratios. In this method, overgrowth is prevented by stopping the polymerization as soon as the nano rods form. When the reaction starts, the initiator molecules are consumed rapidly during polymerization and depleted after the nano rod formation. Therefore the overgrowth of polyaniline is suppressed due to lack of initiator molecules.

3.8.2 FTIR Analysis

The FTIR spectrum of PANI nano rods is given in figure 3.10.

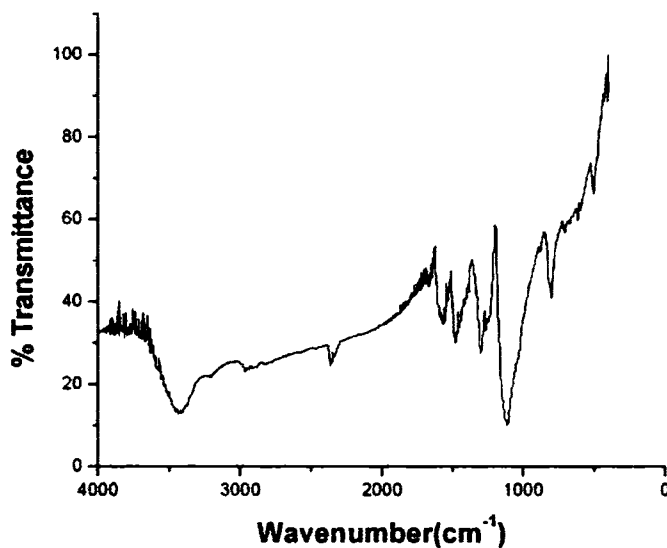


Fig. 3.10 FTIR spectrum of HCl doped PANI nano rods

The spectra show all the characteristic peaks of doped polyaniline as already reported. [1,5]. It is observed that peaks in the spectrum of PANI nano rods are sharper compared to those in micro sized PANI.

3.8.3 X.R.D Analysis

The X.R.D spectra of PANI (micro sized) and PANI nano rod samples(all in powder form) with different aniline to APS feed ratios are given in figure 3.11.

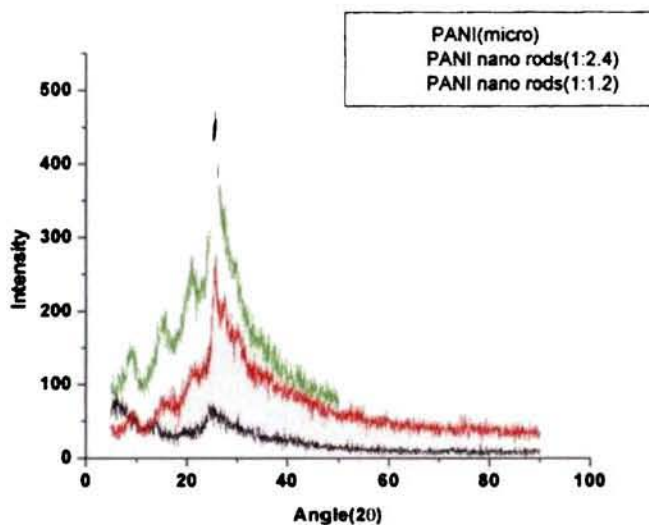


Fig. 3.11 X.R.D spectra of PANI (micro) and PANI nano rod samples

HCl doped PANI shows only amorphous peaks at 25° and 15° , while PANI nano rods show a sharp crystalline peak of much higher intensity at 25° and amorphous peaks at 9° , 15° and 21° . The peak at 25° is common to both the samples and is characteristic of the degree of Π conjugation in PANI [1]. Since PANI nano rods exhibit a sharper and more intense peak at 25° , it has better Π conjugation. It is also observed that, for PANI nano rod samples, the crystallinity decreases with increased addition of APS. As the APS content increases, the rate of polymerization as well as the chain length increases. If the

polymerization rate exceeds a certain limit, it may adversely affect the orderly arrangement of the benzenoid and quinonoid units.

3.8.4 TEM Analysis

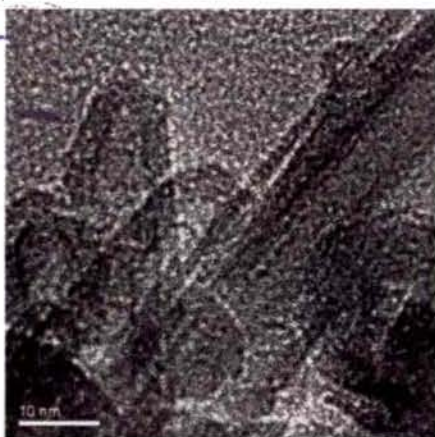


Fig. 3.12a TEM image of a PANI nano rod

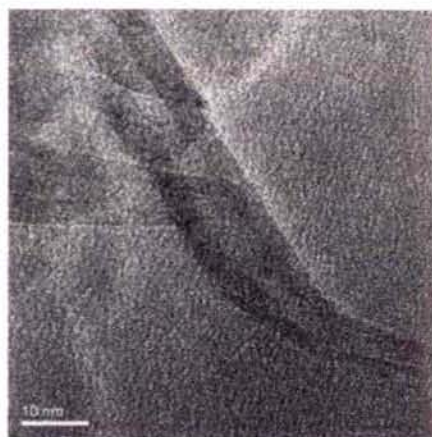


Fig. 3.12b TEM image of another PANI nano rod

TEM images of PANI nano rods (in powder form) are given in figure 3.12a and figure 3.12b.

The average diameter of PANI nano rods is found out to be 10-15nm.

3.8.5 D.C Electrical Conductivity studies

The temperature dependent D.C electrical conductivity plots of PANI nano rod samples synthesized with various aniline to APS feed ratios are given in figure 3.13. The samples are taken in the form of pressed pellets, applying uniform pressure. The measurements are taken using 4-probe technique.

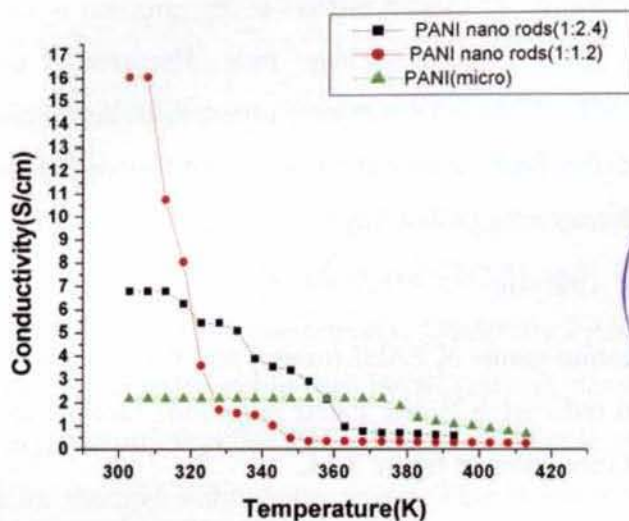


Fig. 3.13. Temperature dependent D.C electrical conductivity plots of HCl doped PANI nano rods synthesized with various aniline to APS feed ratios and HCl doped PANI (micro).

The PANI nano rods exhibit better D.C electrical conductivity than PANI (micro)(2.17S/cm). The better crystallinity of PANI nano rods implies greater long range order favouring effective charge transfer along the chains. This results in higher electrical conductivity. PANI nano rods synthesized with aniline to APS feed ratio 1:1.2 has better room temperature D.C electrical conductivity (16S/cm) than PANI nano rods with aniline to APS feed ratio 1:2.4(7S/cm). This is because of the improved crystallinity of the sample with lower APS loading as explained in section 3.8.3. The conductivity of PANI nano rods is observed to decrease almost exponentially with temperature, unlike the nearly flat temperature dependent behaviour of PANI(micro). The possible reason may be the

greater scattering of the charge carriers at the nano rod walls and at the intersections between different nano rods. The smaller aspect ratio (Length (of the order of nanometers) is not much large compared to diameter) of the PANI nanorods as compared to carbon nano tubes enhances the scattering probability.

3.8.6 T.G.A Analysis

The thermo grams of PANI (micro) and PANI nano rods (aniline to APS feed ratio is 1:1.2) and PANI nano rods (aniline to APS feed ratio is 1:2.4) are given in figure 3.14.

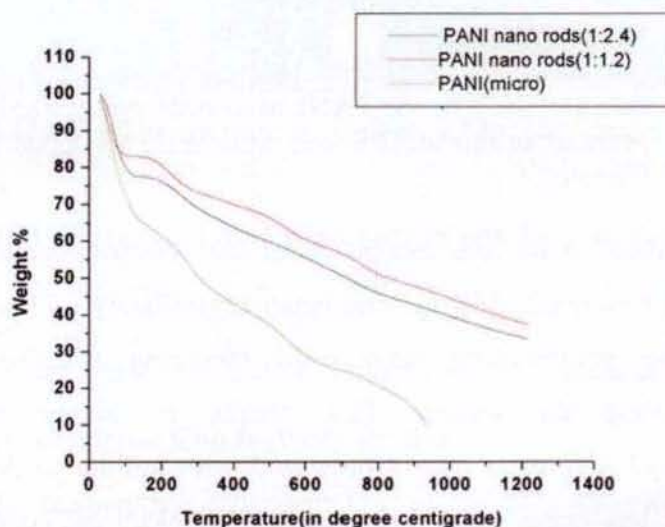


Fig. 3.14 Thermo grams of PANI (micro), PANI nano rods (1:1.2) and PANI nano rods (1:2.4)

Weight loss up to 100⁰ C is mainly due to the evaporation of adsorbed water molecules. Loss of dopants become prominent from a

temperature of 250⁰ C. Degradation of the polymer backbone starts at around 400⁰ C [34].

Up to 300⁰C, PANI(micro) exhibits 50% weight loss, while the corresponding weight loss for PANI nano rods(1:2.4) is 31%, and that for PANI nano rods(1:1.2) is 27%.At 900⁰C, the weight loss for PANI(micro) is 86% and PANI nano rods(1:2.4) and PANI nano rods(1:1.2) are 57% and 52% respectively. Obviously PANI nano rod samples are more thermally stable than PANI (micro), possibly due to their better crystallinity.For the PANI nano rod sample with higher APS feed ratio, thermal stability decreases. This is because, as more amount of APS is added, the chain length increases. This slows down the heat transport along the chains, causing faster degradation. Another possible reason is the better crystallinity of the PANI nano rod sample with lower APS feed ratio.

3.9 Conclusions

Polyaniline (micro sized) samples doped with various acids are synthesized and their structural, electrical and photoluminescence properties are investigated. A comparative study of the photoluminescent properties of polyaniline doped with different acids are carried out.Orthophosphoric acid doped PANI exhibits the highest P.L emission, making it suitable for the fabrication of optoelectronic devices. Temperature dependent D.C electrical conductivity studies reveal that HCl doped PANI has the highest room temperature D.C electrical conductivity which stays almost constant with temperature (above room temperature).

The structural, morphological, electrical and thermal properties of polyaniline nano rod samples are investigated. The polyaniline nano rod samples exhibit better crystallinity as compared to micro sized PANI. TEM measurements reveal that they are rod like in shape. The entire polyaniline nano rod samples show better D.C electrical conductivity and thermal stability as compared to micro sized PANI. The crystallinity of the PANI nano rod samples is found to decrease with increase in the APS feed ratio. Obviously the polyaniline nano rod sample with the lowest APS feed ratio exhibits the highest room temperature D.C electrical conductivity and thermal stability.

References

- [1] M Amrithesh, S Aravind, S Jayalekshmi, R S Jayasree, J. Alloys Compd 458 (2008) 532
- [2] A Pud, N Ogurtsov, A Korzhenko, G Shapoval, Prog. Polym. Sci 28 (2003) 1701
- [3] C Y Yang, Y Cao, P Smith, A J Heeger, Synth. Met. 53(1993)293
- [4] Y Long, Z Chen, N Wang, J Li, M Wan, Physica B 344(2004)82
- [5] J Jang, J Bae, K Lee, Polymer 46(2005)3677
- [6] S J Tans, A R M Verschueren, C Dekker, Nature, 393(1998)49
- [7] R Q Long, R T Yang, J. Am. Chem. Soc. 123(2001)2058
- [8] Z Wang, M Chen, H L Li, Mater. Sci. Eng. A 328(2002)33
- [9] Z Wei, Z Zhang, M Wan, Langmuir 18(2002)917
- [10] J Stejskal, M Spirkova, A Riede, M Helmstedt, P Mokreva, J Prokes, Polymer 40 (1999)2487

- [11] A J Bellamy, *The Infra-red spectra of Complex Molecules*, Second ed., John Wiley & Sons, New York, 1962
- [12] S Tao, Bi Hong, Z Kerong, *Spectrochim Acta Part A* 66(2007)1364
- [13] G.M. do Nascimento, M.L. A. Temperini, *J.Raman Spectrosc.* 39 (2008), 772
- [14] G Messina, A Paoletti, S Santangelo, A Taliaferro Tucciarone, *J.Appl. phys.* 89 (2001)1053
- [15] V Baranauskas, H J Ceragidi, A C Peterlevitz, J C R Quispe, *J.Phys: Conference series* 61(2007)71
- [16] X Zhang, J Zhang, Z Liu, *Appl.Phys.* A80(2005)1813
- [17] H K Chaudhari, D S Kelkar, *Polym.Int.* 42(1997)380
- [18] T A Skotheim, R L Elsenbaumer, J R Reynolds(Eds), *Hand Book of Conducting Polymers*, Marcel Dekker, Inc., New York, 1998, p945-946
- [19] S W Liu, J Yue, R J Wehmschulte, *Nano Lett.* 2(2002)1439
- [20] J Y Shimano, A G MacDiarmid, *Synth.Met.* 123(2001)251
- [21] J R G Thorne, J G Master, S A Williams, A G Mac Diarmid, R M Hochstrasser, *Synth.Met.* 49/50(1992)423
- [22] M K Ram, G Mascetti, S Paddue, E Maccioni, C Nicolini, *Synth. Met.* 89 (1997)63
- [23] M Wohlgenannt, Z V Vardeny, *J.Phys:Condens.Matter* 15(2003)R83
- [24] A Kohler, J S Wilson, R H Friend, *Adv.Mater* 14(2002)701
- [25] N J Turro, *Modern Molecular Photo Chemistry*, University Science Books, California, CL, 1991
- [26] A B Kaiser, *Phys.Rev.* B40(1989)2806

- [27] Reghu Menon, C O Yoon, D Moses, A J Heeger, Phys. Rev B, 48(1993)17685
- [28] K Lee, S Cho, S H Park, A J Heeger, C W Lee, S H Lee, Nature 441 (2006)65
- [29] T A Skotheim, R L Elsenbaumer, J R Reynolds (Eds), Hand Book of Conducting Polymers, Marcel Dekker, Inc., New York, 1998, p27-84
- [30] A J Heeger, Phys.Scr. T102(2002)30
- [31] M Ahlskog, M Reghu, A J Heeger, J.Phys:Condens. Matter 9 (1997) 4145
- [32] Y Long, Z Chen, N Wang, J Li, M Wan, Physica B 344(2004)82
- [33] V L Covalan, S D'Antone, G Ruggeri, E Chiellini, Macromolecules 33 (2000)6685
- [34] L.Abell, S.J.Pomfret, P.N.Adams, A.P.Monkman, Synth. Met. 84 (1997), 127-128

Chapter 4

STUDIES ON PANI (HCl)-PMMA COMPOSITES

<i>Contents</i>	4.1 Introduction
	4.2 Preparation of PMMA sheets
	4.3 Synthesis of PANI-PMMA composites
	4.4 FTIR Analysis
	4.5 Raman Studies
	4.6 Photoluminescence(P.L) studies
	4.7 D.C electrical conductivity studies
	4.8 Thermo Gravimetric Analysis
	4.9 Mechanical strength measurements
	4.10 Conclusions

4.1 Introduction

In spite of many of their attractive electrical and optical properties, a large number of the conducting polymers have low mechanical strength and are difficult to process [1-2]. By making composites with suitable conventional polymers, the physical properties such as mechanical strength and processibility can be improved [2-14]. In addition to it, the properties of the guest polymer can be beautifully blended with that of the host polymer. Polymer composites can be prepared either by mechanical blending or by chemical insitu polymerisation. Of the two, chemical polymerisation gives more uniform composition [1].

Polyaniline (PANI) has attracted global interest because of its excellent electrical properties, stability in air and ease of synthesis [15]. In suitably doped form, its applicability as hole-injecting electrode in electro luminescent devices is one of the hot areas of research in the field of polymer optoelectronics [16-19]. Its composites with many other polymers are also being pursued for optoelectronic applications [20,21]. Polyaniline can be prepared in bulk form using chemical oxidative polymerization or in thin film form using plasma polymerization technique, electrochemical deposition, spin coating or solution casting [22].

One of the negative aspects of polyaniline is its comparatively low mechanical strength, which limits its applications to some extent [2]. By making composites with polymethylmethacrylate (PMMA), the mechanical strength of polyaniline can be improved [20]. Also the excellent optical properties of PMMA can be suitably incorporated into the host polymer. In this chapter, the focus is on the structural, optical, electrical, thermal and mechanical characterization of PANI-PMMA composites.

4.2 Preparation of PMMA sheets

In order to fully exploit the excellent optical properties and the mechanical strength of PMMA, we have worked with bulk polymerized PMMA instead of the widely used emulsion polymerized PMMA. The monomer methylmethacrylate (MMA) is washed first with 20% sodium hydroxide solution to remove the inhibitors and then with distilled water. The initiator benzoyl peroxide is added to MMA and stirred for

2-3 hours at around 80⁰C till the solution becomes viscous. The resulting solution is poured into a dish and kept for drying till crystal clear PMMA sheets are obtained

4.3 Synthesis of PANI-PMMA composites

Freshly distilled aniline (A.R grade) is mixed with 1.5M hydrochloric acid. PMMA dissolved in toluene is added to it. Ammonium persulphate (APS) dissolved in water is added drop wise to the resulting mixture with continuous stirring. Aniline to APS weight ratio is fixed at 3.37. The temperature is maintained at around -10⁰C and stirring is allowed to proceed for 4-5 hours. The precipitate obtained is filtered, washed several times and dried. Since the synthesis temperature is low and the molarity of the oxidant high, the amount of unutilized reagents is very small. Hence the synthesis is very much environment friendly.

4.4 FTIR Analysis

The FTIR spectrum of PANI-PMMA composite (Fig 4.1) shows all the major peaks of HCl doped PANI as well as PMMA [20, 22-25]. This confirms the fact that PANI has been dispersed as an interpenetrating network in the PMMA matrix.

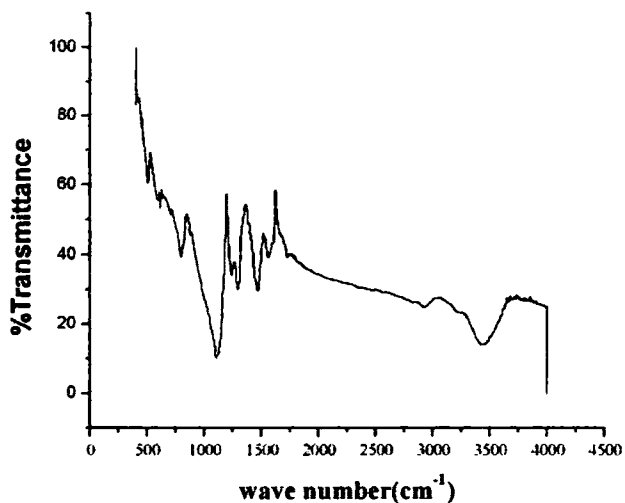


Fig. 4.1 FTIR spectrum of PANI (HCl)-PMMA composite

Table 4.1 The wave numbers of various vibration peaks observed and the corresponding assignment of vibrations

Wave No: (cm⁻¹)	Assignment of Vibrations
3436	N-H Stretching Vibration in PANI
1726	C=O Stretching in PMMA
1564	C=N Stretching in PANI
1467	O-CH ₃ Deformation in PMMA
1298	C-N Stretching mode of benzenoid unit of PANI
1241	C-O Stretching in PMMA
1107	Quinonoid unit vibration of doped PANI
871	Skeletal vibration of PMMA
799	C-C and C-H stretch for the benzenoid unit of PANI

4.5 Raman Studies

The Raman spectra of PANI (HCl) and PANI (HCl)-PMMA composite (1:1) is shown in figure 4.2.

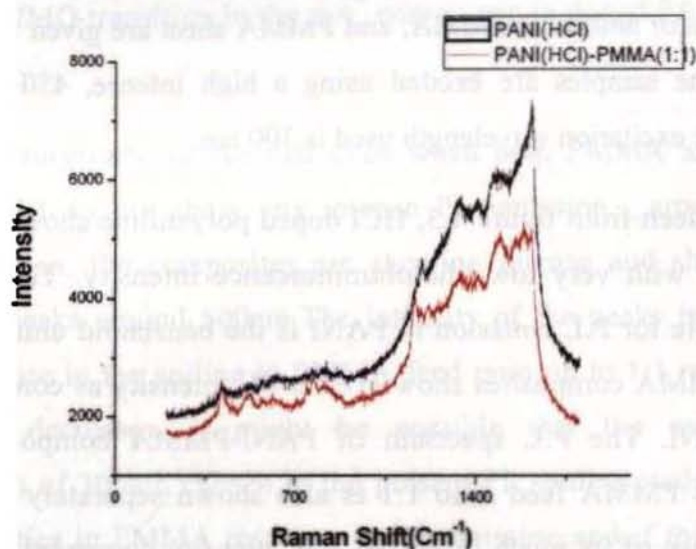


Fig. 4.2 Raman spectra of PANI (HCl) and PANI (HCl)-PMMA (1:1) composite

PANI(HCl) exhibits all the significant vibrations as reported in section 3.4. PANI(HCl)-PMMA composite shows all the major vibrations of PANI(HCl). Additionally it exhibits the peaks of PMMA at 771cm^{-1} (C-C skeletal mode vibration), 818cm^{-1} (C-O-C symmetric stretching mode), 966cm^{-1} (CH_2 rock) and 1217cm^{-1} (C-O vibration). The C=O vibration of PMMA at 1720cm^{-1} is blue shifted to 1620cm^{-1} in the composite [26]. This highlights the possibility of electron transfer between the bulky C=O group of PMMA and NH group of PANI. Thus the formation of PANI(HCl)-PMMA composite is confirmed.

4.6 Photoluminescence(P.L) studies

The photoluminescence spectra of HCl doped PANI and HCl doped PANI-PMMA composites(all in powder form) with different feed ratios of aniline to PMMA, and PMMA sheet are given in figures 4.3-4.5. The samples are excited using a high intense, 450W xenon lamp. The excitation wavelength used is 300 nm.

As seen from figure 4.3, HCl doped polyaniline shows a broad spectrum with very low photoluminescence intensity. The species responsible for P.L emission in PANI is the benzenoid unit [27-28]. PANI-PMMA composites show greater PL intensity as compared to pure PANI. The P.L spectrum of PANI-PMMA composite with aniline to PMMA feed ratio 1:1 is also shown separately in figure 4.4 because of its much increased P.L intensity compared to PANI and other PANI-PMMA composites. For comparison, the P.L spectrum of pure PMMA is shown in figure 4.5. Since the intensity of the P.L emission peak of PMMA centered on 450 nm is much smaller compared to that of PANI and PANI-PMMA composites, it is shown separately.

The analysis of the P.L spectra shows that though pure PMMA shows a P.L emission peak at 450 nm, it is much reduced in intensity compared to that of PANI and PANI-PMMA composites. As mentioned earlier, the P.L spectrum of HCl doped PANI is quite broad and featureless. Coming to the spectrum of PANI-PMMA composites, it is seen that the P.L emission intensity increases

drastically with increase in PMMA content in the composites, till it saturates for the 1:1 feed ratio. The emission peak is centered at around 502 nm in all the composites which could be attributed to HOMO/LUMO transition in the π - π^* energy gap in doped PANI [28-30].

It is surprising to see that even when both PMMA and HCl doped PANI do not show any intense PL emission, around the 500nm region, the composites are showing intense and sharp PL emission peaks around 500nm. The intensity of the peaks increases with increase in the aniline to PMMA feed ratio up to 1:1 ratio and thereafter decreases. It might be possible that the excitation wavelength of 300nm chosen in the present PL studies could excite the impurities in PMMA resulting in PL emission and if this is the case the intensity of the emission peak will increase with increase in PMMA content. However in the present case, definitely, this is not the situation, since the intensity of PL emission in PMMA is much less (fig 4.5) compared to that in the composites. Also the emission peak in PMMA is around 450nm where as that in the composites is just above 500nm. The enhancement of the PL emission intensity in the composites with increase in PMMA content can be explained as follows.

There are electron donating groups such as $>NH$ in PANI and electron withdrawing groups such as $>C=O$ in PMMA. This combination enhances the π electron mobility in the composites. So as PMMA content increases in the composites the combination probability

and hence the π electron mobility increases further. This in turn favours the formation of singlet excitons. The singlet exciton states so formed decay radiatively to the ground state resulting in enhanced photoluminescence [20, 31]. The P.L emission intensity decreases for the PANI (HCl)-PMMA (1:2) composite and the spectrum turns broad and featureless. This may be due to the increased barrier width attributed by the increased PMMA content (PMMA is insulating). This decreases the Π electron mobility and thereby the luminescence intensity. This observation is well supported by the reduced D.C electrical conductivity value observed for the composite synthesized in this feed ratio, as detailed in the next section.

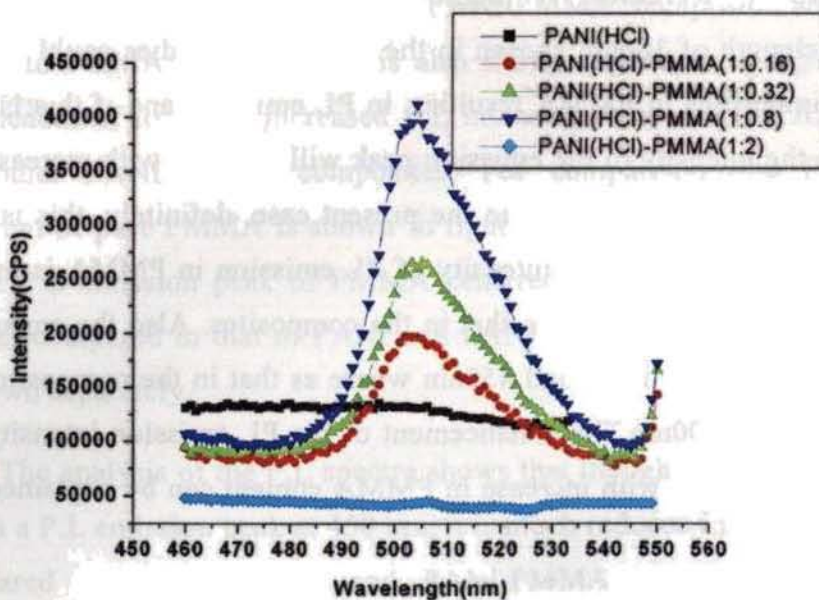


Fig. 4.3 Photoluminescence emission spectrum of HCl doped PANI and HCl doped PANI-PMMA composites synthesized with different aniline to PMMA feed ratios.

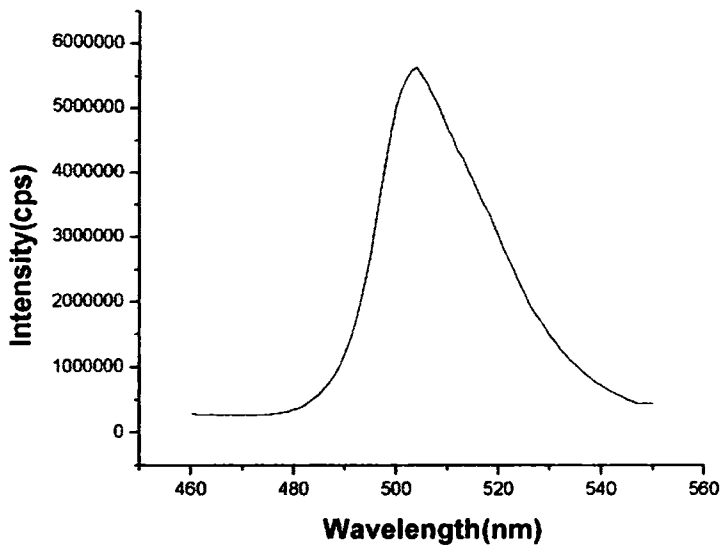


Fig. 4.4 Photoluminescence emission spectrum of PANI (HCl)-PMMA composite with aniline to PMMA feed ratio 1:1.

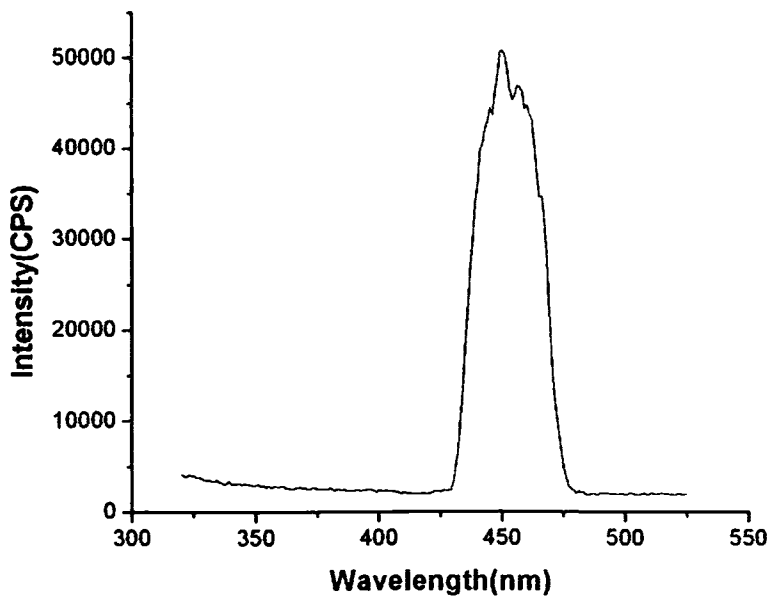


Fig. 4.5 Photoluminescence emission spectrum of PMMA

4.7 D.C electrical conductivity studies

Temperature variation of D.C electrical conductivity of HCl doped PANI and HCl doped PANI-PMMA composites, measured using 2-probe technique, are shown in figures 4.6 and 4.7. All samples are taken in the form of pressed pellets, applying uniform pressure. The temperature range chosen is 10K-300K.

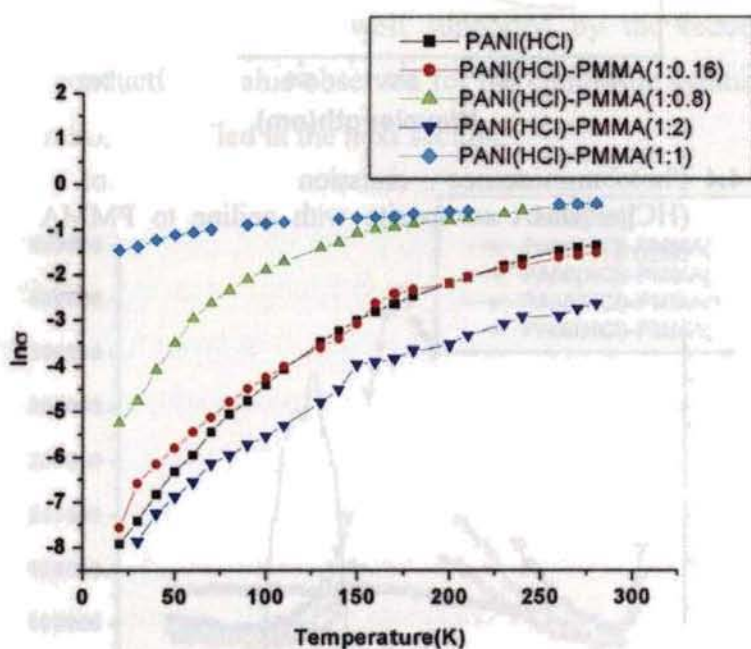


Fig. 4.6 $\ln\sigma$ vs. temperature plots of PANI (HCl) and PANI (HCl)-PMMA composites, measured using 2-probe technique

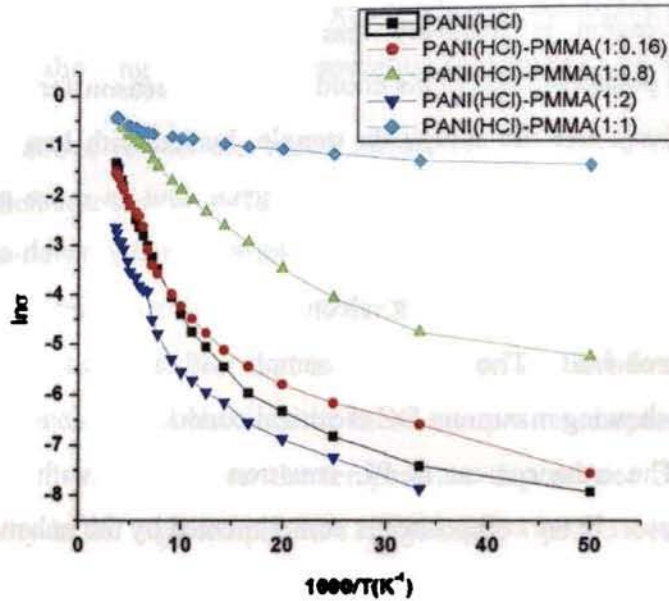


Fig. 4.7 $\ln\sigma$ vs. $1000/T$ plots of PANI (HCl) and PANI (HCl)-PMMA composites measured using 2 probe technique

From the figure it is obvious that the DC electrical conductivity of the composites is higher than that of HCl doped PANI and also it increases with increase in PMMA content in the composites up to 1:1 ratio and thereafter decreases for the 1:2 ratio. This result is all the more interesting since PMMA is an insulator. The increase in conductivity is explained as follows. In PANI-PMMA composites, the conducting PANI regions are interconnected by insulating PMMA regions. By adding PMMA, increase in conductivity occurs due to electronic tunneling through non-conducting PMMA separating mesoscopic conducting PANI islands [32]. Particles in PANI and PANI-PMMA are comprised of ordered regions surrounded by disordered or partly disordered regions. PANI is more disordered and contains localized spinless bipolarons. On the other hand, PANI-PMMA's

disordered region is relatively less disordered and contains partly delocalized polarons[33-37]. This could be another reason for the increase in conductivity. For the composite sample, loaded with less amount of PMMA, the conductivity increase is marginal. But as more amount of PMMA is added, the conductivity increases appreciably which can be due to increased enhancement in π electron mobility owing to increased tunneling probability. The composite sample with aniline to PMMA feed ratio 1:1 is showing maximum DC electrical conductivity and PL emission intensity. The enhancement in PL emission intensity with increase in PMMA content in the composites is complimented by the enhancement in DC electrical conductivity with increase in PMMA content. The enhancement in π electron mobility with increase in PMMA content is the common major factor contributing towards both of these mechanisms.

The reason for the decrease in D.C electrical conductivity for the 1:2 ratio is the presence of higher amount of PMMA, which is a known insulator. The higher PMMA content in the composite lowers the Π electron mobility as discussed earlier. As evident from the figure, the most conducting sample in the set, PANI(HCl)-PMMA (1:1) is showing a flat temperature dependence compared to the less conducting samples. Even for the less conducting samples, the variation in D.C electrical conductivity with temperature is less beyond about 150K up to 300K (figure 4.6). This is in close agreement with the earlier reports on the temperature dependence of D.C electrical conductivity in doped PANI thin films, where the less conducting samples are showing

temperature dependence to some extent, whereas the highly conducting samples are showing quite flat temperature response [15,38-39].

The above results are based on the D.C electrical conductivity measurements in the range 10K-300K using 2-probe technique.4-probe measurement technique, which is more accurate, could not be used in the above temperature range due to limitations of the apparatus. Taking into consideration, the fact that much attention has not been given to the high temperature behaviour of these composite samples, we have carried out investigations on the temperature dependence of electrical conductivity in the high temperature range using 4-probe technique.

The results are shown in fig4.8.

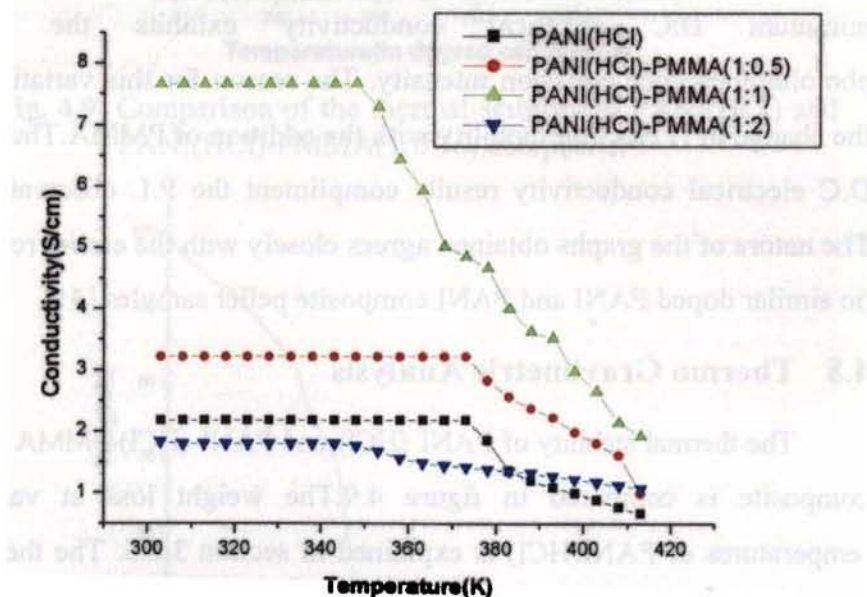


Fig. 4.8 Temperature variation of D.C electrical conductivity of PANI (HCl) and PANI (HCl)-PMMA composites measured using 4 probe technique.

The samples show negligible variation of conductivity with temperature from room temperature to about 360K characteristic of highly conducting samples[40]. The room temperature D.C electrical conductivity of HCl doped PANI is 2.17S/cm while that of HCl doped PANI-PMMA composite synthesized in the 1:1 ratio is 7.66S/cm. It decreases to 1.79S/cm for aniline to PMMA feed ratio 1:2. The D.C electrical conductivity is almost constant up to about 360K and thereafter decreases monotonically. The decrease in D.C electrical conductivity at high temperatures could be due to enhanced charge carrier scattering at elevated temperatures. The sample with the maximum D.C electrical conductivity (1:1) shows the maximum photoluminescence emission intensity, while the sample with the minimum D.C electrical conductivity exhibits the least photoluminescence emission intensity. The reason for this variation is the change in Π electron mobility with the addition of PMMA. Thus the D.C electrical conductivity results compliment the P.L observations. The nature of the graphs obtained agrees closely with the earlier reports on similar doped PANI and PANI composite pellet samples [41].

4.8 Thermo Gravimetric Analysis

The thermal stability of PANI (HCl) and PANI (HCl)-PMMA (1:1) composite is compared in figure 4.9. The weight loss at various temperatures of PANI(HCl) is explained in section 3.8.6. The thermal stability of PANI(HCl)-PMMA(1:0.16) composite is more or less the same as compared to PANI(HCl). Even though the thermal stability of PMMA is much less (figure 4.10), the thermal stability of the composite

does not drop considerably. The reason may be explained as follows. As the PMMA feed ratio increases, the electrical conductivity increases. Consequently the thermal conductivity also increases, compensating for the low thermal stability of PMMA.

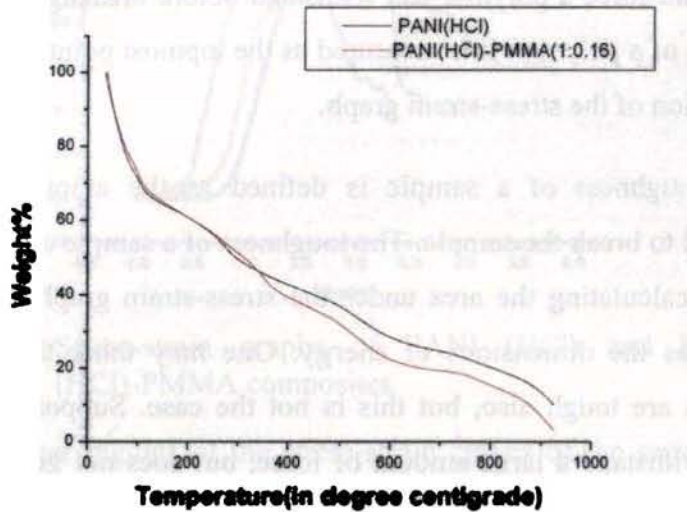


Fig. 4.9 Comparison of the thermal stability of PANI(HCl) and PANI(HCl)-PMMA(1:0.16) composite.

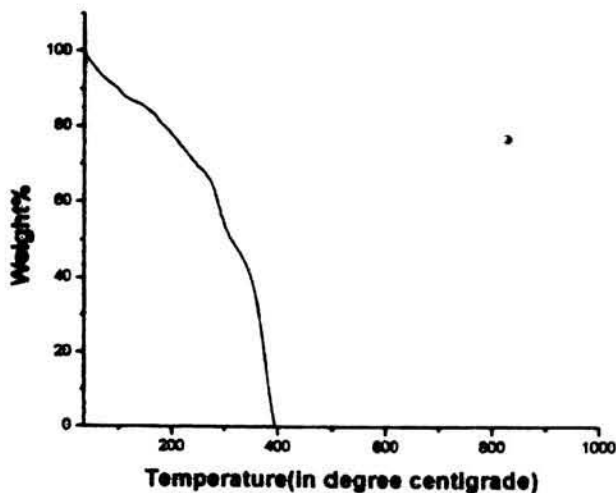


Fig. 4.10 T.G.A plot of PMMA

4.9 Mechanical strength measurements

Three major parameters related to mechanical strength measurements are strength, toughness and young's modulus. The maximum force a polymer can withstand before breakage is called the strength of a polymer. It is measured as the topmost point in the straight line region of the stress-strain graph.

Toughness of a sample is defined as the amount of energy required to break the sample. The toughness of a sample could be found out by calculating the area under the stress-strain graph, because the latter has the dimensions of energy. One may think that all strong samples are tough also, but this is not the case. Suppose the sample could withstand a large amount of force, but does not get compressed much before it breaks. Then, the sample is really strong, but not tough. But if a large elongation occurs for a greater applied stress and the sample withstands greater force before it breaks, the specimen is indeed strong as well as tough[42-44]. The desired objective is to prepare samples with considerable strength and toughness. The stress to strain ratio of the sample is termed the young's modulus. It is calculated from the slope of the linear region of the stress-strain graph.

The samples are pressed into pellets under uniform pressure. Stress is applied on the samples by a probe of 5mm diameter and the corresponding stroke is measured. The stress-strain graphs of PANI(HCl) and PANI (HCl)-PMMA composites of various weight ratios are given in the figure 4.11.

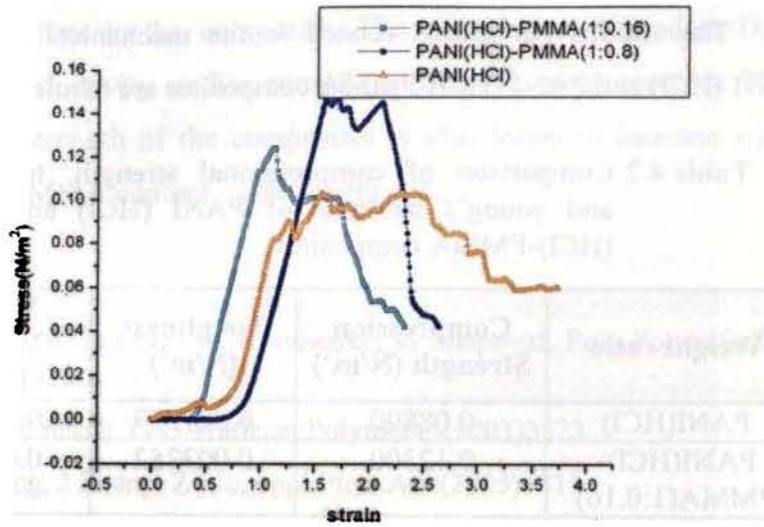


Fig. 4.11 Stress-strain graphs of PANI (HCl) and PANI (HCl)-PMMA composites

The linear regions of the stress-strain curves of the samples are given in figure 4.12.

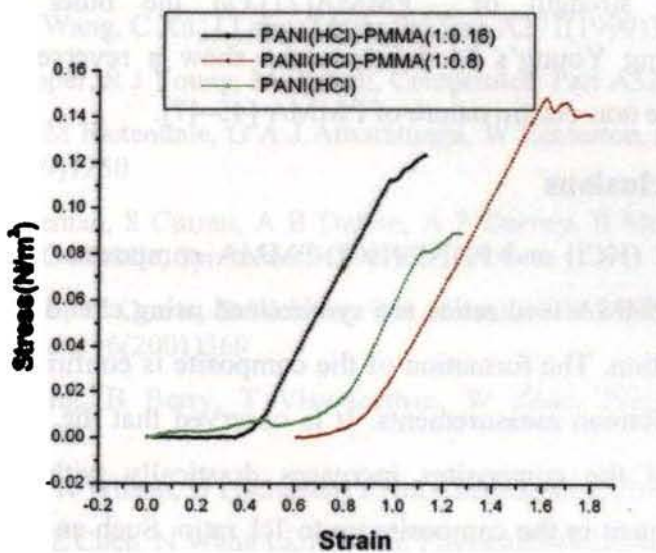


Fig. 4.12 Linear portion of stress-strain graphs

The various parameters related to the mechanical strength of PANI (HCl) and PANI (HCl)-PMMA composites are tabulated below.

Table 4.2 Comparison of compressional strength, toughness and young's modulus of PANI (HCl) and PANI (HCl)-PMMA composites

Weight ratio	Compression Strength (N/m ²)	Toughness (N/m ²)	Young's Modulus (N/m ²)
PANI(HCl)	0.08890	0.001589	0.020697
PANI(HCl)-PMMA(1:0.16)	0.12300	0.003252	0.020051
PANI(HCl)-PMMA(1:0.8)	0.14780	0.005494	0.019230

The compression strength and toughness are found to increase with increased weight ratios of PMMA. This is due to the good mechanical strength of PMMA[21]. On the other hand, the corresponding Young's Modulus values show a reverse trend. The reason is the non-elastic nature of PMMA [45-47].

4.10 Conclusions

PANI (HCl) and PANI (HCl)-PMMA composites with various aniline to PMMA feed ratios are synthesized using chemical oxidative polymerization. The formation of the composite is confirmed from the FTIR and Raman measurements. It is observed that the P.L emission intensity of the composites increases drastically with increase in PMMA content in the composite up to 1:1 ratio. Such an enhancement in the emission intensity is due to the increase in Π electron mobility, brought about by the presence of electron donating and electron

accepting groups in the composite. The temperature dependent D.C electrical conductivity studies compliment the P.L measurements. The mechanical strength of the composites is also found to increase with increase in PMMA content in the composite.

References

- [1] A Pud, N Ogurtsov, A Korzhenko, G Shapoval, Prog.Polym.Sci28 (2003)1701
- [2] A Mirmohseni, G G Wallace, Polymer44(2003)3523
- [3] X Zhang, J Zhang, Z Liu,Appl.Phys.A80(2005)1813
- [4] E T Thostensona, Z Renb, T W Choua,Compos. Sci.Technol.61 (2001)1899
- [5] K T Lau,D Hui,Compos.Pt.B-Eng.33(2002)263
- [6] R H Baughman, A A Zakhidov, W A Heer,Science197(2002)787
- [7] L Dai,A W H Mau,Adv.Mater.13(2001)899
- [8] Z Jia, Z Wang, C Xu, J Lang, Mater.Sci.Eng.A271(1999)395
- [9] C A Cooper, R J Young, M Halsall, Composites: Part A32(2001)401
- [10] I Musa, M Baxendale, G A J Amaratunga, W Eccleston, Synth.Met. 102(1999)1250
- [11] J N Coleman, S Curran, A B Dalton, A P Darvey, B McCarthy, W Blau, R C Barklie, Synth.Met.102 (1999)1174
- [12] H S Woo, R Czerw, S Webster, D L Caroll, J W Park, J H Lee, Synth.Met.116(2001)369
- [13] C H Song, B Berry, T Viswanathan, W Zhao, Polym.Prepr.41 (2000)1102
- [14] Y Sun, S R Wilson, D I Schuster, J.Am.Chem.Soc.123(2001)5348
- [15] Y Long, Z Chen, N Wang Li, M Wan, PhysicaB344 (2004)82
- [16] Y Yang, A J Heeger, Appl.Phys.Lett.64 (1994)1245

- [17] Y Yang, E Westerweele, C Zhang, P Smith, A J Heeger, *J.Appl. Phys.*77 (1995)694
- [18] G Gustafsson, Y Cao, G M Treacy, F K Lavetter, N Colaneri, A J Heeger, *Nature*357 (1992)477
- [19] S A Carter, M Angelopoulos, S Karg, P J Brock, J C Scott, *Appl. Phys.Lett.*70 (1997)2067
- [20] M Amrithesh, S Aravind, S Jayalekshmi, R S Jayasree, *J.Alloys Compd.*449 (2008)176
- [21] V R Gowariker, N V Viswanathan, Jayadev Sreedhar, *Polymer Science, New Age International(p) Limited, New Delhi, 1996, p-220*
- [22] T A Skotheim, R L Elsenbaumer, J R Reynolds (Eds), *Hand Book of Conducting Polymers, Marcel Dekker, Inc., New York, 1998*
- [23] M Amrithesh, S Aravind, S Jayalekshmi, R S Jayasree, *J.Alloys Compd.*458 (2008)532
- [24] J Jang, J Bae, K Lee, *Polymer*46 (2005)3677
- [25] A J Bellamy, *The Infra-red spectra of Complex Molecules, Second ed., John Wiley & Sons, New York, 1962*
- [26] X XingSheng, M Hai, Z Qijing, Z Yunsheng, *J.Opt.A: Pure Appl. Opt.*4 (2002)237
- [27] R Sainz, A M Benito, M T Martinez, J F Galindo, J Sotres, A M Baro, B Corraze, O Chauvet, A B Dalton, R H Baughman, W K Maser, *Nanotechnol.*16(2005)S150
- [28] J Y Shimano, A G MacDiarmid, *Synth.Met.*123 (2001)251
- [29] D.L.Wise, G.E.Wnek, D.J.Trantalo, T.M.Cooper, J.D.Gresser (Eds), *Electrical and optical polymer systems Fundamentals, Methods and Applications, Marcel Dekker, INC. Newyork, 1998*
- [30] H.Lim, J.H.Choi, *J.Chem.Phys*124 (2006)014710
- [31] D.L.Wise, G.E.Wnek, D.J.Trantalo, T.M.Cooper, J.D.Gresser (Eds), *Photonic Polymer Systems-Fundamentals, Methods and Applications, Marcel Dekker, INC. Newyork, 1998, p344*
- [32] A B Kaiser, *Rep.prog.Phys.*64 (2001)1

- [33] B Wessling, P K Kahol, A Raghunathan, B J McCormick, *Synth. Met.* 119(2001)197
- [34] J M Ginder, A F Richter, A G MacDiarmid, A J Epstein, *Solid State Commun.* 63(1987)97
- [35] P K Kahol, A J Dyakonov, B J McCormick, *Synth. Met.* 89(1997)17
- [36] P K Kahol, A Raghunathan, B J McCormick, A J Epstein, *Synth. Met.* 101(1999)815
- [37] B Wessling, *Synth. Met.* 102(1999)1396
- [38] M Reghu, Y Cao, D Moses, A J Heeger, *Phys. Rev. B* 47 (1993)1758
- [39] M Reghu, C O Yoon, D Moses, A J Heeger, Y Cao, *Phys. Rev. B* 48 (1993)17685
- [40] K Lee, S Cho, S H Park, A J Heeger, C-W Lee, S H Lee, *Nature* 441 (2006)65
- [41] R Murugesan, E Subramania N, *Bull. Mater. Sci.* 26(2003)529
- [42] F W Billmeyer Jr, *Text Book of Polymer Science*, John Wiley & Sons, New York, 1970
- [43] D B V Parker, *Polymer Chemistry*, Applied Science Publishers Ltd, London, 1974
- [44] David J William, *Polymer Science and Engineering*, Prentice-Hall, New Jersey, 1971
- [45] G Odian, *Principles of Polymerization*, 3rd ed., J Wiley, New York, 1991
- [46] B Z Jang, *Advanced Polymer Composites: Principles and Applications*, ASM International, Materials Park, OH, 1994
- [47] D. I. Bower, *An introduction to polymer physics*, Cambridge university press, Newyork, 2002, p164-169

.....*SC*.....

Chapter **5**

STUDIES ON PANI (HCl)-MWNT COMPOSITES

<i>Contents</i>	5.1 Introduction
	5.2 Synthesis of PANI and PANI-MWNT Composites
	5.3 TEM Analysis
	5.4 SEM Analysis
	5.5 X.R.D Analysis
	5.6 Raman Analysis
	5.7 FTIR Analysis
	5.8 D.C electrical conductivity studies
	5.9 Thermoelectric power studies
	5.10 T.G.A
	5.11 Conclusions

5.1 Introduction

One of the major attractions of polyaniline(PANI) is that it can be easily made highly conducting through proper doping[1-4].Making composites of PANI with suitable materials is another method to enhance its conductivity[3,5-6]. Multi Walled Carbon Nano Tube (MWNT) is one such highly pursued material due to its high electrical conductivity, mechanical strength and thermal stability [7]. Although there have been a few reports on the synthesis and characterization of Polyaniline-carbon nanotube composites [8-10], a systematic study on its temperature dependent D.C electrical conductivity, especially in the high temperature

solution used and low mass of Cl^- ions. Actually only less than 1% of the available charge carriers contributes to the conductivity of doped PANI. If all the charge carriers do contribute, the room temperature conductivity of doped PANI would be comparable to that of copper [19]. In fact PANI is only partially crystalline, with conducting metallic islands separated by large amorphous regions as evident from the X.R.D spectrum (see fig5.7). The characteristic metallic conductivity in doped PANI is limited by strong disorder [19].

The room temperature D.C electrical conductivity of PANI(HCl)-MWNT composites increases initially with increase in MWNT loading and thereafter saturates at 28S/cm (1:0.4), almost 4 times higher than that observed for pristine MWNTs(7S/cm) used in the present work. Due to the large aspect ratio (Length is very large compared to diameter) and surface area of MWNTs, MWNTs may serve as conducting bridges between scattered PANI islands, boosting the charge delocalization [8]. There is also a possibility of charge transfer from the quinonoid unit of polyaniline to the carbon nanotubes, since carbon nano tubes are good electron acceptors and doped PANI is a good electron donor. The improved crystallinity of PANI with the addition of MWNT as evident from the XRD investigations is another reason for the increase in conductivity. Particularly the peak at 25° , representing the extent of Π conjugation [1, 9, 20] becomes sharper and more intense on MWNT addition, facilitating greater charge transport due to enhanced carrier mobility. PANI (HCl)-MWNT composite

region, in doped composite samples is quite scanty. Moreover similar investigations reported earlier are centered on thin film samples and the investigations on powder samples in the form of pressed pellets of PANI or its composites are quite scarce [11-12]. In this chapter, the structural, morphological, electrical and thermal studies on PANI (HCl)-MWNT composites in powder form are described.

5.2 Synthesis of PANI and PANI-MWNT Composites

HCl doped PANI is prepared by chemical oxidative polymerization method using ammonium persulphate (APS) as oxidant at a synthesis temperature of around -10°C . Details are given in section 3.2.

For preparing HCl doped PANI-MWNT composites with different aniline to MWNT feed ratios, high pure MWNT (purchased from SUN NANO) is dispersed in 1.5M HCl solution. Freshly distilled aniline (A.R grade) is added to it. APS dissolved in water is added drop wise to the mixture with continuous stirring for 4-5 hours. The synthesis temperature is maintained at around -10°C . The precipitate obtained is filtered, washed and dried.

5.3 TEM Analysis

The morphology of PANI-MWNT composites is found out based on the TEM images. The TEM image of HCl doped PANI is shown in figure 5.1. Figures 5.2-5.3 depict the TEM images of HCl doped PANI-MWNT composites synthesized in the aniline monomer to MWNT feed ratios 1:0.1 and 1:0.5 (weight/weight) respectively. All samples are taken in pellet form.

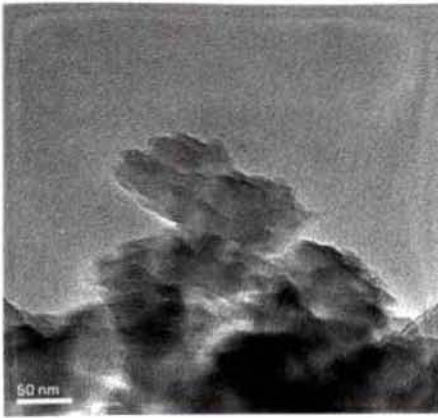


Fig. 5.1 TEM image of PANI (HCl)

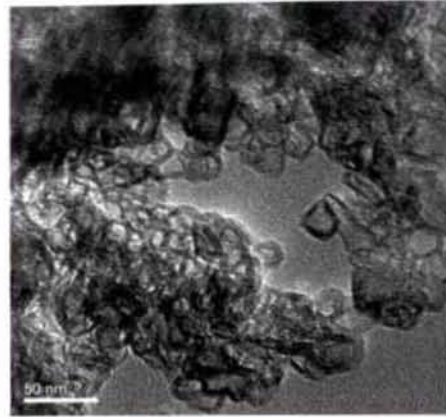


Fig. 5.2 TEM image of PANI (HCl)-MWNT (1:0.1) composite

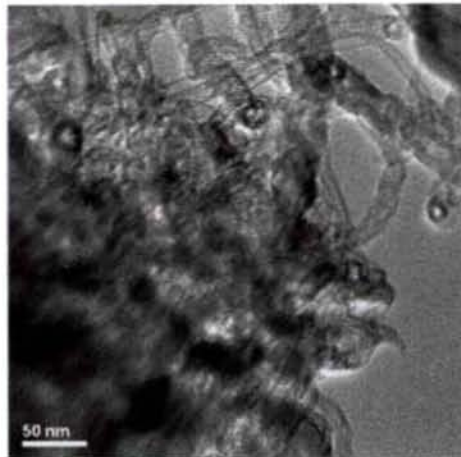


Fig. 5.3 TEM image of PANI(HCl)-MWNT(1:0.5) composite

Figures 5.2&5.3 clearly indicate the presence of both PANI and MWNT in the composite. The rod-like and coiled like structures of MWNT in the composite are clearly seen in the TEM images, which suggest the following possibilities. MWNTs can exist as bundles with special gaps between them. Aniline molecules occupy these gaps due to strong π - π electron interaction between

the MWNTs and aniline monomers and are then in situ polymerized. As polymerization proceeds, the long chain PANI molecules would break the MWNT bundles into individual nano tubes. The MWNTs are thus dispersed individually into the PANI matrix. In addition to this, PANI macromolecules can also be adsorbed at the surface of MWNTs, forming a tubular shell of the composite [9]. Due to the large aspect ratio (Length is very large compared to diameter) and surface area of the MWNTs, they act as 'conducting bridges' connecting PANI domains, forming a 3D network structure[8].

5.4 SEM Analysis

The SEM images of PANI (HCl) and PANI (HCl)-MWNT (1:0.5) composite (both in powder form) are given in figures 5.4 and 5.5.

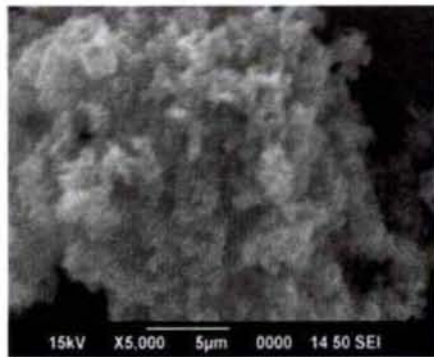


Fig. 5.4 SEM image of PANI (HCl)

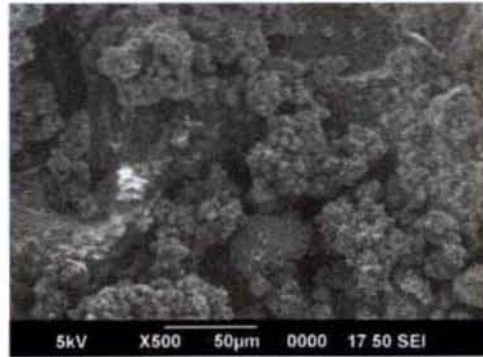


Fig. 5.5 SEM image of PANI (HCl)-MWNT

The SEM images give the surface morphology of the samples. From figure 5.5, it is clear that aniline is polymerized between the wedges of MWNTs as well as on the tube surfaces, as described earlier in section 5.3.

5.5 X.R.D Analysis

The X.R.D spectrum of MWNT is given in figure 5.6 and those of PANI(HCl) and PANI(HCl)-MWNT composites with various aniline to MWNT feed ratios are given in figure 5.7. All the samples are taken in powder form.

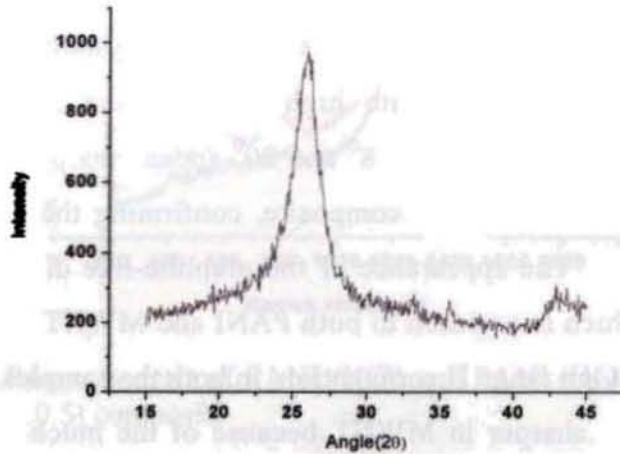


Fig. 5.6 X.R.D spectrum of MWNT

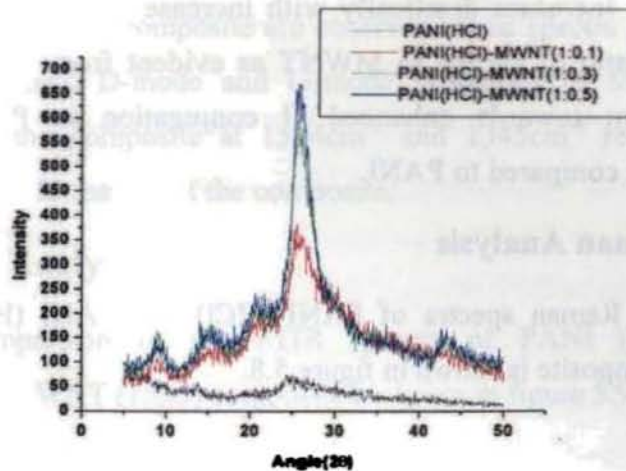


Fig. 5.7 X.R.D spectra of PANI (HCl) and PANI (HCl)-MWNT composites

PANI shows amorphous peaks at around 8° and 20° and somewhat sharper peaks at 15° and 25° . MWNT has a highly crystalline peak at 25° which is much more intense and sharper than that of PANI at the same position. An additional crystalline peak appears at around 43° with reduced intensity [8-9]

PANI-MWNT composites show the crystalline peaks of MWNT at 25° and 43° with high intensity and sharpness. The amorphous peaks of PANI at 8° and 20° appear sharper in the XRD spectrum of PANI-MWNT composite, confirming the formation of the composite. The appearance of the graphite-like diffraction peak at 25° [9], which is common to both PANI and MWNT, indicates the presence of long range Π conjugation, in both the samples. This peak is very much sharper in MWNT because of the much enhanced Π conjugation in MWNT. The crystallinity of PANI-MWNT composite increases drastically with increase in MWNT content in the feed ratio of aniline to MWNT as evident from figure 5.7. All these point towards enhanced Π conjugation in PANI-MWNT composite compared to PANI.

5.6 Raman Analysis

The Raman spectra of PANI (HCl) and PANI (HCl)-MWNT (1:0.5) composite is shown in figure 5.8.

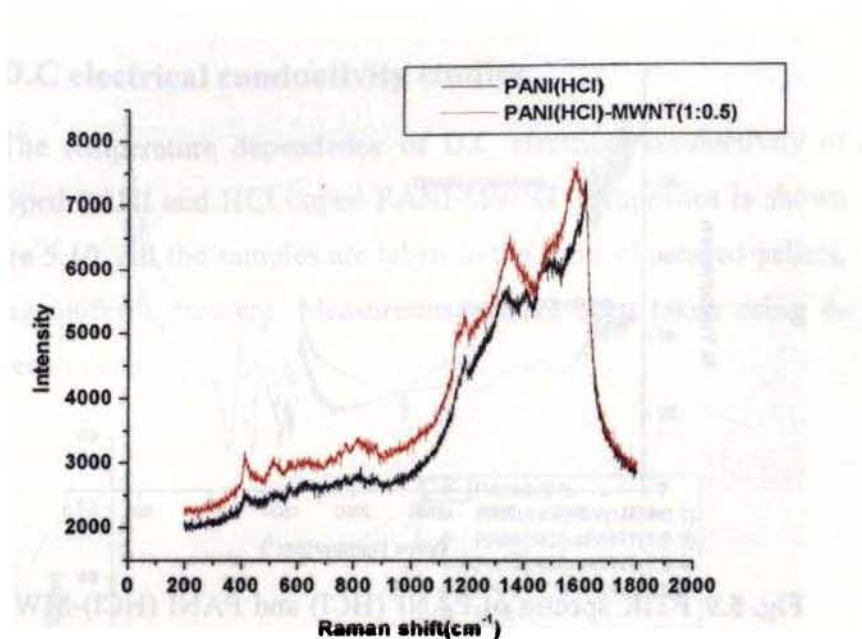


Fig. 5.8 Raman spectra of PANI (HCl) and PANI (HCl)-MWNT (1:0.5) composite

All the characteristic Raman frequencies of PANI (HCl) and PANI (HCl)-MWNT composite are observed in the spectra [9, 13-14]. The characteristic D-mode and G-mode vibrations of MWNT are observed in the composite at 1574cm^{-1} and 1345cm^{-1} respectively, confirming the formation of the composite.

5.7 FTIR Analysis

A comparison of the FTIR spectra of PANI (HCl) and PANI (HCl)-MWNT (1:0.5) composite is shown in figure 5.9.

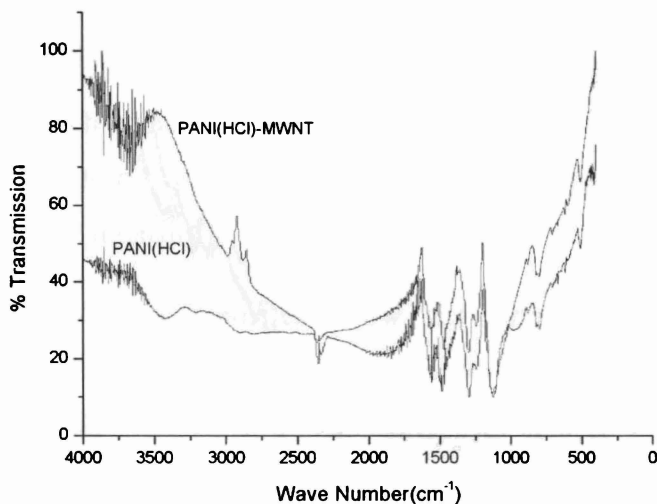


Fig. 5.9 FTIR spectra of PANI (HCl) and PANI (HCl)-MWNT composite (1:0.5)

The two spectra resemble each other closely with only small shifts in absorption wave numbers. Both the spectra show all the characteristic vibrations of HCl doped PANI. [4] However, it is observed that the NH stretching vibration occurs at around 3500cm^{-1} in HCl doped PANI, whereas the NH stretching vibration seems to have shifted to 3000cm^{-1} in HCl doped PANI-MWNT composite. This could be due to the interaction of MWNT with the lone pair electrons of nitrogen. Since the characteristic C=C vibrations of MWNT are more or less in the same frequency range as those in HCl doped PANI, the presence of MWNT in the composite cannot be clearly established from the FTIR spectra. But the TEM, SEM, XRD and Raman investigations, described earlier clearly establish the formation of PANI(HCl)-MWNT composite.

5.8 D.C electrical conductivity studies

The temperature dependence of D.C electrical conductivity of HCl doped PANI and HCl doped PANI-MWNT composites is shown in figure 5.10. All the samples are taken in the form of pressed pellets, applying uniform pressure. Measurements have been taken using 4-probe technique.

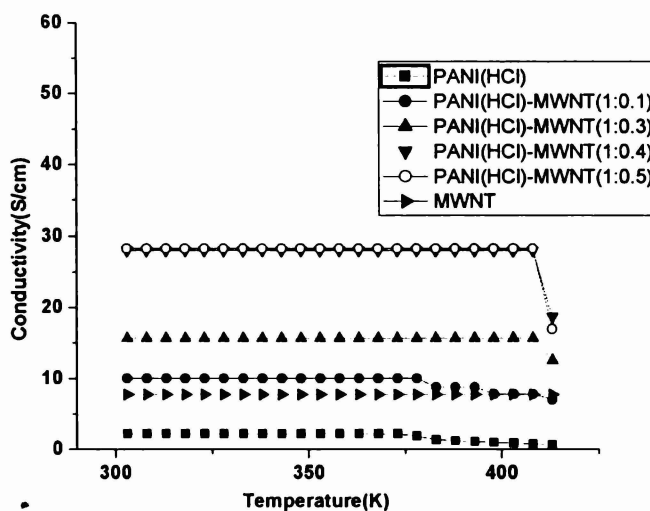


Fig. 5.10 Temperature dependent D.C electrical conductivity plots of PANI (HCl) and PANI (HCl)-MWNT composites with various aniline to MWNT feed ratios

All the samples exhibit negligible variation of electrical conductivity with temperature, characteristic of highly conducting samples [1,15-18]. HCl doped PANI shows a flat temperature dependence of D.C electrical conductivity (room temperature conductivity is 2.17S/cm). The reasonably high electrical conductivity of HCl doped PANI is attributed to the high molarity of dopant acid

solution used and low mass of Cl^- ions. Actually only less than 1% of the available charge carriers contributes to the conductivity of doped PANI. If all the charge carriers do contribute, the room temperature conductivity of doped PANI would be comparable to that of copper [19]. In fact PANI is only partially crystalline, with conducting metallic islands separated by large amorphous regions as evident from the X.R.D spectrum (see fig5.7). The characteristic metallic conductivity in doped PANI is limited by strong disorder [19].

The room temperature D.C electrical conductivity of PANI(HCl)-MWNT composites increases initially with increase in MWNT loading and thereafter saturates at 28S/cm (1:0.4), almost 4 times higher than that observed for pristine MWNTs(7S/cm) used in the present work. Due to the large aspect ratio (Length is very large compared to diameter) and surface area of MWNTs, MWNTs may serve as conducting bridges between scattered PANI islands, boosting the charge delocalization [8]. There is also a possibility of charge transfer from the quinonoid unit of polyaniline to the carbon nanotubes, since carbon nano tubes are good electron acceptors and doped PANI is a good electron donor. The improved crystallinity of PANI with the addition of MWNT as evident from the XRD investigations is another reason for the increase in conductivity. Particularly the peak at 25° , representing the extent of Π conjugation [1, 9, 20] becomes sharper and more intense on MWNT addition, facilitating greater charge transport due to enhanced carrier mobility. PANI (HCl)-MWNT composite

synthesized in the 1:0.5 ratio exhibits room temperature D.C electrical conductivity same as that of the 1:0.4 ratio composite sample.

One of the interesting observations is that, D.C electrical conductivity of PANI (HCl) and MWNT samples is almost constant with temperature. A comparatively sudden jump in conductivity with temperature, at high temperatures is observed only for PANI (HCl)-MWNT composite samples. The decrease in D.C electrical conductivity with temperature becomes sharper with increase in MWNT content in the composites. The results may be explained as follows.

For PANI (HCl) sample, the D.C electrical conductivity stays constant at 2.17S/cm up to 373K. In the temperature range 373K-378K, it exhibits a marginal drop to 1.85S/cm. Thereafter, there is a gradual(not sharp) decrease of conductivity to about 0.7S/cm at 413K. The nominal decrease in D.C electrical conductivity at higher temperatures is due to elevated charge carrier scattering at high temperatures arising from enhanced carrier mobility. The MWNT exhibits quite flat temperature dependence of conductivity up to the maximum temperature of investigation (A conductivity of 7S/cm is observed in the range 303K-413K). This is a consequence of the long range order prevailing in the MWNT system as observed from the X.R.D spectrum (fig 5.6)

For the PANI (HCl)-MWNT (1:0.1) composite, the D.C electrical conductivity stays constant at 10S/cm up to 373K. A marginal drop to

8.8S/cm is observed at 383K. Thereafter conductivity decreases to 7S/cm at 413K. The drop in conductivity with temperature is more or less gradual and not sharp and is comparable to the behaviour of PANI (HCl) sample. PANI (HCl)-MWNT composite samples with aniline to MWNT feed ratio at or above 1:0.3 exhibit a comparatively sharper drop in conductivity with temperature at high temperatures. The D.C electrical conductivity in all the above three samples, remains constant up to a particular temperature. For example, for PANI(HCl)-MWNT(1:0.3) composite sample, the D.C electrical conductivity remains constant at 15.7S/cm from 303K-408K and decreases from 15.7S/cm to 12.5S/cm in the temperature range 408K-413K. The sample with feed ratio 1:0.4 shows a much sharper decrease in conductivity within the same temperature range (from 28S/cm to 19S/cm). PANI(HCl)-MWNT(1:0.5) composite sample exhibits a sharp drop in conductivity from 28S/cm to 17S/cm at 413K.

From the TEM images, it is clear that aniline molecules are polymerized in the special gaps between the MWNT bundles. They are also adsorbed at the surface of MWNTs and subsequently polymerized. Thus MWNTs may serve as 'conducting bridges' connecting the isolated PANI islands, boosting the charge mobility. At higher temperatures, the increased mobility of the charge carriers may give rise to enhanced scattering effects from the intersections of PANI and MWNTs. As the MWNT content increases in the composites, the number of interfaces also increases leading to greater charge scattering. This can be the reason for the observed sharp drop in conductivity in

PANI (HCl)-MWNT composite samples with higher MWNT content, compared to other samples.

PANI (HCl)-MWNT composite (1:0.5 feed ratio) exhibits the highest room temperature D.C electrical conductivity of 28S/cm (almost equal to that of 1:0.4 ratio) which stays constant upto 408K. The sample with 1:0.4 feed ratio shows the same value of D.C electrical conductivity within the temperature range 303K-408K. The stable and reasonably high D.C electrical conductivity observed for the composite sample even at elevated temperatures offers prospects of applications in the fabrication of devices working at high temperatures. An almost flat response of D.C electrical conductivity with temperature has been reported earlier on MWNT and PANI(EB)-MWNT composite samples in the temperature range 27K-300K[7]. Similarly an almost constant temperature response of D.C electrical conductivity and a sharp decrease at high temperatures has been observed on the pellet samples of sulphuric acid doped PANI and its metal oxalate composites with trivalent metal ions[21]. But a similar study has not been attempted on doped PANI-MWNT composites yet.

5.9 Thermoelectric power studies

The temperature dependent thermoelectric power plots of PANI (HCl) and PANI (HCl)-MWNT composite (1:0.5) are shown in figures 5.11 and 5.12 respectively. All the samples are taken in the form of pressed pellets, applying uniform pressure.

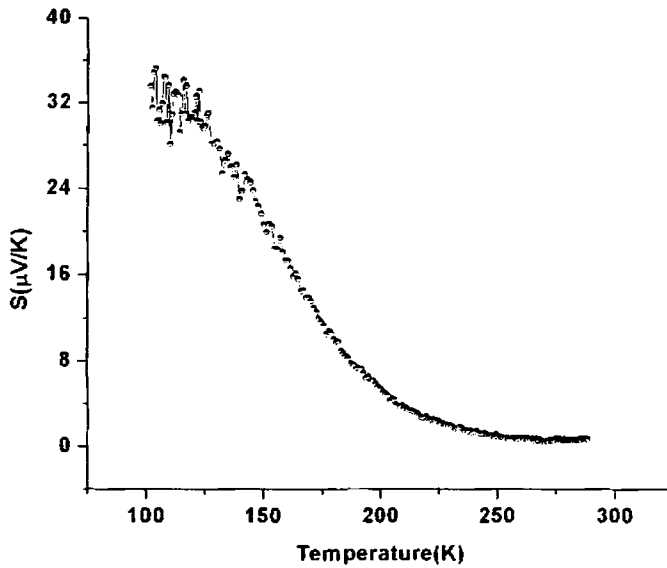


Fig. 5.11 Temperature dependent thermo power of PANI (HCl)

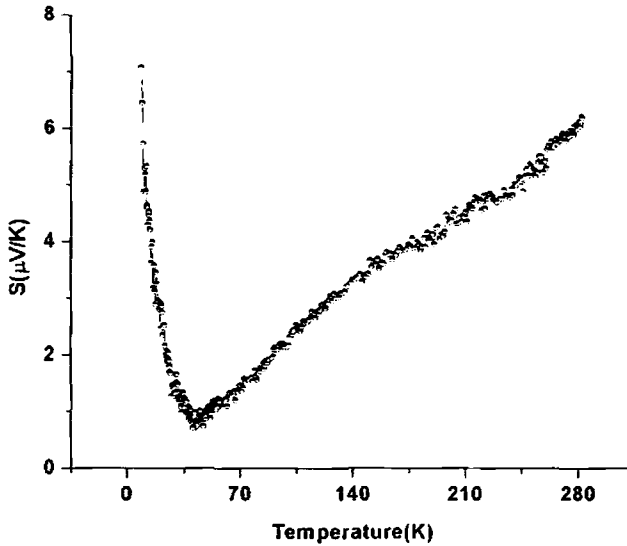


Fig. 5.12 Temperature dependent thermo power of PANI(HCl)-MWNT (1:0.5) composite

The room temperature thermo power of PANI (HCl)-MWNT composite is about $6.8\mu\text{V/k}$, which is about 8 times higher than that of

HCl doped PANI ($0.8 \mu\text{V/k}$). The positive thermo power value observed for HCl doped PANI establishes its semi metallic nature [1]. The positive and much higher thermo power value of PANI(HCl)-MWNT composite is very close to the value obtained for CSA doped PANI films showing metallic behaviour [1]. The magnitude and sign of thermo power are consistent with the results obtained for a number of partially doped p-type conducting polymers [1,22-24]. The positive sign of the thermo power agrees with the calculated band structure of the metallic emeraldine salt with a three quarter-filled Π band with one hole per repeat unit [25]. PANI(HCl) shows an exponential decrease of thermo power with temperature, while PANI(HCl)-MWNT composite (1:0.5) exhibits a nearly linear response, after an initial decrease. The possible reason may be explained as follows. PANI (HCl) is mostly amorphous in nature. On the other hand, PANI (HCl)-MWNT composite is considerably crystalline. Increase in crystallinity implies increase in chain orientation. As the chain orientation increases, the temperature dependence of thermo power shifts from its U-shaped behaviour to linear nature [26]. Thus the absence of linear temperature dependence for PANI (HCl) is due to the higher degree of disorder and the formation of metallic islands which suppresses the intrinsic conductivity [1]. The D.C electrical conductivity also rises with rise in crystallinity as already observed. The thermo power results thus compliment the D.C electrical conductivity studies.

5.10 T.G.A

The thermo grams of PANI (HCl), MWNT and PANI (HCl)-MWNT composite (1:0.5) composite are shown in figure 5.13. All samples are taken in powder form.

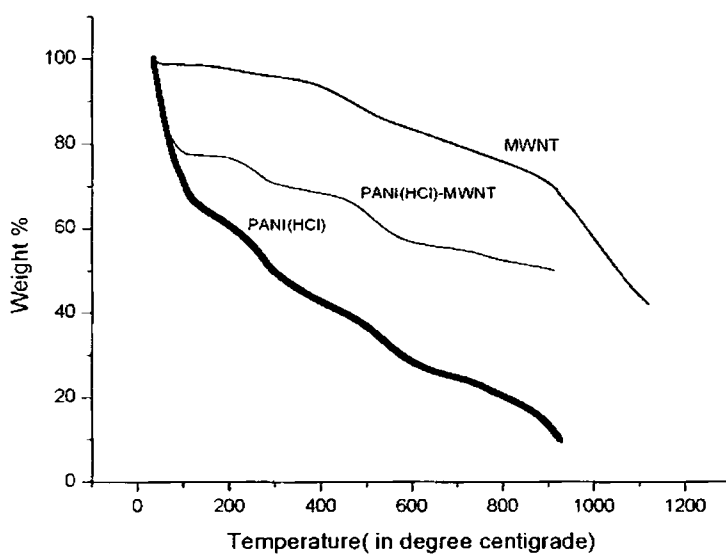


Fig. 5.13 Thermo grams of PANI (HCl), MWNT and PANI (HCl)-MWNT (1:0.5) composite

Weight loss up to 100⁰ C is mainly due to the evaporation of adsorbed water molecules. Loss of dopants become prominent from a temperature of 250⁰ C. Degradation of the polymer backbone starts at around 400⁰ C. [27]. From the thermo grams, we see that the thermal stability of PANI(HCl)-MWNT(1:0.5) composite is remarkably better compared to HCl doped PANI. For example at 300⁰C, weight loss of HCl doped PANI is about 50% whereas that of the HCl doped PANI-MWNT composite is only 30%. At 900⁰C, the weight loss for HCl doped PANI is 86% whereas that for the

composite is only 50%. Obviously thermal stability increases with the addition of MWNT possibly due to the better thermal conductivity of MWNT [8].

5.11 Conclusions

HCl doped PANI-MWNT composites are synthesized by chemical insitu polymerization and their structural, thermal, morphological and electrical studies are carried out.

The so synthesized PANI-MWNT composites show quite high room temperature D.C electrical conductivity, very good thermal stability, a nearly flat temperature dependent conductivity response and quite high positive thermo power value comparable to doped polymers showing metallic conductivity. The present study is relevant where there is increased demand for identifying polymer/organic materials with high mobility charge carriers for the fabrication of transistors and microprocessors. The stable D.C electrical conductivity observed in the PANI (HCl)-MWNT composite even at high temperatures highlights the prospects of application of these composites in the fabrication of devices capable of operating at high temperatures.

References

- [1] Reghu Menon, C O Yoon , D Moses, A J Heeger , Y Cao , Phys. Rev.B 48(1993) 17685
- [2] A Pud, N Ogurtsov, A Korzhenko, G Shapoval, Prog.Polym.Sci 28 (2003)1701
- [3] C Y Yang , Y Cao, P Smith, A J Heeger, Synth.Met.53(1993)293

- [4] M Amrithesh, S Aravind, S Jayalekshmi, R S Jayasree, J. Alloys Compd. 458(2008)532
- [5] P Banarjee, B M Mandal, Synth. Met. 74(1995)257
- [6] A Pron, M Zagorska, Y Nicolau, F Genoud, M Nechtschein, Synth. Met. 84(1997) 89
- [7] R Sainz, A M Benito, M T Martinez, J F Galindo, J Sotres, A M Baro, B Corraze, O Chauvet, A B Dalton, R H Baughman, W K Maser, Nano technol. 16(2005)S150
- [8] H Zengin, W Zhou, J Jin, R Czrew, DW Smith, Jr., L Echegoyen, D L Carroll, S H Foulger, J Ballato, Adv. Mater. 14(2002)1480
- [9] X Zhang, J Zhang, Z Liu, Appl. Phys. A 80(2005) 1813
- [10] G B Blanchet, C R Fincher, F Gao, Appl. Phys. Lett. 82(2003)1290
- [11] H Liu, X B Hu, J Y Wang, R I Boughton, Macromolecules 35 (2002) 9414
- [12] Y Cao, P Smith, A J Heeger, Synth. Met. 48(1992)91
- [13] S Tao, B Hong, Z Kerong, Spectrochim Acta Part A 66 (2007)1364
- [14] G M do Nascimento, M L A Temperini, J. Raman Spectrosc. 39 (2008) 772
- [15] K Lee, S Cho, S H Park, A J Heeger, C W Lee, S H Lee, Nature 441 (2006)65
- [16] T A Skotheim, R L Elsenbaumer, J R Reynolds (Eds), Hand Book of Conducting Polymers, Marcel Dekker, Inc., New York, 1998, p27-84
- [17] H Liu, X B Hu, J Y Wang, R I Boughton, Macromolecules 35 (2002) 9414
- [18] Y Long, Z Chen, N Wang, J Li, M Wan, Physica B 344(2004)82
- [19] J Y Shimano, A G MacDiarmid, Synth. Met. 123 (2001)251
- [20] S W Liu, J Yue, R J Wehmschulte, Nano Lett. 2 (2002)1439
- [21] R Murugesan, E Subramanian, Bull. Mater. Sci. 26 (2003)529

- [22] H Yan, T Ohta, N Toshima, *Macromol.Mater.Eng.*286 (2001)139
- [23] Y W Park, C O Yoon, C H Lee, H Shirakawa, Y Suezaki, K Akagi, *Synth.Met.*28 (1989) D27
- [24] Y W Park, A J Heeger, M A Dury, A G MacDiarmid, *J.Chem. Phys.*73 (1980)946
- [25] C O Yoon, M Reghu, D Moses, A J Heeger, Y Cao, *Phys.Rev.*B48 (1993)14080
- [26] F Wudl, R O Angus, F L Lu, P M Allemand, D J Vachon, M Nowak, Z X Liu, A J Heeger, *J.Am.Chem.Soc.*109 (1987)3677
- [27] L.Abell, S.J.Pomfret, P.N.Adams, A.P.Monkman, *Synth. Met.* 84(1997)127

.....803.....

Chapter **6**

OPTICAL TRANSITION GAP ANALYSIS IN POLYMER FILMS

<i>Contents</i>	6.1	Introduction
	6.2	Synthesis of powder samples
	6.3	Film preparation
	6.4	Film thickness measurement
	6.5	FTIR Analysis
	6.6	Optical absorption studies
	6.7	Conclusions

6.1 Introduction

Studies described in the earlier chapters are centered on powder samples. But as far as technological interests are concerned, fabrication of films is essential. Though there are many methods to fabricate polymer films (described earlier in chapter1), solution casting is the most widely used technique owing to its simplicity. In this chapter, the optical transition gap analysis of some selected polymer films is reported. The samples selected include,

- a) PANI (HCl) and PANI (HCl)-MWNT composite films
- b) PANI (emeraldine base (EB)) films cast from m-cresol as well as NMP

Though extensive investigations have been reported on the electrical conductivity behaviour of doped PANI both in bulk and thin film forms [1-4], detailed investigations on the optical characterization of PANI thin films are scanty. Reports on the room temperature D.C electrical conductivity of acid (sulphuric acid, camphor sulphonic acid, toluene sulphonic acid etc) doped PANI in the form of pressed pellets is reported to lie in the range 0.5-2S/cm[5-7]. D.C electrical conductivity measurements have been carried out on PANI pellets doped with hydrochloric acid (HCl), Camphor Sulphonic acid (CSA) and ortho phosphoric acid (H_3PO_4) as described earlier in chapter3. A maximum conductivity of 2.17S/cm has been recorded for HCl doped PANI. In HCl doped PANI-MWNT composite pellet samples, the highest room temperature D.C electrical conductivity of 28S/cm has been observed in HCl doped PANI-MWNT composite with 50% MWNT loading(chapter5). The room temperature D.C electrical conductivity values observed in thin films of HCl doped PANI and HCl doped PANI-MWNT composite, both cast from m-cresol is about 10S/cm and 40S/cm respectively. In this chapter, a comparative study of the optical transitions of HCl doped PANI, HCl doped PANI-MWNT composite and the emeraldine base (EB) form of PANI (all in thin film forms) is attempted. The first two samples constitute the conducting state and the third sample constitutes the insulating state of PANI. Such an investigation has been carried out mainly because 1. HCl doped PANI and HCl doped PANI-MWNT composite samples show quite high room temperature D.C electrical conductivity and 2. though extensive investigations have been reported on the electrical conductivity behaviour of acid doped

PANI samples and their various composites [2-4,6], a comparative study on the various optical transitions in PANI films in the conducting and insulating forms is quite scanty.

6.2 Synthesis of powder samples

PANI (HCl) and PANI (HCl)-MWNT composite samples are synthesized according to the procedure described earlier in chapters 3 and 5 respectively. PANI (EB) is prepared by dedoping HCl doped PANI salt with 1.5M NH₄OH.

6.3 Film preparation

0.2 g of the polymer sample in powder form is dissolved in 2 ml of m-cresol by stirring continuously for about 12 hours. The obtained solution is spread uniformly on ultrasonically clean glass substrates and allowed to dry in a hot air oven kept at 70 degrees. The same procedure is adopted for preparing films of all the samples.

6.4 Film thickness measurement

The film thickness is measured using a DEKTAK 6M STYLUS PROFILER. The recorded thickness of all the films falls in the range 35 μm to 45 μm.

6.5 FTIR Analysis

The FTIR analysis of PANI (HCl) and PANI (HCl)-MWNT composite samples is carried out earlier in chapters 3 and 5 respectively.

The FTIR spectrum of PANI (EB) is shown in figure 6.1.

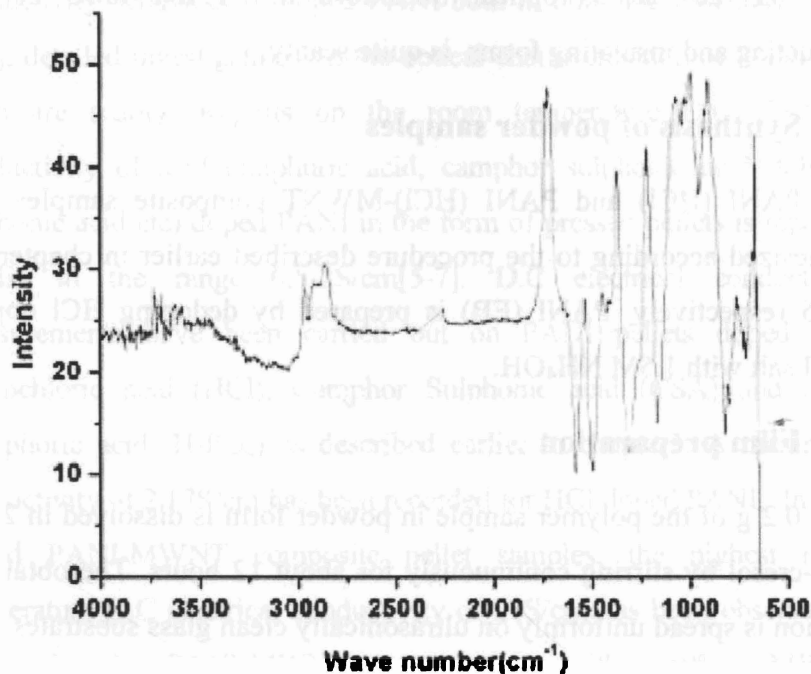


Fig. 6.1 FTIR spectrum of PANI (EB)

The major peaks observed at 1584 cm^{-1} , 1488 cm^{-1} , 1308 cm^{-1} , 1171 cm^{-1} and 827 cm^{-1} are in good agreement with the already reported peaks of PANI (EB) confirming its formation [8-9].

6.6 Optical absorption studies

The optical absorption spectra of PANI (EB) cast from NMP, PANI (EB) cast from m-cresol, PANI (HCl) and PANI (HCl)-MWNT composite both cast from m-cresol are shown in figures 6.2-6.5.

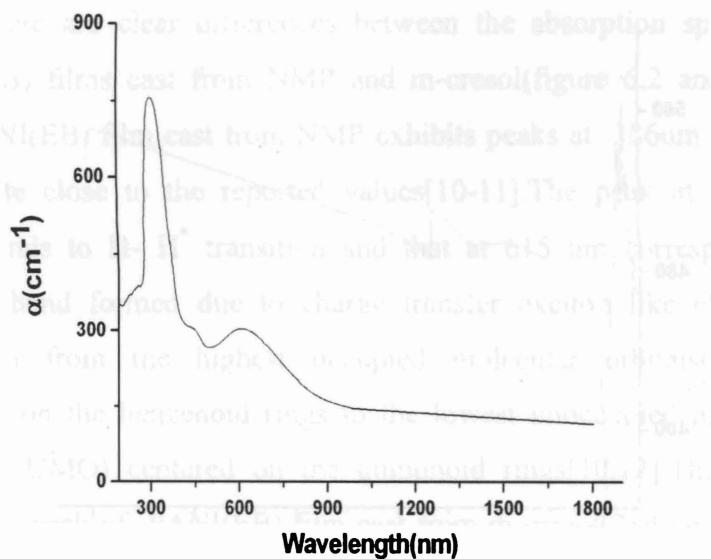


Fig. 6.2 Optical absorption spectrum of PANI (EB) film cast from NMP

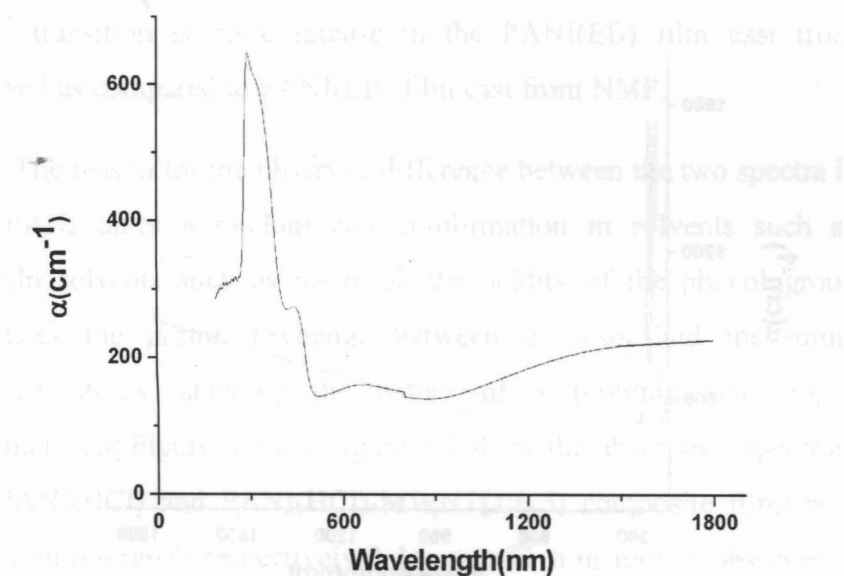


Fig. 6.3 Optical absorption spectrum of PANI (EB) film cast from m-cresol

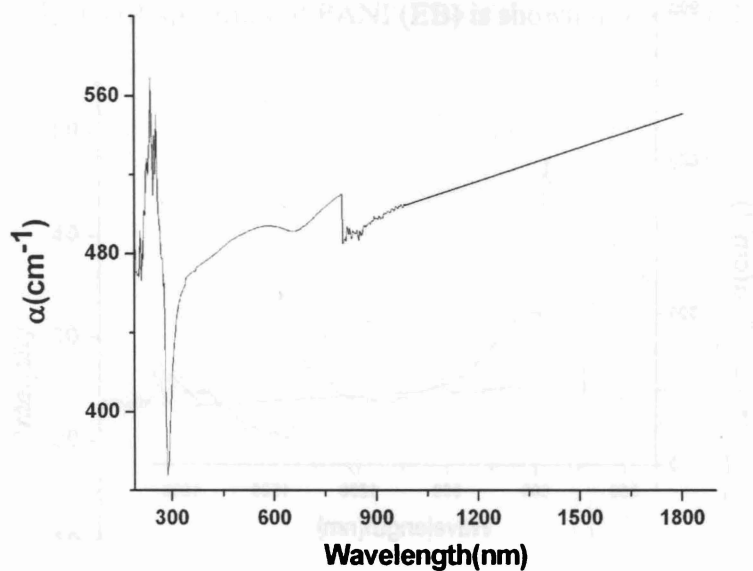


Fig. 6.4 Optical absorption spectrum of PANI (HCl) film cast from m-cresol

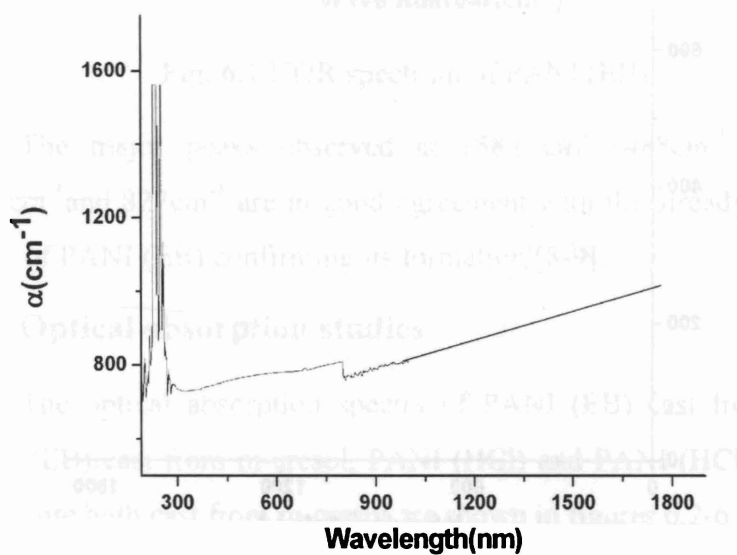


Fig. 6.5 Optical absorption spectrum of PANI (HCl)-MWNT (1:0.5) composite film cast from m-cresol

There are clear differences between the absorption spectra of PANI(EB) films cast from NMP and m-cresol (figure 6.2 and figure 6.3). PANI(EB) film cast from NMP exhibits peaks at 306 nm and 615 nm, quite close to the reported values [10-11]. The peak at 306 nm corresponds to Π - Π^* transition and that at 615 nm corresponds to exciton band formed due to charge transfer exciton like electronic transition from the highest occupied molecular orbitals (HOMO) centered on the benzenoid rings to the lowest unoccupied molecular orbitals (LUMO) centered on the quinonoid rings [10,12]. The Π - Π^* transition peak of PANI(EB) film cast from m-cresol (289 nm) is very close to that observed for PANI(EB) film cast from NMP, while the exciton band of EB decreases in intensity for the film cast from m-cresol. The transition peak at 458 nm which corresponds to polaron to Π^* transition is more intense in the PANI(EB) film cast from m-cresol as compared to PANI(EB) film cast from NMP.

The reason for the observed difference between the two spectra is that PANI takes a random coil conformation in solvents such as NMP. In solvents such as m-cresol, the acidity of the phenol group facilitates the proton exchange between m-cresol and the imine nitrogen atoms, showing the nature of a protonic acid doped system [10,13]. Figure 6.4 and figure 6.5 show the absorption spectrum of PANI(HCl) and PANI(HCl)-MWNT(1:0.5) composite films (both cast from m-cresol) respectively. Polaron to Π^* transition is observed in both the doped films at around 480 nm as a low intensity kink. Both the spectra exhibit absorption peak at around 790 nm which corresponds to

Π to polaron transition [10,14-15]. The peak corresponding to Π - Π^* transition has been reduced to a very weak kink in both PANI(HCl) and PANI(HCl)-MWNT films. A free carrier tail extending to the near infrared (NIR) region is observed in HCl doped PANI and HCl doped PANI-MWNT composite films, which is characteristic of a highly conducting state [10]. However a similar free carrier tail is also observed in the EB film cast from m-cresol, possibly due to the moderate doping effect of m-cresol [10]. In the EB film cast from NMP, the free carrier tail is not observed.

The photon absorption in many amorphous materials is found to obey the Tauc relation given by, $(\alpha h\nu) = B (h\nu - E)^n$

Here α is the absorption coefficient in eVcm^{-1} , $h\nu$ the photon energy, B a constant and the index n is connected with the distribution of the density of states. For direct allowed transition energy gap, $n=1/2$ and for indirect allowed transition energy gap, $n=2$. $(\alpha h\nu)^2$ as a function of photon energy $h\nu$ gives direct allowed transition energy gap. $(\alpha h\nu)^{1/2}$ as a function of photon energy $h\nu$ gives indirect allowed transition energy gap [16-18]. The direct allowed transition energy gaps of PANI(EB) film cast from NMP and PANI(EB) film cast from m-cresol are shown in figures 6.6 and 6.7 respectively.

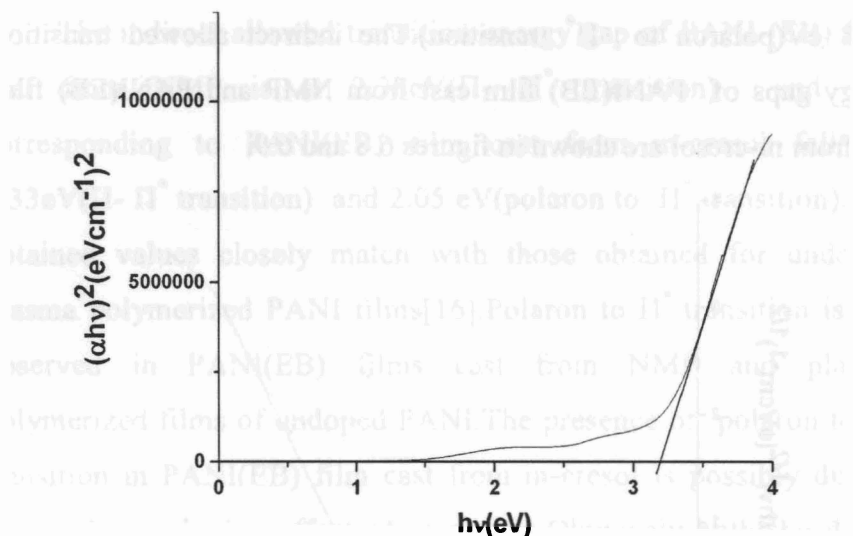


Fig. 6.6 Direct allowed transition energy gap of PANI (EB) film cast from NMP

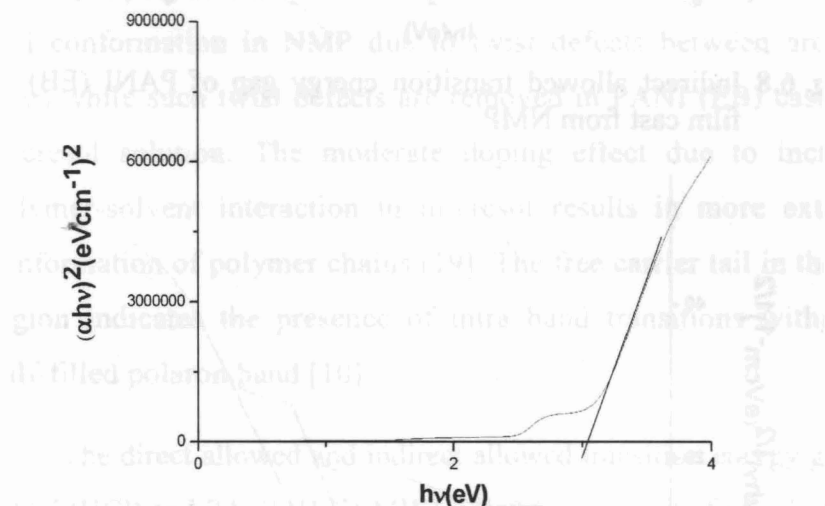


Fig. 6.7 Direct allowed transition energy gap of PANI (EB) film cast from m-cresol

The direct allowed transition energy gap of PANI (EB) film cast from NMP falls at 3.12 eV (Π - Π^* transition), while that corresponding to PANI(EB) film cast from m-cresol falls at 3.0 eV and

2.508 eV (polaron to Π^* transition). The indirect allowed transition energy gaps of PANI(EB) film cast from NMP and PANI(EB) film cast from m-cresol are shown in figures 6.8 and 6.9.

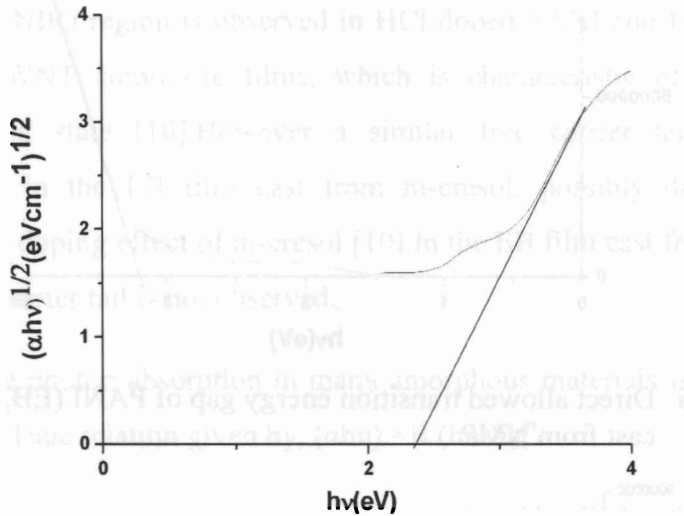


Fig. 6.8 Indirect allowed transition energy gap of PANI (EB) film cast from NMP

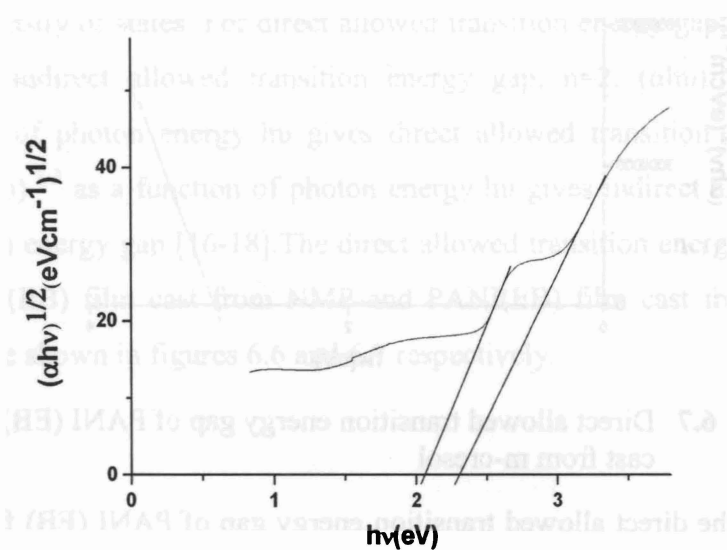


Fig. 6.9 Indirect allowed transition energy gap of PANI (EB) film cast from m-cresol

The indirect allowed transition energy gap of PANI (EB) film cast from NMP is at 2.38eV(Π - Π^* transition) and that corresponding to PANI(EB) film cast from m-cresol falls at 2.33eV(Π - Π^* transition) and 2.05 eV(polaron to Π^* transition). The obtained values closely match with those obtained for undoped plasma polymerized PANI films[16]. Polaron to Π^* transition is not observed in PANI(EB) films cast from NMP and plasma polymerized films of undoped PANI. The presence of polaron to Π^* transition in PANI(EB) film cast from m-cresol is possibly due to the moderate doping effect of m-cresol. Obviously both the direct allowed and indirect allowed transition energy gaps decrease for PANI (EB) films cast from m-cresol. PANI (EB) takes up a random coil conformation in NMP due to twist defects between aromatic rings while such twist defects are removed in PANI (EB) cast from m-cresol solution. The moderate doping effect due to increased polymer-solvent interaction in m-cresol results in more extended conformation of polymer chains [19]. The free carrier tail in the NIR region indicates the presence of intra band transitions within the half-filled polaron band [10].

The direct allowed and indirect allowed transition energy gaps of PANI (HCl) and PANI (HCl)-MWNT(1:0.5) composite films (both cast from m-cresol) are shown in figures 6.10-6.13.

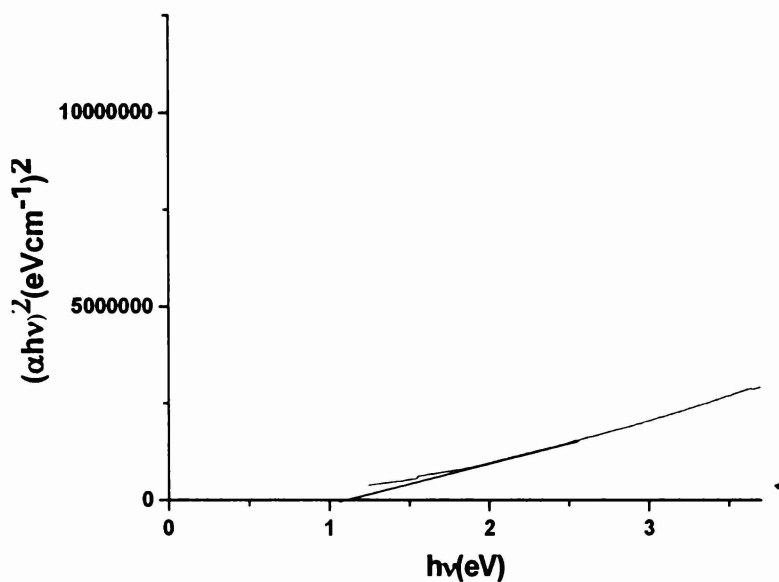


Fig. 6.10 Direct allowed transition energy gap of PANI (HCl) film

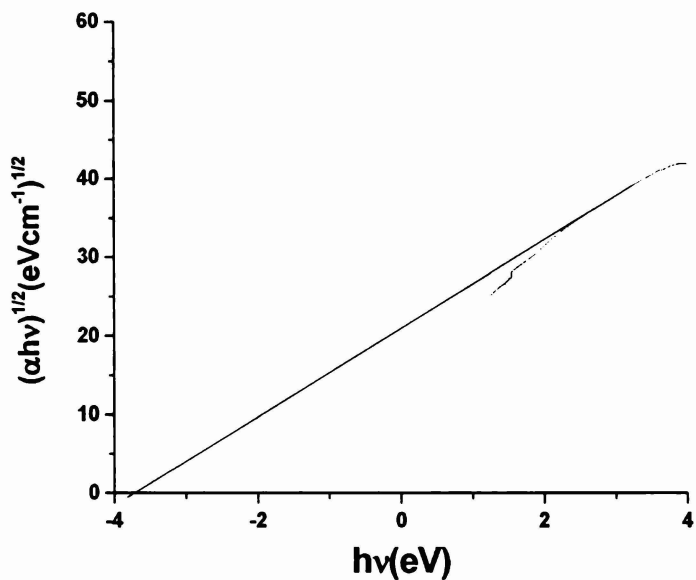


Fig. 6.11 Indirect allowed transition energy gap of PANI(HCl) film

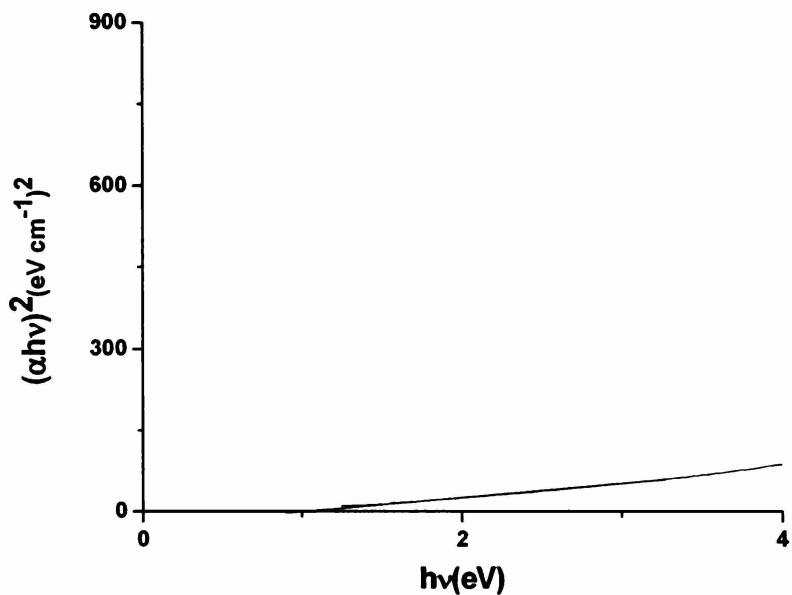


Fig. 6.12 Direct allowed transition energy gap of PANI(HCl)-MWNT(1:0.5) composite film

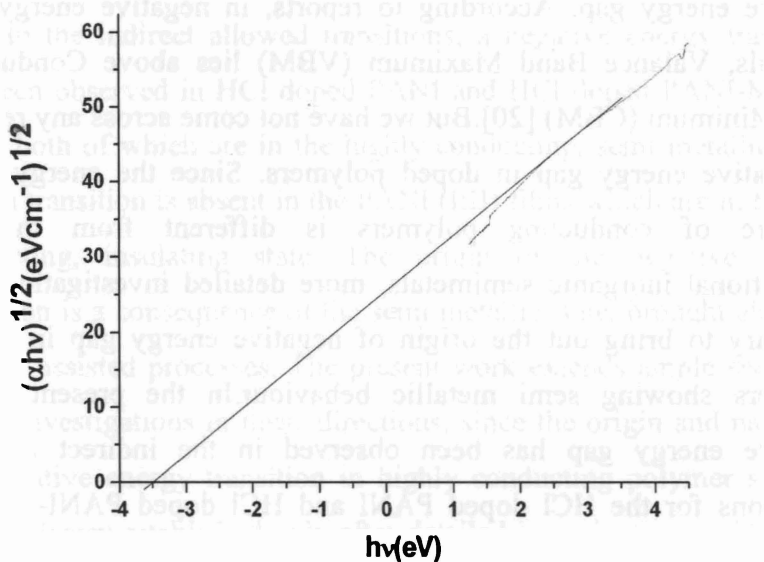


Fig. 6.13 Indirect allowed transition energy gap of PANI (HCl)-MWNT (1:0.5) composite film

As the polaron band gets more dispersed in energy, Π - Π^* transition becomes very weak due to the elimination of band gap between Π band and polaron band[10]. In that case the transition energy gap corresponds to that between polaron band and Π^* band. The direct allowed transition energy gap of PANI(HCl) cast from m-cresol is 1.09eV while the indirect transition energy gap is -3.7eV. The direct allowed transition energy gap of PANI(HCl)-MWNT film cast from m-cresol is 0.91147eV and indirect allowed transition energy gap is -3.58eV. Negative energy gap has already been reported in inorganic systems such as $\text{InN}_x\text{Sb}_{1-x}$, $\text{Hg}_{1-x-y}\text{Cd}_x\text{Mn}_y\text{Te}$ and HgTe-CdTe [20-23]. Techniques like XPS, HREELS, magneto phonon resistance and magneto transport measurements have been employed to establish the presence of negative energy gap. According to reports, in negative energy gap materials, Valance Band Maximum (VBM) lies above Conduction Band Minimum (CBM) [20]. But we have not come across any reports of negative energy gap in doped polymers. Since the energy band structure of conducting polymers is different from that of conventional inorganic semimetals, more detailed investigations are necessary to bring out the origin of negative energy gap in doped polymers showing semi metallic behaviour. In the present work, negative energy gap has been observed in the indirect allowed transitions for the HCl doped PANI and HCl doped PANI-MWNT composite films which are in the semi metallic state (as given earlier, the D.C electrical conductivity values of HCl doped PANI and HCl doped PANI-MWNT composite films are 10S/cm and 40S/cm

respectively.)[24]. Both the PANI (EB) films, which are in the insulating state, do not show any negative energy transition. The existence of the negative energy transition is a consequence of the semi metallic state of the polymer, which is in agreement with the earlier observation of negative energy gap in semi metallic inorganic systems. Moreover the negative energy transition is observed only in the indirect allowed transition whereas it is absent in the direct allowed transition. Thus phonons do play a significant role in the origin of negative energy transition. The origin and nature of such a transition in highly conducting doped polymers can be clearly established only after detailed investigations employing more sophisticated techniques.

6.7 Conclusions

In the indirect allowed transitions, a negative energy transition has been observed in HCl doped PANI and HCl doped PANI-MWNT films, both of which are in the highly conducting, semi metallic state. Such a transition is absent in the PANI (EB) films which are in the low conducting, insulating state. The origin of the negative energy transition is a consequence of the semi metallic state, brought about by phonon assisted processes. The present work extends ample scope for future investigations in these directions, since the origin and nature of the negative energy transition in highly conducting polymer systems can be clearly established only after detailed investigations using more sophisticated techniques.

References

- [1] K Lee, S Cho, S H Park, A J Heeger, C W Lee, S H Lee, *Nature*441 (2006)65
- [2] Y Long,Z Chen,N Wang,J Li,M Wan,*PhysicaB*344(2004)82
- [3] E R Holland,S J Pomfret,P N Adams,A P Monkman ,*J.Phys.: Condens. Matter*8(1996)2991
- [4] A Mirmohseni, G G Wallace, *Polymer*44 (2003)3523
- [5] R Murugesan,E Subramanian,*Bull.Mater.Sci*26(2003)529
- [6] H Liu,X B Hu,J Y Wang,R I Boughten, *Macromolecules* 35(2002)9414
- [7] Y Cao,P Smith,A J Heeger,*Synth.Met*48(1992)91
- [8] Y Geng,J Li,Z Sun,X Jing, F Wang,*Synth.Met*96(1998)1
- [9] J Tang,X Jing,B Wang,F Wang,*Synth.Met*24(1988)231
- [10] D L Wise,G E Wnek,D J Trantalo,T M Cooper,J D Gresser(Eds), *Electrical and optical polymer systems Fundamentals, Methods and Applications*, Marcel Dekker, INC.Newyork,1998,p359-386
- [11] P Rannou, A Pron, M Nechtsheim, *Synth.Met.*101 (1999)827
- [12] H Lim, J H Choi, *J.Chem.Phys*124 (2006)014710
- [13] J K Avlyanov, Y Min, A G MacDiarmid, *Synth.Met.* 72(1995)65
- [14] S Stafstrom, J L Bredas, A J Epstein, H S Woo, D B Tanner, W S Huang, A G MacDiarmid,*Phys.Rev.Lett.*,59(1987)1464
- [15] N C Baird, H Wang, *Chem.Phys.Lett.*202 (1993)50
- [16] C Joseph Mathai, S Saravanan, M R Anantharaman, S Venkitachalam, S Jayalekshmi, *J.Phys.D:Appl.Phys*35 (2002)2206
- [17] J Tauc, *Optical properties of solids*, A Ables, North-Holland, Amsterdam, 1970, p277

- [18] E A Davis, N F Mott, *phil.Mag.*22 (1970)903
- [19] Y Xia, A G MacDiarmid, A J Epstein, *Macromolecules*27 (1994) 7212
- [20] T D Veal, I Mahboob, C F McConville, *Phys.Rev.Lett*92 (2004)136801
- [21] S Kuroda, T Okamoto, H J Kwon, K Takita, *Semicond. Sci. Technol.*7 (1992) B42
- [22] C A Hoffman, J R Meyer, F J Bartoli, Y Lansari, J W Crook Jr., J F Schetzina, *Phys.RevB* 40(6)(1989)3867
- [23] C Y Moon, S-H Wei, *Phys.Rev.B*74 (2006)045205
- [24] M.Amrithesh, K.P.Chandni, S.Jayalekshmi, Febin Kurian, S.J.Varma, *Optoelectron.Adv.Mater (RC)*, 3(2) (2009)149

Chapter 7

PHOTOACOUSTICS: THEORY AND EXPERIMENT

<i>Contents</i>	7.1 Introduction
	7.2 History of Photo Acoustic effect
	7.3 Photo Induced Processes
	7.4 Detection methods
	7.5 Photoacoustic effect in condensed media
	7.6 Rosencwaig-Gersho theory
	7.7 Open photo acoustic cell configuration
	7.8 Thermal diffusivity measurements on PANI (HCl) and PANI (HCl)-MWNT Composites
	7.9 Experimental Setup
	7.10 Experimental procedure
	7.11 Analysis of thermal diffusivity results
	7.12 Conclusions

7.1 Introduction

Spectroscopy deals with the study of interaction of energy with matter. In the field of high-energy physics, the radiation is sufficiently energetic to perturb and in some cases, even transform the matter with which it interacts. In the oldest form of spectroscopy, the energy is usually too low to perturb the material under study. In optical spectroscopy, the energy exists in the form of optical photons or quanta with wavelength ranging from 1\AA in the X-ray region to more

than 10^6 \AA in the far – infrared[1]. Because of its versatility, range and nondestructive nature, optical spectroscopy remains a most important and widely used tool for investigating and characterizing the properties of matter.

Conventional spectroscopy can be categorized into two.

- a) That which involves the study of the photons that are transmitted through the material of interest; that is, the study of those photons that do not interact with the material.
- b) That which involves the study of light that is scattered or reflected from the material, that is, those photons that have undergone some interaction with the material.

Almost all conventional optical methods are variations of these two basic techniques[2-12]. This has been a scientific tool for over a century, and it has proven invaluable in studies on reasonably clean media, such as solutions and crystals and on reflective surfaces. There are, however several instances where conventional transmission spectroscopy is inadequate even for the case of clear, transparent materials, such as to measure a very weak absorption. This problem occurs for all forms of matter. Over the years, various techniques have been developed to overcome this difficulty, such as derivative spectroscopy which has proven to be generally inadequate. In addition, there are substances, both organic and inorganic, that are not readily amenable to the conventional transmission or reflection modes of optical spectroscopy. These are usually highly light-scattering

materials, such as powders, amorphous solids, gels etc. There are a number of materials that are optically opaque and have dimensions that far exceed the penetration depth of the photons.

In recent years, thermal wave physics has emerged as an effective analytical tool for the characterization of such materials[13-16]. These methods are based on the generation of thermal waves due to a transient temperature change within the sample after illumination with a pulsed or chopped optical radiation[17-30]. During the past three decades, another optical technique called photoacoustic spectroscopy (PAS) has been developed to study those materials that are unsuitable for the conventional transmission or reflection methodologies. PAS is different from the conventional techniques chiefly in that even though the incident energy is in the form of optical photons, the interaction of these photons with the material under investigation is studied not through subsequent detection and analysis of some of the photons, but rather through a direct measure of the energy absorbed by the material as a result of its interaction with the photon beam[31-37].

In PAS, the sample is always placed in a closed cell or chamber. In the case of gases and liquids, the sample fills the entire chamber. In the case of solids, the sample fills only a portion of the chamber, and the rest of the chamber is filled with a non-absorbing gas such as air. In addition, the chamber also contains a sensitive microphone. The sample is illuminated with monochromatic light that passes through an electromechanical chopper for modulation. If any of the incident photons are absorbed by the sample internal energy levels within the

sample are excited. Upon subsequent de-excitation of these energy levels, all or part of the absorbed photon energy is transformed into heat energy through non-radiative de-excitation processes. In a gas this heat energy appears as kinetic energy of the gas molecules, while in a solid or liquid, it appears as vibrational energy of ions or atoms. Since the incident radiation is intensity or frequency modulated, the internal heating of the sample is also modulated.

Since photo acoustics measures the internal heating of the sample, it is clearly a form of calorimetry, as well as a form of optical spectroscopy. There are many calorimetric techniques by which one can detect and measure the heat produced during the process. By employing a conventional calorimeter based on the usual temperature sensors such as thermistors and thermopiles, one can measure the temperature rise. These classical techniques have several disadvantages compared to photo acoustic spectroscopy in terms of sensitivity, and speed at which measurements can be made. More suitable calorimetric techniques measure heat production through volume and pressure changes produced in the sample or in an appropriate transducing material in contact with the sample.

In gaseous samples, volume changes can be quite large as a result of internal heating. In these cases, a sensitive capacitor microphone proves to be an excellent detector. When dealing with liquids or bulk solid samples, it is possible to measure heat production through subsequent pressure or stress variations in the sample itself by means of

always, possible to employ a piezoelectric detector, as in the case of powdered or gel sample. In these cases, a gas is used as a transducing medium, coupling the sample to a microphone. The periodic heating of the sample from the absorption of the optical radiation results in a periodic heat flow from the sample to the gas, which itself does not absorb the optical radiation. This in turn produces pressure and volume changes in the gas that drive the microphone.

Photo acoustics is, much more than spectroscopy. Photo acoustics can be used to measure the absorption or excitation spectrum, the life time of excited states and the energy yield of radiative processes. These are all spectroscopic measurements. On the other hand, photo acoustics can also be used to measure thickness of layers and thin films and to perform a variety of other non-spectroscopic investigations. In such studies the calorimetric or acoustic aspect of photo acoustics plays a dominant role. Thus photo acoustic studies can be performed on all types of materials – inorganic, organic and biological and on all states of matter.

7.2 History of Photo Acoustic effect

The photo acoustic effect is the process of conversion of optical energy into acoustical perturbation when modulated light interacts with matter kept in a cavity. Light absorbed by the sample will excite a fraction of the ground state molecular population into higher energy levels. These excited states will subsequently relax through a combination of radiative and non-radiative path ways. The non-

region of the excitation light beam and create a pressure wave that propagates away from the source. The pressure wave is then detected with a suitable sensor such as microphone.

The photo acoustic effect in both nongaseous and gaseous matter was discovered by Alexander Graham Bell in the year 1880. He showed that the solar radiation, dispersed with a prism and chopped at an audio frequency is absorbed by different materials to varying amounts depending upon the wavelength and produced varying audio signals. One of the transmitters of Bell called as photo phone consisted of a voice-activated mirror (which was activated by sound waves of a voice), a selenium cell and an electrical telephone receiver [6]. The intensity modulated sunlight was then focused onto a selenium cell. Since electrical resistance of selenium varies with the intensity of light falling on it, the voice modulated beam of sunlight resulted in electrically reproduced telephonic speech.

Bell demonstrated that the photo acoustic effect in solids was dependent on the absorption of light and that the strength of the acoustic signal was in turn, dependent on how strongly the incident light was absorbed by the material in the cell. He concluded that “The nature of the rays that produces sonorous effects in different substances depends upon the nature of the substances that are exposed to the beam, and that the sounds in every case are due to those rays of the spectrum that are absorbed by the body”. Bell thus correctly deduced the intrinsic optical absorptive dependence of the photo acoustic effect.

Though Bell had prophesized the scope of his novel observation, after the initial flurry of interest generated by his original work, experimentation (for nearly 50 years) with the photo acoustic effect remained almost in a dormant state. The effect was obviously considered as being no more than an interesting curiosity of no great scientific or practical value. Further more, the experiments were difficult to perform and were quantitative since they required the investigator's ear to be the signal detector. After the advent of microphones, Veingerov of Leningrad was able to observe this effect in gaseous samples. Between 1950 and 1970, the photo acoustic gas analyzer employing a conventional light source gave way to the more sensitive gas chromatographs and the spectrograph was overtaken by the more versatile infrared spectrophotometer. During this period, the photo acoustic effect was primarily employed to study vibrational life times and other aspects of radiation less de-excitation in gases. The advent of lasers in the early 1970's paved a new way in the photo acoustic spectroscopy of gaseous samples. But the applications of this technique has been effectively and efficiently extended to liquids and solids only after the successful formulation of general theoretical model by Rosencwaig and Gersho in mid seventies [1, 37].

Subsequent developments in the theoretical aspects of photo thermal phenomena are mere extensions of the modifications of R-G model. Modifications to the R-G theory by McDonald and Wetsel in 1978, by taking into account the contribution from thermally

induced vibrations in the sample are somewhat intriguing. By this time, a new form of photo acoustic configuration, namely open photo acoustic cell (OPC) had emerged. This was a major renaissance in the field of PA technique. Thermal and optical characterization of materials in solid or liquid state becomes more simple, accurate and sensitive in OPC configuration. If the sample is in solid form, it can be mounted on the OPC and from the signal amplitude or phase dependence on the modulation frequency of the excitation beam, one can easily evaluate the thermal parameters such as thermal diffusivity of the sample.

7.3 Photo Induced Processes

The absorption of photons by atoms or molecules will result in a series of processes or effects in a material. The excited level may lose its energy by radiative processes, such as spontaneous or stimulated emission, and by non radiative processes which mainly results in heat generation. If the photon energy is high enough, direct photochemical changes may take place. Destructive changes may take place at very high power densities of the incident light. A schematic representation of various photo-induced processes and main channels of photo-induced changes that occur in condensed matter is given in the following figure.

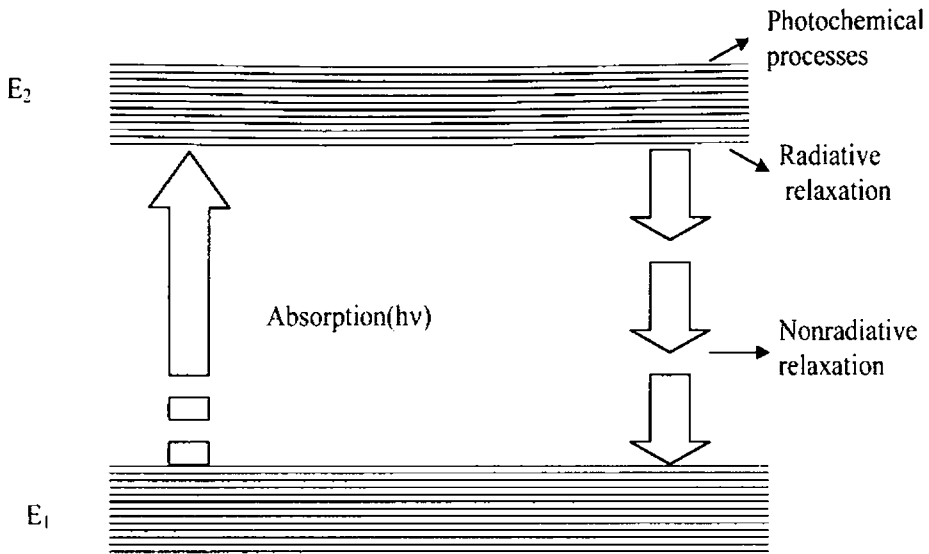


Fig. 7.1 A schematic representation of photo-induced processes

In the figure E_1 and E_2 represent the energies of the lower and upper levels and

$E_2 - E_1 = h\nu$ is the energy of the absorbed photon. The absorbed power in the sample I_{abs} is in accordance with

$$I_{\text{abs}} = I_0 [1 - \exp(-\infty L)] \cong \infty IL \dots\dots\dots (7.1)$$

with $\infty L \ll 1$. Here I and L are the incident light intensity and the sample length respectively and ∞ is the absorption coefficient.

Now, the absorbed energy will be liberated through radiative, nonradiative or chemical processes and each of these processes has specific quantum yield [38-39].

If n_r , n_{nr} and n_{pc} are the quantum yields of radiative, nonradiative and photochemical processes respectively, the total quantum yield of all the channels of de-excitation is given by

$$n_r + n_{nr} + n_{pc} = 1 \dots\dots\dots (7.2)$$

Accordingly, the intensity I_{abs} of the laser radiation absorbed over all these channels is

$$I_{abs} = I_r + I_{nr} + I_{pc} \dots\dots\dots (7.3)$$

where $I_r = n_r I_{abs}$, $I_{nr} = n_{nr} I_{abs}$ and $I_{pc} = n_{pc} I_{abs}$ are the amount of energy liberated through the radiative, nonradiative and photochemical processes respectively.

Measurement of the energy absorbed or that released through any of these relaxation channels facilitates the study of various properties and parameters of the sample.

7.4 Detection methods

Spectroscopy is the measurement and interpretation of EM radiation absorbed or emitted when the molecules or atoms or ions of a sample move from one state to another. The laser based spectroscopic techniques can be divided into

- a) Absorption method
- b) Radiative emission
- c) Non Radiative emission

The absorption method is the basic and the simplest approach and by using this technique, information regarding the optical properties and composition of the sample can be obtained by varying different parameters such as intensity, wave length, etc. of the light beam that passes through or get reflected from the sample. However a variety of external parameters such as surface quality, influence of stray light etc have a pronounced effect on the accuracy of the conventional absorption measurements. In such situations, radiative or non radiative emission measurements are more appropriate. The non radiative relaxation of photo-excited state usually results in heating of the sample. The liberated heat energy not only carries the information regarding the absorbed energy but contains details regarding the thermal properties of the sample as well. A group of such spectroscopic methods on the measurement of photo induced heating of the sample are called photo thermal methods

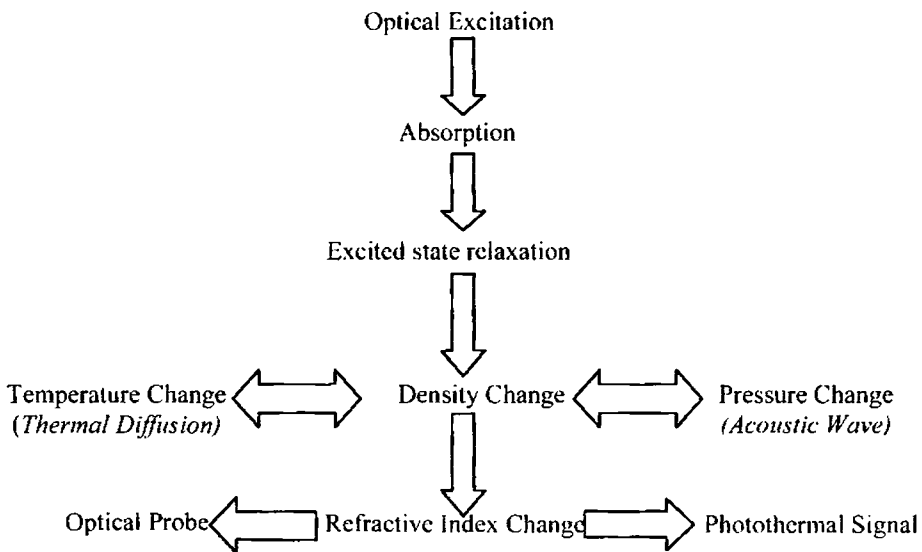


Fig. 7.2 Schematic diagram of photo thermal effects

The thermalisation of a sample as a result of non radiative relaxation brings about changes in many parameters such as density, pressure, refractive index etc. If the temperature change occurs in a faster time scale, then it will result in a pressure change in the sample.

Pressure transducers such as microphones, piezo electric crystals etc are commonly used to monitor the pressure waves associated with rapid ample heating. The branch of photo thermal spectroscopy based on the pressure wave measurement is known as photo acoustic technique.

Detection Techniques

Table 7.1 Various detection schemes

Thermodynamic Parameter	Measured Property	Detection Technique
Temperature	Temperature Infrared Emission	Calorimetry Photothermal Radiometry
<i>Pressure</i>	<i>Acoustic Wave</i>	<i>Photoacoustic Spectroscopy</i>
Density	Refractive Index Surface Deformation	P T Lens P T Interferometry P T Deflection P T Refraction P T Diffraction Surface Deflection

7.5 Photoacoustic effect in condensed media

Photoacoustic spectroscopy has been proved to be a powerful analytical tool for samples such as powders, opaque materials and even living tissues. In condensed matter, absorbed light is converted partially or totally into heat by non-radiative transitions. In the atoms or molecules, the excited level may lose its energy by spontaneous or stimulated emission. The non-radiative process mainly results in heat wave generation. For the heat wave generation, many excitation mechanisms can be used such as pulsed electrical heating or irradiation with laser etc. If the energy is high enough, direct photochemical changes such as photo decomposition, photo-ionization etc, of the excited molecule may take place. Destructive changes such as vaporization of the sample and plasma generation may take place as a result of photon-matter interaction at very high power densities of incident light.

The photo acoustic technique is essentially a closed cavity detection of energy liberated by atoms or molecules through non radiative de-excitation mechanisms subsequent to light absorption by a sample. When a solid sample is irradiated with a modulated optical radiation, the energy liberated through the non-radiative channel will result in the generation of thermal waves within the sample. The thermal waves diffused through the sample to the surrounding gas (say a cavity) carry information regarding the thermal properties of the sample.

The most widely used model for describing photo acoustic effect on condensed sample in a gas-microphone cell was originally developed by Rosencwaig and Gersho in 1976[37]. It is valid for acoustic wavelengths much greater than the dimensions of the sample and gas column.

7.6 Rosencwaig-Gersho theory

The Rosencwaig-Gersho theory is a one dimensional heat flow model for the analysis of the production of a photo acoustic signal in a cell [37]. This theory is sufficient to describe the photo acoustic signal generation in condensed media. According to R-G theory with gas-microphone detection, the signal depends on the generation of an acoustic pressure disturbance at the solid-gas interface. The generation of the surface pressure disturbance, in turn depends on periodic temperature at the sample-gas interface. The formulation of R-G model is based on the light absorption and thermal wave propagation in an experimental configuration as in figure 7.1.

Here a cylindrical cell of length L and diameter D is considered. Assume that the length L is small compared to the wavelength of the acoustic signal. The sample is considered to be in the form of a disk having diameter D and thickness l . The sample is mounted so that its front surface is exposed to the gas (air) within the cell and its back surface is a poor thermal conductor of thickness l_b . The length l_g of the gas column in the cell is then given by $l_g = L - l - l_b$. Further assumption is that the gas and backing materials are not light absorbing.

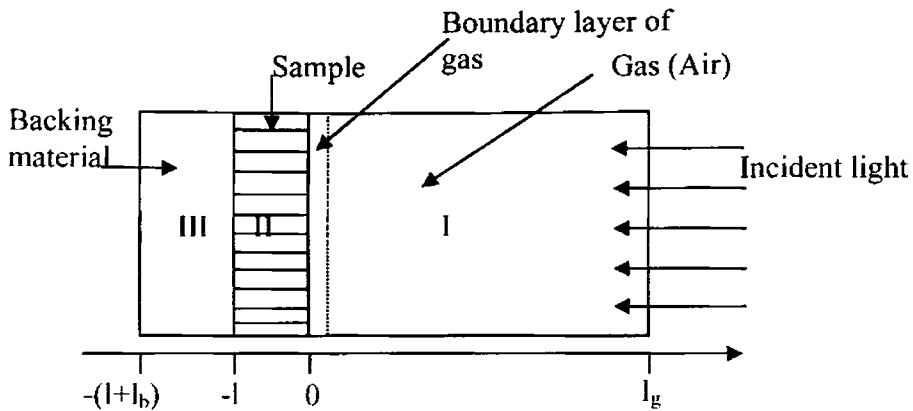


Fig.7.3 Schematic diagram of photoacoustic setup

Let k_i , ρ_i , C_i , and α_i represent the thermal conductivity, density, specific heat and thermal diffusivity respectively of the material i . Then $a_i = (\omega/2\alpha_i)^{1/2}$ is the thermal diffusion co-efficient and $\mu_i = 1/a_i$ is the thermal diffusion length of the material. i can be s , g and b for solid, gas and backing material respectively. ω denotes the chopping frequency of the incident light beam in radians per second.

Assume that the sinusoidally chopped monochromatic light with wavelength λ is incident on the solid with intensity

$$I = (1/2) I_0 (1 + \cos \omega t) \dots\dots\dots (7.4)$$

The thermal diffusion equation in the three regions can be written as[5]

$$\frac{\partial^2 \varphi}{\partial t^2} = \frac{1}{\alpha_b} \frac{\partial \varphi}{\partial t}, \quad -l-l_b \leq x \leq -l \quad \text{Region III} \dots\dots\dots (7.5)$$

$$\frac{\partial^2 \varphi}{\partial t^2} = \frac{1}{\alpha_g} \frac{\partial \varphi}{\partial t}, \quad 0 \leq x \leq -l_g \quad \text{Region I} \dots\dots\dots (7.6)$$

$$\frac{\partial^2 \varphi}{\partial t^2} = \frac{1}{\alpha_s} \frac{\partial \varphi}{\partial t} - A \exp(\beta x) [1 + \exp(j\alpha x)], \quad -l \leq x \leq 0 \text{ Region II} \dots\dots\dots (7.7)$$

where $A = \frac{\beta I_0 \eta}{2k_s} \dots\dots\dots (7.8)$

Here φ is the temperature and η is the light conversion efficiency. The real part of the complex-valued solution $\varphi(x, t)$ of the above equations is the solution of physical interest and represents the temperature in the cell relative to the ambient temperature as a function of position and time. Thus, the actual temperature field in the cell is given by,

$$T(x,t) = \text{Re}[\varphi(x, t)] + \phi \dots\dots\dots (7.9)$$

where Re denotes "the real part of" and ϕ is the ambient (room) temperature.

The complex amplitude of the periodic temperature distribution, θ at the solid-gas boundary ($x=0$) is given by

$$\theta = \frac{\beta I_0}{2k_s(\beta^2 - \sigma_s^2)} \left(\frac{(r-1)(b+1)\exp(\sigma_s l) - (r+1)(b-1)\exp(-\sigma_s l) + 2(b-r)\exp(-\beta l)}{(g+1)(b+1)\exp(\sigma_s l) - (g-1)(b-1)\exp(-\sigma_s l)} \right) \dots\dots (7.10)$$

Where

$$b = \frac{k_b a_b}{k_s a_s}, \quad g = \frac{k_g a_g}{k_s a_s}, \quad r = (1-j) \frac{\beta}{2a_s} \quad \text{and} \quad \sigma_s = (1+j)\alpha_s \dots\dots\dots (7.11)$$

The main source of acoustic signal arises from the periodic heat flow from the solid to the surrounding gas. The periodic heating causes the boundary layer of gas to expand and contract periodically. This can

be thought of as the action of an acoustic piston on the rest of the gas column, producing an acoustic pressure signal that travels through the entire gas column. The displacement of the gas piston due to the periodic heating can be estimated using the ideal gas law,

$$\delta x(t) = 2\pi\mu_g \frac{\bar{\phi}(t)}{T_0} = \frac{\theta\mu_g}{\sqrt{2}T_0} \exp\left[j\left(\omega t - \frac{\pi}{4}\right)\right] \dots\dots\dots (7.12)$$

where the average dc temperature of the gas boundary layer is set as the dc temperature at the solid surface, $T_0 = \phi + \theta_0$, ϕ being the ambient temperature at the cell walls. Assuming that the rest of the gas responds to the action of the piston adiabatically, the acoustic pressure in the cell due to the displacement of the gas piston can be obtained from the adiabatic gas law $PV^\gamma = \text{constant}$, where P is the pressure, V is the gas volume in the cell, and γ the ratio of the specific heats. Thus the incremental pressure is

$$\delta P(t) = \frac{\gamma P_0}{V_0} \delta V = \frac{\gamma P_0}{l_g} \delta x(t) \dots\dots\dots (7.13)$$

where P_0 and V_0 are the ambient pressure and volume respectively and $-\delta V$ is the incremental volume. Then from equations (7.12) & (7.13)

$$\delta P(t) = Q \exp\left[j\left(\omega t - \frac{\pi}{4}\right)\right] \dots\dots\dots (7.14)$$

where

$$Q = \frac{\gamma P_0 \theta}{\sqrt{2} l_g a_g T_0} \dots\dots\dots (7.15)$$

The actual physical pressure variation is given by the real part of $\delta P(t)$ and Q specifies the complex envelope of the sinusoidal pressure variation.

Substituting for θ

$$Q = \frac{\beta I_0 \mathcal{P}_0}{2\sqrt{2}k_s l g_a g T_0 (\beta^2 - \sigma_s^2)} \times \left(\frac{(r-1)(b+1)\exp(\sigma_s l) - (r+1)(b-1)\exp(-\sigma_s l) + 2(b-r)\exp(-\beta l)}{(g+1)(b+1)\exp(\sigma_s l) - (g-1)(b-1)\exp(-\sigma_s l)} \right) \dots\dots (7.16)$$

Thus, equation (7.16) can be used to evaluate the amplitude and phase of the acoustic pressure wave produced in the cell by photo acoustic effect. It can be observed that interpretation of the full expression for $\delta P(t)$ is difficult because of the complex expression of Q . Some physical insight can be gained if certain special cases according to the optical opaqueness of solids are examined. For each category of optical opaqueness, three cases according to the relative magnitude of the thermal diffusion length μ_s , as compared to the physical length l and the optical absorption length μ_β can be considered.

Defining $Y = \frac{\mathcal{P}_0 l_0}{2\sqrt{2}l g T_0}$, (7.17)

CASE I: Optically Transparent solids ($\mu_\beta > 1$)

1. *Case Ia : Thermally Thin Solids ($\mu_s \gg l ; \mu_s \gg \mu_\beta$)*

We can set $e^{-\beta l} \cong 1 - \beta l$, $e^{\pm \sigma l} \cong 1$ and $|t| > 1$ in equation (7.17) and hence we obtain

$$Q = \frac{(1-i)\beta l}{2a_g} \left(\frac{\mu_b}{k_b} \right) Y \dots\dots\dots (7.18)$$

Thus the acoustic signal is proportional to βl and varies as f^1 . In addition, the thermal properties of the backing material come into play in the expression for Q.

2. *Case Ib: Thermally Thin Solids ($\mu_s > l ; \mu_s < \mu_\beta$)*

Here we can set $\exp(-\beta l) \cong 1 - \beta l$, $e^{\pm \sigma l} \cong 1 \pm \sigma_s l$ and $|t| < 1$ in equation (7.17).

$$\text{Then } Q = \frac{(1-j)\beta l}{2a_g} \left(\frac{\mu_b}{k_b} \right) Y \dots\dots\dots (7.19)$$

This equation is identical with equation (7.18) and hence the acoustic signal behaves in the same fashion.

3. *Case Ic: Thermally Thick Solids ($\mu_s > l ; \mu_s \ll \mu_\beta$)*

In this case we set $\exp(-\beta l) \cong 1 - \beta l$, $e^{\pm \sigma l} \cong 0$ and $|t| \ll 1$ in equation (7.17)

$$\text{Now } Q = -j \frac{\beta l}{2a_g} \left(\frac{\mu_s}{k_s} \right) Y \dots\dots\dots (7.20)$$

The acoustic signal is now proportional to $\beta\mu_s$ rather than βl . This means that light absorbed within the first thermal diffusion length contributes to the signal, although light is being absorbed throughout the length of the solid. Moreover, μ_s being less than the thickness l , thermal properties of the backing material will not influence the signal. Here the signal varies as $f^{3/2}$ with the modulation frequency.

CASE II: Optically Opaque Solids

Case II a: Thermally Thin Solids ($\mu_s \gg l ; \mu_s \gg \mu_\beta$)

In equation (7.17), we set $\exp(-\beta l) \cong 0, e^{\pm\sigma l} \cong 1$ and $l \gg 1$

Then we obtain

$$Q = \frac{(1-j)}{2a_g} \left(\frac{\mu_b}{k_b} \right) Y \dots\dots\dots (7.21)$$

Here the photo acoustic signal is independent of β , which is valid for a perfect black absorber. The signal depends on the thermal properties of the backing material and varies as $1/f$.

Case II b: Thermally Thick Solids ($\mu_s < l ; \mu_s > \mu_\beta$)

We set $\exp(-\beta l) \cong 0, e^{-\sigma l} \cong 0$ and $l \gg 1$ in equation (7.17)

We obtain
$$Q = \frac{(1-j)}{2a_g} \left(\frac{\mu_s}{k_s} \right) Y \dots\dots\dots (7.22)$$

Though equations (7.21) & (7.22) are similar, in the present case there is no contribution from the thermal properties of the backing material.

Case II c: Thermally Thick Solids ($\mu_s \ll l$; $\mu_s < \mu_\beta$)

We set $\exp(-\beta l) \cong 0$, $e^{-\sigma l} \cong 0$ and $|r| < 1$ in equation (7.17). Then we obtain

$$Q = \frac{-j\beta\mu_s}{2a_g} \left(\frac{\mu_s}{k_s} \right) Y \dots\dots\dots (7.23)$$

The photo acoustic signal will be proportional to $\beta\mu_s$. The signal is independent of the thermal properties of the backing material and varies as $f^{3/2}$.

A theoretical analysis of the photo acoustic effect applied to different cases has been discussed and can be applied to the study of any kind of sample.

The photo acoustic measurements can be done in two different configurations (1) By heat transmission and (2) By heat reflection configurations. The photo acoustic cell can be designed for the two configurations. The simplest and convenient form of a cell that can be used for heat transmission configuration is the open photo acoustic cell.

7.7 Open photo acoustic cell configuration

Open photo acoustic cell (OPC) configuration is a modified form of conventional photo acoustic cell configuration. In the OPC, the solid sample can be mounted directly on top of the microphone, leaving a small volume of air in between the sample and microphone. It is an open cell detection configuration in the sense that the sample is placed on top of the detection system as in the case of piezoelectric and

pyroelectric detection. Consequently this configuration is a minimum volume detection scheme and hence the signal strength will be much greater than that in conventional PA configurations. The major advantage of this configuration is that samples having large sizes can also be studied, whereas in conventional PA cells, sample size should be small enough to be contained inside the PA cavity. A schematic representation of the typical OPC is shown in figure 7.4.

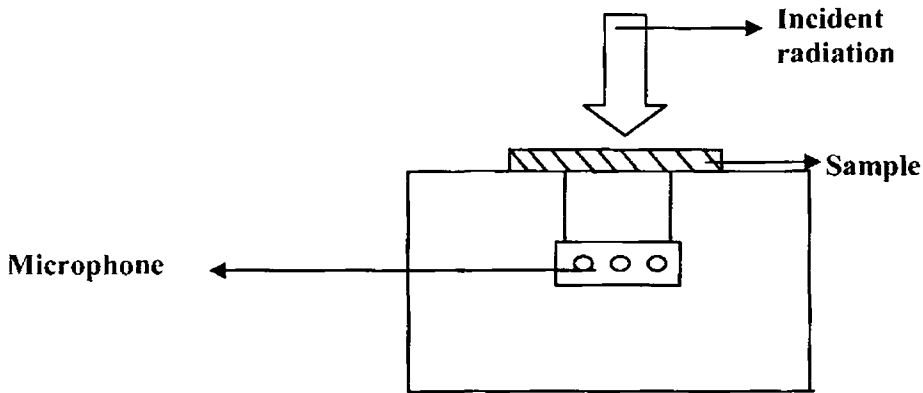


Fig. 7.4 OPC configuration

According to R G theory, the pressure variations in the acoustic chamber for an OPC detection configuration is given by,

$$Q_{th} = \frac{\gamma P_0 I_0 (\alpha_g \alpha_s)^{1/2} e^{j(\omega t - \pi/2)}}{2\pi T_0 l_g K_g f \sinh(l_s \sigma_s)} \dots\dots\dots (7.24)$$

where γ is the ratio of specific heats of air, I_0 is the intensity of incident light beam, $P_0(T_0)$ is the ambient pressure (temperature), f is the modulation frequency, l_i, k_i and α_i are the thickness, thermal conductivity

and thermal diffusivity of the medium i , where $i=g$ refers to the gas and $i=s$ refers to the sample under investigation. Also $\sigma_i=(1+i)a_i$, where thermal diffusion co-efficient, $a_i= \frac{\sqrt{\omega}}{\sqrt{2\alpha_i}}$

For a thermally thin sample, ($l_s\alpha_s \ll 1$), the above equation reduces to,

$$Q_{th} \approx \frac{\gamma P_0 (\alpha_g)^{1/2} \alpha_s e^{j(\omega t - 3\pi/4)}}{(2\pi)^{3/2} T_0 l_g l_s k_s f^{3/2}} \dots\dots\dots (7.25)$$

In this case, the amplitude of the photo acoustic signal varies as $f^{1.5}$

At higher modulation frequencies, the sample becomes thermally thick, ($l_s\alpha_s \gg 1$), so that photo acoustic signal obeys the equation,

$$Q_{th} \approx \frac{\gamma P_0 I_0 (\alpha_g \alpha_s)^{1/2}}{\pi T_0 l_g k_s} \frac{e^{-l_s \sqrt{\frac{\pi f}{\alpha_s}}}}{f} e^{j(\omega t - \frac{\pi}{2} - l_s \alpha_s)} \dots\dots\dots (7.26)$$

From the last equation it is obvious that for thermally thick sample, the amplitude of photo acoustics signal varies as $(1/f)\exp(-b\sqrt{f})$, where $b=l_s\sqrt{\pi/\alpha_s}$, whereas phase decreases linearly with \sqrt{f} , namely,

$$\Phi_{th} = -\pi/2 - b\sqrt{f} \dots\dots\dots (7.27).$$

Hence the thermal diffusivity can be evaluated either from the amplitude or phase of the PA signal obtained under heat transmission configuration. A necessary condition that should be satisfied for employing OPC configuration is that the specimen under investigation should be opaque at the incident wavelength. Though the phase and

amplitude of the PA signal contains clear signature of the thermal transport properties of the specimen, phase data is more reliable for OPC since the amplitude data depends on many external parameters such as surface quality and detector response at different wavelengths.

However for plate shaped specimens, the contribution to the PA signal from the thermo elastic bending due to the temperature gradient existing in the specimen cannot be neglected, especially when the sample is in the thermally thick region. The existence of temperature gradient causes an expansion of the sample parallel to the sample surface, thereby inducing bending along the thickness direction. Such a vibrating sample acts as a mechanical piston; this is otherwise known as drum effect. For an optically opaque sample, in the thermally thick regime, the pressure fluctuation in the air chamber of the OPC detector from the thermo elastic displacement is given by[40],

$$Q_{el} \approx \frac{3\alpha_T R^4 \gamma P_0 l_0 \alpha_s \left[\left(1 - \frac{1}{z}\right)^2 + \frac{1}{z^2} \right]^{\frac{1}{2}} e^{j(\omega t + \pi/2 + \Phi)}}{4\pi R_c^2 l_s^2 l_g k_s f} \dots\dots\dots (7.28)$$

Where $z = b\sqrt{f}$, $\Phi = \tan^{-1}(1/(z-1))$ and α_T is the sample thermal expansion co-efficient. R is the radius of the front hole of the microphone and R_c is the radius of the OPC air chamber. The above equation means that the thermo elastic contribution, at high frequencies varies as f^1 and the phase Φ follows the expression

$$\Phi_{el} \approx \Phi_0 + \tan^{-1}(1/(z-1)) \dots\dots\dots (7.29)$$

Thus for thermally thick sample, if thermo elastic contribution is dominant, the thermal diffusivity value can be evaluated from the modulation frequency dependence of the signal phase.

In the next section of this chapter, the thermal diffusivity analysis of PANI (HCl) and PANI (HCl)-MWNT composites are carried out. The thermal diffusivities are calculated using thermo elastic bending formula applied to open photo acoustic technique in transmission configuration.

Experimental

7.8 Thermal diffusivity measurements on PANI (HCl) and PANI (HCl)-MWNT composites

Although PANI and its composites have been widely investigated over the years, their thermal properties have been unfortunately ignored. For the fabrication of devices capable of working in the high temperature region, the thermal behaviour of such materials has to be studied in detail.

In this section, thermal diffusivity measurements on PANI (HCl) and PANI (HCl)-MWNT composites with different aniline to MWNT feed ratios are described. The thermal diffusivity of the composite depends on the thermal conductivity as well as thermal diffusivity of its components[41-42].MWNT is a material with good thermal conductivity as already described in chapter5.So it is relevant to study the variation of thermal diffusivity of the composites with varying aniline to MWNT feed ratios.

7.9 Experimental Setup

The experimental setup consists of a) *Laser source* b) *Open Photoacoustic cell (OPC)* c) *Mechanical chopper* d) *Lock-in-amplifier*.

- a) The *Laser source* used in the present investigation is **He-Ne laser** (6328 \AA) of power 20 mW. The original laser beam has a spot size of 0.7mm and is used without focusing to avoid lateral heat flow.
- b) A *conventional OPC* made of stainless steel of radius 2cm (figure 7.5) is used in which the sample is placed directly on top of microphone by leaving a small volume of gas in between the two. Such OPC's can be used only in the heat transmission configuration. The microphone used is a highly sensitive electret microphone (Knowles FG 3329). Shielded wires are used to take electrical connections directly from the microphone. The samples can be fixed on to the sample chamber by means of vacuum grease.

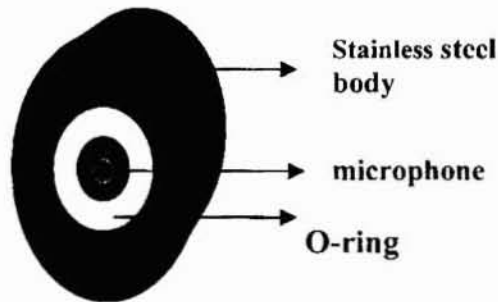


Fig. 7.5 Open photo acoustic cell

- c) The model *SR 540 mechanical chopper* is used to square-wave modulate the intensity of the optical signal. The unit can chop light sources at rates from 4Hz-4 kHz. The choice of operating frequency is influenced by several factors. In general, phase jitter, background noise and lock-in-amplifier noise all degrade at low frequencies. For frequencies from 4Hz to 400Hz, the six slot blade is used whereas for frequencies from 400 Hz to 4 kHz, the thirty slot blade is used.
- d) The *Lock-in amplifier* used in the present study is *Stanford Research model (SR 830)*. Lock-in amplifiers are used to detect and measure very small AC signals (upto nanovolts). Accurate measurement may be made even when the small signal is obscured by noise sources many thousands of times larger. Lock-in amplifiers use a technique known as phase-sensitive detection to single out the component of the signal at a specific reference frequency and phase. Noise signals at frequencies other than the reference frequency are rejected and do not affect the measurement. According to Fourier theorem any input signal can be represented as the sum of many sine waves of differing amplitudes, frequencies and phases. The lock-in amplifier multiplies the signal by a pure sine wave at the reference frequency. All components of the input signal are multiplied by the reference simultaneously. The average of the product of two sine waves is zero unless the frequencies are exactly the same. The product of this multiplication yields a DC output signal proportional to the component of the signal whose frequency is exactly locked to the reference frequency. The low pass filter, which follows the

multiplier, provides the averaging which removes the products of the reference with components at all the other frequencies. In the general case, the input consists of signal plus noise. Noise is represented as varying signals at all frequencies. The ideal lock-in only responds to noise at the reference frequency. Noise at other frequencies is removed by the low pass filter following the multiplier. This “bandwidth narrowing” is the primary advantage that a lock-in amplifier provides. Only inputs at frequencies at the reference frequency result in an output. A schematic of the experimental setup is shown in figure 7.6.

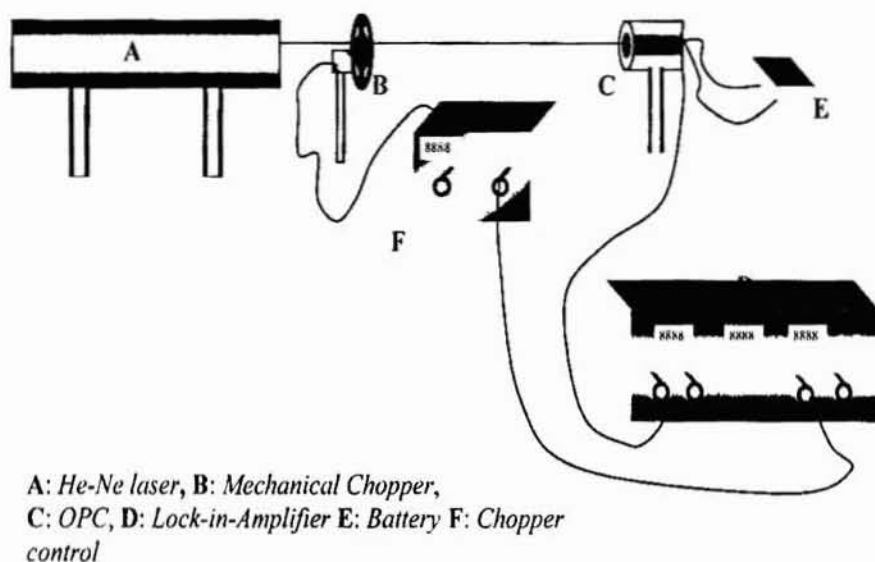


Fig. 7.6 Photo acoustics setup

7.10 Experimental procedure

In the OPC, the solid plate like sample is fixed on the top of the microphone using vacuum grease at the edges, leaving a small volume

of air in between the sample and microphone and the sample is irradiated at its surface facing the ambient. This configuration is a minimum volume PA detection scheme and hence the signal strength is much greater than the conventional PA configuration. A cross-sectional view of the OPC used in the experiment is shown in the figure 7.6. Continuous-wave laser emission at 6328\AA from a He-Ne laser of 20 mW is used as the source of excitation. The original laser beam has a spot size of 0.7mm and is used without focusing to avoid lateral heat flow. The signal is detected using a highly sensitive electret microphone kept in the side chamber. A mechanical chopper is used to modulate the laser beam at the desired frequency. The PA signal is produced in a small volume of air in between the sample and microphone. The phase and amplitude as a function of modulation frequency is recorded using dual phase lock-in-amplifier.

Hence the thermal diffusivity α_s of the sample can be easily evaluated from either a signal amplitude plot or a phase plot. A necessary condition for employing the OPC configuration is that the sample would be optically opaque at the incident wavelength. Though the phase and amplitude of the PA signal contains clear signature of the thermal transport properties of the sample, phase data are more reliable since the amplitude data depend on many external parameters such as sample surface quality and the detector response at different modulation frequencies.

7.11 Analysis of thermal diffusivity results

Plots of phase vs frequency^{1/2} plots of PANI (HCl) and PANI (HCl)-MWNT composites with various aniline to MWNT feed ratios are given in

figures 7.7-7.10. Samples are taken in the form of pressed pellets of 1mm thickness and 1.2cm diameter, applying uniform pressure.

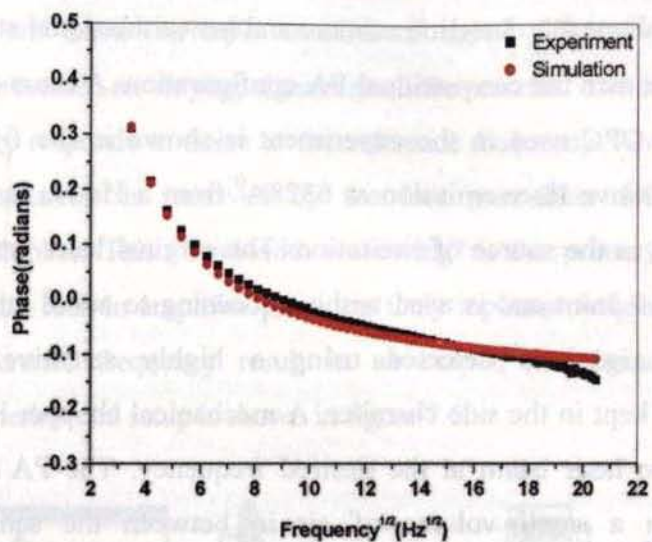


Fig. 7.7 Phase vs. square root of frequency plot of PANI (HCl)

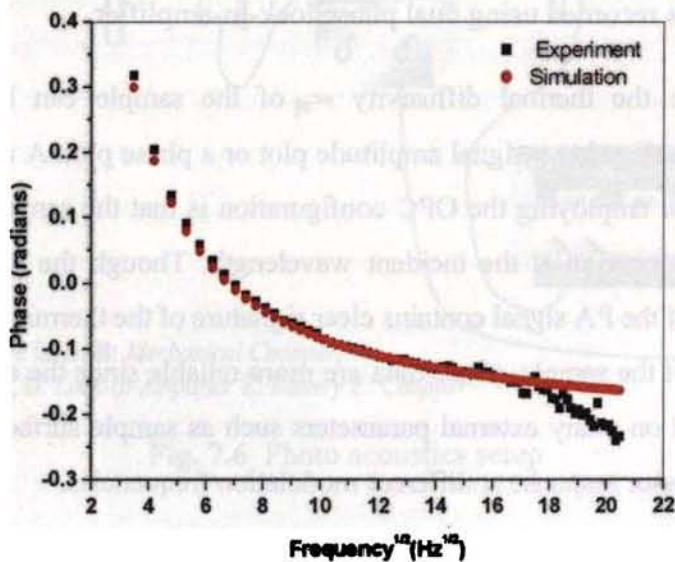


Fig. 7.8 Phase vs. square root of frequency plot of PANI (HCl)-MWNT (1:0.1) composite

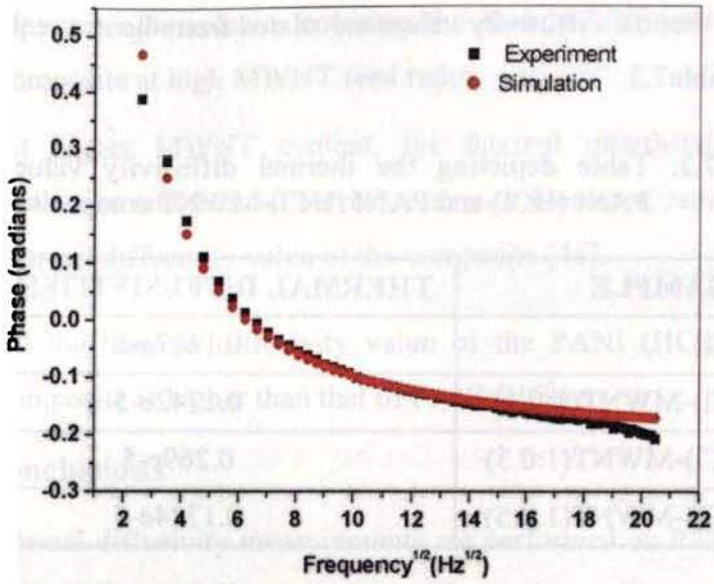


Fig. 7.9 Phase vs. square root of frequency plot of PANI (HCl)-MWNT (1:0.3) composite

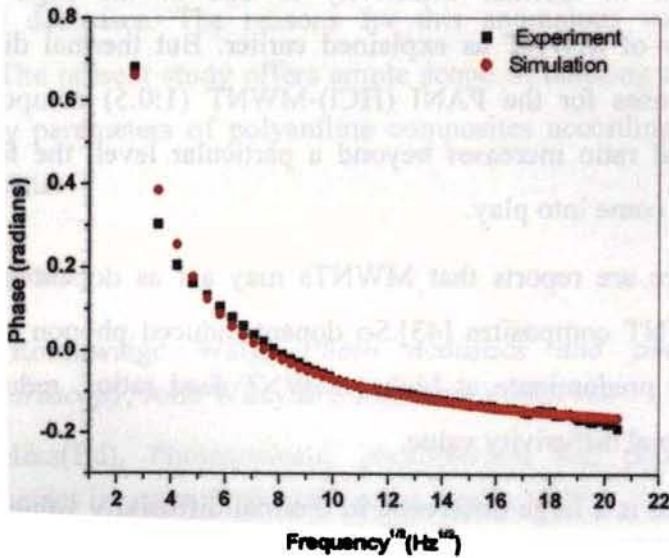


Fig. 7.10 Phase vs. square root of frequency plot of PANI (HCl)-MWNT (1:0.5) composite

The thermal diffusivity values calculated from the above plots are given in table7.2.

Table 7.2. Table depicting the thermal diffusivity values of PANI (HCl) and PANI (HCl)-MWNT composites

SAMPLE	THERMAL DIFFUSIVITIES (m^2s^{-1})
PANI(HCl)	0.1427e-5
PANI(HCl)-MWNT(1:0.1)	0.1742e-5
PANI (HCl)-MWNT(1:0.3)	0.269e-5
PANI (HCl)-MWNT(1:0.5)	0.1724e-5

The thermal diffusivity values of the composites increase with increase in MWNT loading up to 1:0.3 ratio. Obviously the enhancement in thermal diffusivity is due to the high thermal conductivity of MWNT as explained earlier. But thermal diffusivity value decreases for the PANI (HCl)-MWNT (1:0.5) composite. As MWNT feed ratio increases beyond a particular level, the following effects may come into play.

- a) There are reports that MWNTs may act as dopant in PANI-MWNT composites [43].So dopant induced phonon scattering may predominate at higher MWNT feed ratios, reducing the thermal diffusivity value.
- b) There is a large difference in thermal diffusivity value between PANI and MWNT.This thermal diffusivity mismatch [44] may

play a major role in lowering the thermal diffusivity of the composite at high MWNT feed ratios.

- c) At higher MWNT content, the thermal interfacial contact resistance and thermal barrier resistance increases, reducing the thermal diffusivity value of the composite [45].

Still the thermal diffusivity value of the PANI (HCl)-MWNT (1:0.5) composite is higher than that of PANI (HCl).

7.12 Conclusions

Thermal diffusivity measurements are performed on PANI (HCl) and PANI (HCl)-MWNT composites with varying aniline to MWNT feed ratios. It is found that the thermal diffusivity value for the composite increases with MWNT loading up to 1:0.3 ratio and thereafter decreases. The reasons for this anomalous variation are studied. The present study offers ample scope in tailoring the thermal diffusivity parameters of polyaniline composites according to device requirements.

References

- [1] A Rosenwaigc Waig, *Photo acoustics and photoacoustic spectroscopy*, John Wiley & Sons, New York,1980
- [2] P Hess(Ed), *Photoacoustic, photothermal and photochemical processes in gases*, Springer-Verlag, Berlin,1989
- [3] P Hess, J Pelzl(Eds), *photo acoustic and photo thermal phenomena*, Springer-Verlag,Berlin,1988

- [4] S E Bialkowski, *Photothermal Spectroscopy Method Chemical Analysis*, Wiley, New York, 1996
- [5] G Chen, *Phys.Rev.B*, 57(1998)14958
- [6] E Luscher, P Kurpiun, H Coufal, R Tilgner, *Photoacoustic effect: principles and applications*, Friedr. Vieweg & Sohn, Braunschweig, 1984
- [7] J A Sell(Ed), *Photo thermal investigations of solids and fluids*, Academic Press, Boston, 1989
- [8] P Hess(Ed), *Photo acoustic and photo thermal processes at surfaces and thin films*, Springer-Verlag, Berlin, 1989
- [9] A Mandelis (Ed), *Photo acoustic and thermal wave phenomena in semiconductors*, North Holland, New York, 1987
- [10] Y H Pao(Ed), *Optoacoustic spectroscopy and detection*, Academic press, New York, 1977
- [11] D Bicanic (Ed), *proceedings of seventh international topical meeting on photo acoustic and photo thermal phenomena*, 1991
- [12] J Badoz, D Fournier(Eds), *Photo acoustic and photo thermal spectroscopy*, *J.de Phys.*, Colloque C6(Les Editions de Physique, Les Ulis), 1983
- [13] Yu G Gurevich, G Gonzalez da la Cruz, G Logvinov, M N Kasyanchuk, *Semiconductors*, 32(11)(1998)1179
- [14] A Mandelis, *Physics Today*, August(2000)29
- [15] George Biranbaum, Bert A Auld(Ed), *Sensing for materials characterization, processing and manufacturing*, The American Society for Nondestructive Testing, Inc., Columbus, 1998
- [16] A Mandelis (Ed), *Principles and Perspectives of Photo thermal and Photo acoustic Phenomena*, Elsevier, Oxford, 1992

- [17] H Vargas, L C M Miranda, *Phys.Rep.*, 161(2)(1988)43
- [18] D Fournier, A C Boccara, A Skumanich, N M Amer, *J.Appl. Phys.* 59 (3)(1986)787
- [19] I A Vitkin, C Christifields, A Mandelis, *Appl.Phys.Lett.*, 54 (1989) 2392
- [20] A Mandelis, M M Zver, *J.Appl.Phys.*, 57(1985)4421
- [21] H Coufal, *Appl.Phys.Lett.*, 45(1984)516
- [22] A Mandelis, *Nondestructive Evaluation*, PTR Prentice Hall, Englewood Cliffs, New Jersey, 1994
- [23] R L Thomas, *Anal. Sciences*, April (2001)17
- [24] H Shinoda, T Nakajima, K Ueno, N Koshida, *Nature*, August (1999) 400
- [25] H Vargas, L C M Miranda, *Review of Scientific Instruments*, 74(1)(2003)794
- [26] P Helander, *J.Photoacoust.*, 1(1982)103
- [27] Achamma Kurian, K P Unnikrishnan, Sajan D George, Pramod Gopinath, V P N Nampoori, C P G Vallabhan, *Spectrochimica Acta part A*, 59(2003)487
- [28] P R Bajra, *Revista Physicae*, 1(2000)1
- [29] J R D Pereira, A M Mansanares, E C de Silva, J Palangana, M L Baesso, *Molecular Crystals and Liquid Crystals*, 332(1999)569
- [30] F Scudeiri, M Bertolotti, *Proce. 10th Conference of Photo acoustic and Photo thermal Phenomena*, AIP, New York, 1999
- [31] A Rosenwaig, *Science*, 181(1973)657
- [32] A Rosenwaig, *Phys.Today*, 29(1975)23

- [33] A Rosencwaig, *Anal.Chem.*,47(6)(1975)502
- [34] A Rosencwaig, *Rev.Sci.Instrum.*,48(1977)1133
- [35] A Rosenwaig, *Opt.Commun.*,7(1973)305
- [36] A Rosenwaig, *Anal.Chem.*,47(1975)592
- [37] A Rosenwaig A Gersho., *J.Appl.Phys.*47(1976)64
- [38] K K R Mukherjee, *Fundamentals of Photochemistry*, New Age International, NewDelhi,1978
- [39] Dieter K. Schroder. *Semiconductor material and device characterization*. John Wiley 3rd Ed., 2005.
- [40] L F Perondi, L C M Miranda, *J.Appl.Phys.*62(7)(1987)2955
- [41] V Pilla, D T Balogh, R M Faria, T Catunda, *Rev.Sci.Instrum.*74, 91(2003)866
- [42] A Salzar, *Euro.J.Phys.*24 (2003)1
- [43] H Zengin, W Zhou, J Jin, R Czrew, D W Smith.Jr, L Echegoyen, D L Carroll, S H Foulger, J Ballato, *Adv.Mater*, 14(2002)1480
- [44] P J Mendoza, A Mandlies, L Nicolaidis, J Huaretta, E M Rodriguez, *Anal.Sci.*17 (2001) S29
- [45] D Forunier, J P Roger, A Bellouati, C Boue, H Stamm, F Lekstani, *Anal.Sci.* 17(2001) S158



Chapter **8**

SUMMARY AND FUTURE PROSPECTS

Contents

- 8.1 Towards conducting polymers**
 - 8.2 Missing links**
 - 8.3 Focus of the present work**
 - 8.4 Summary of the work done**
 - 8.5 Scope for further work**
-

8.1 Towards conducting polymers

Mankind has always been in the pursuit of new materials for better performance. This quest for excellence started from the early years of civilization. Discovery of metals was a major breakthrough in technological development. This paved way for progress in the fields such as industry, agriculture, medicine, communication, defence and transport. Despite having high electrical conductivity, strength and durability, metals suffered from many drawbacks like heavy weight and susceptibility to corrosion. The realization that polymers, once scouted as insulators, could conduct electricity provided the cutting edge. The electrical conductivity of conducting polymers could be tuned from insulating to metallic through proper doping and optimization of synthesis conditions. In addition to good electrical conductivity, many of the conducting polymers exhibit significant photoluminescence and

electroluminescence, making them compatible for use as hole injecting electrodes as well as emissive layers in polymer LEDs. Compared to conventional metals, they are light, resistant to corrosion, easily processible and cheap. These advantageous aspects boost their applications as effective discharge layers as well as conducting resists in electron beam lithography, in the metallization of printed circuit boards, as excellent corrosion protection layers for metals and in electromagnetic shielding.

8.2 Missing links

In spite of the rapid flourish in conducting polymer research, there are gap areas which have to be addressed in depth. The conduction mechanism in polymers is still controversial. Metallic conductivity has already been achieved in polymers. But the origin of metallic nature in such materials is still not properly understood. There has not been much focus on the photo luminescent properties of doped conducting polymers, especially PANI and its composites. The origin and nature of various optical transitions are still to be explored. The processibility of conducting polymers and their composites in the form of films has to be improved.

8.3 Focus of the present work

The materials selected for the present study are PANI doped with various dopants, PANI-PMMA composites, MWNT, PANI-MWNT composites, and films of PANI and PANI-MWNT composites. The motivation for selecting these materials is,

- a) PANI is a material with excellent electrical and optical properties.
- b) These materials have numerous technological applications.
- c) The luminescent behaviour of PANI and PANI-PMMA composites are not well studied.
- d) The semi metallic nature of PANI and PANI-MWNT composites has to be explored in depth.
- e) The optical transition energy gaps of films of PANI and its composites and the origin of various optical transitions have to be addressed in detail.
- f) Aniline monomer is comparatively cheap and PANI can be easily synthesized using chemical oxidative polymerization.

8.4 Summary of the work done

PANI samples doped with three different acids-HCl, CSA and H_3PO_4 , are synthesized using chemical oxidative polymerization technique with APS as oxidant. FTIR and Raman spectra show all the reported peaks of doped PANI. There is a small shift in Raman wave numbers corresponding to PANI doped with various acids. A comparison of the X.R.D spectra of the samples reveals that PANI (H_3PO_4) exhibits the highest extent of crystallinity. The peak at 25° , in particular, corresponding to the degree of π conjugation, is very sharp and intense in orthophosphoric acid doped PANI. The incorporation of the bulky PO_4^- group demands more orderly arrangement of the polymer chains resulting in better crystallinity. The

P.L studies of the samples are performed with excitation wavelength chosen at 365nm. (This is because the π - π^* transition wavelength of the benzenoid unit, the unit responsible for photoluminescence in PANI, corresponds to about 330 nm.) Emission is observed at around 450nm. Highest P.L emission intensity is recorded for PANI (H_3PO_4), followed by PANI(HCl) and PANI(CSA). The high P.L emission intensity of PANI (H_3PO_4) is due to the more orderly arrangement of benzenoid and quinonoid units (i.e., better Π conjugation) in it, as evident from the X.R.D spectrum. As Π conjugation increases, the probability for singlet exciton formation, the species mainly responsible for photoluminescence in conjugated polymers, increases. The decay of singlet excitons thus formed to the ground state results in photoluminescence. The possible reason for PANI (HCl) to show slightly higher P.L emission as compared to PANI (CSA) may be the presence of lighter dopant ions in HCl doped PANI (Cl^-), with higher mobility compared to the heavier dopant ions (SO_3^-) in CSA doped PANI. All the three samples show negligible variation of D.C electrical conductivity with temperature. PANI (HCl) has the highest room temperature D.C electrical conductivity possibly due to the presence of lighter Cl^- ions. PANI (H_3PO_4) exhibits slightly higher room temperature D.C electrical conductivity as compared to PANI (CSA), despite the presence of bulky PO_4^- ions in it. The possible reason may be the better crystallinity of PANI (H_3PO_4), which compensates for the heaviness of the dopant ions.

Nanomaterial research has come to the forefront of global research and development programmes recently, owing to the versatile applications of nano materials in all walks of science and technology. Samples with nano scale dimensions have properties entirely different from their bulk counter parts. Nano scale device engineering has reduced the size of electronic devices to amazingly smaller dimensions. In the present work, HCl doped PANI nano rods are produced using dispersion polymerization technique with APS as oxidant. The advantages of dispersion polymerization are its high yield and the absence of byproducts. Samples are prepared with various aniline to APS feed ratios. The FTIR spectrum of PANI nano rods is similar to PANI (micro), but the peaks are sharper. X.R.D spectra clearly indicate that PANI nano rods are more crystalline as compared to PANI (micro). The peak at 25° , in particular, is more intense and sharper for PANI nano rods, indicating better Π conjugation. As the APS feed ratio increases, crystallinity decreases. This is because as APS loading increases, the rate of polymerization also increases. If the rate of polymerization exceeds a particular limit, the orderly arrangement of benzenoid and quinonoid units may be lost, resulting in reduced crystallinity. The formation of nano rods with average diameter 10-15nm is clear from the TEM images. The PANI nano rods with aniline to APS feed ratio 1:1.2 exhibit D.C electrical conductivity of the order of 16S/cm, compared to that of HCl doped PANI (micro), which is around 2S/cm. The better crystallinity of PANI nano rods implies greater long range order favouring effective charge transfer along the chains. This results in higher electrical conductivity. PANI nano rods

synthesized with aniline to APS feed ratio 1:1.2 has better room temperature D.C electrical conductivity (16S/cm) than PANI nano rods with aniline to APS feed ratio 1:2.4(7S/cm). This is because of the improved crystallinity of the former as explained in section 3.8.3. The conductivity of PANI nano rods is observed to decrease almost exponentially with temperature, unlike the nearly flat temperature dependent behaviour of PANI (micro). The possible reason may be the greater scattering of the charge carriers at the nano rod walls and at the intersections between different nano rods.

PANI nano rods are found to be more thermally stable than PANI (micro), possibly due to their better crystallinity. For the PANI nano rod sample with higher APS feed ratio, thermal stability decreases. This is because, as APS feed ratio increases, the chain length also increases. This slows down the heat transport along the chains, causing faster degradation. Another possible reason is the better crystallinity of the PANI nanorod sample with lower APS feed ratio.

PMMA is a material with good transparency and optical properties. But studies on PANI-PMMA composites are amazingly scarce. These aspects prompted us to carry out detailed investigations on PANI-PMMA composites. In the present work, HCl doped PANI-PMMA composites are synthesized by chemical oxidative polymerization of aniline in the presence of PMMA dissolved in toluene. FTIR and Raman investigations confirm the formation of PANI(HCl)-PMMA composite. The Raman spectrum also highlights the possibility of electron transfer between PANI and PMMA. The

photoluminescence emission spectra of PANI and PANI-PMMA composites are recorded with excitation wavelength chosen at 300nm. The emission falls at around 502nm. PANI(HCl) exhibits negligible photoluminescence emission, while the emission intensity of PANI-PMMA composites increases with increase in PMMA content in the composite. The presence of electron donating group NH in PANI and electron accepting group C=O in PMMA enhances the Π electron mobility and thereby the possibility for exciton formation. As PMMA content increases, the exciton formation probability also increases resulting in enhanced photoluminescence. But as the PMMA content is increased beyond 1:1 feed ratio, the photoluminescence emission intensity decreases. The temperature dependent D.C electrical conductivity results compliment the P.L results. As the PMMA content in the composite increases, the D.C electrical conductivity also increases up to 1:1 feed ratio. Thereafter, it decreases. PMMA may act as conducting bridges connecting the isolated PANI islands, boosting the Π electron mobility and thereby the electrical conductivity. Particles in PANI and PANI-PMMA are comprised of ordered regions surrounded by disordered or partly disordered regions. PANI is more disordered and contains localized spinless bipolarons. On the other hand, PANI-PMMA's disordered region is relatively less disordered and contains partly delocalized polarons. This could be another reason for the increase in conductivity. But as the PMMA content increases beyond a particular value, the Π electron mobility decreases due to the increased barrier width created by the insulating PMMA. Therefore the D.C electrical conductivity as well as P.L emission decreases. The

samples show semi metallic behaviour with negligible variation of conductivity with temperature from room temperature to about 360K. Even though the thermal stability of PMMA is much less, the thermal stability of the composite does not drop considerably, which can be explained as follows. As the PMMA feed ratio increases, the electrical conductivity increases. Consequently the thermal conductivity also increases, compensating for the low thermal stability of PMMA. PANI-PMMA samples exhibit good mechanical strength also.

MWNT is a material with good electrical conductivity and thermal stability. In the present work, PANI (HCl)-MWNT composites are synthesized by chemical oxidative polymerization of aniline in the presence of MWNT. TEM and SEM investigations suggest that MWNTs are dispersed individually into the PANI matrix. In addition to this, PANI macromolecules can also be adsorbed at the surfaces of MWNTs, forming a tubular shell of the composite. Due to the large aspect ratio and surface area of the MWNTs, they act as 'conducting bridges' connecting PANI domains, forming a 3D network structure. The X.R.D investigations suggest that the crystallinity of PANI-MWNT composites are considerably higher than that of PANI. The crystallinity increases with increase in MWNT content in the composite. The intensity and sharpness of the peak at 25° corresponding to the degree of Π conjugation also increases. The X.R.D spectrum of the composite contains all the peaks of PANI as well as MWNT. FTIR and Raman investigations confirm the formation of the composite. The D.C electrical conductivity of the composites is

considerably higher than that of PANI and increases with increase in MWNT content in the composites. The conductivity saturates after 40% MWNT loading (28S/cm, 14 times higher than that of PANI and 4 times higher than that of MWNT). Due to the large aspect ratio (length to diameter ratio) and surface area of MWNTs, MWNTs may serve as conducting bridges between scattered PANI islands, boosting the charge delocalization. There is also a possibility of charge transfer from the quinonoid unit of polyaniline to the carbon nanotubes, since carbon nano tubes are good electron acceptors and doped PANI is a good electron donor. The improved crystallinity of PANI with the addition of MWNT as evident from the XRD investigations is another reason for the increase in conductivity. The samples show semi metallic behaviour, which is well supported by the thermo power measurements. The composite sample exhibits better thermal stability as compared to PANI, possibly due to the better thermal conductivity of MWNT. Thermal diffusivity measurements using photo acoustic technique show that the thermal diffusivity of the composites increases with increase in MWNT content in the composite up to 1:0.3 ratio, and thereafter decreases for the 1:0.5 sample. The results are explained based on the high thermal conductivity of MWNT, thermal interfacial contact resistance and thermal barrier resistance.

Detailed optical absorption investigations are performed on PANI and PANI-MWNT composite films, deposited using solution casting technique. Negative energy gap has been observed for the first time in PANI(HCl) and PANI(HCl)-MWNT composite films, in the

conducting state, corresponding to indirect allowed transition, while it is absent in the insulating PANI(EB) films.

8.5 Scope for further work

The present investigations and the results obtained extend ample scope for further investigations. The important areas to be explored further are

- a) Detailed thermo power and D.C electrical conductivity measurements on all the semi metallic samples from low temperatures to high temperatures (5K-450K) may shed light on the origin and nature of the metallic state in PANI and its composites.
- b) Attempts should be made to optimize the film deposition conditions to get high quality films of PANI and its composites for possible microelectronic and optoelectronic applications.
- c) Though negative energy gap has been observed in highly conducting films of PANI and its composites, the origin and nature of the negative energy gap could not be established based on the results of the present work.
- d) Other areas to be explored in detail include PANI nanorods and the mechanical strength measurements on PANI-MWNT composite samples.

.....ECC.....

